Condition Indicator Analysis for the Enhancement of Power System State Estimators

Project-Related Ph.D. Thesis

Power Systems Engineering Research Center

A National Science Foundation
Industry/University Cooperative Research Center
since 1996

Power Systems Engineering Research

Condition Indicator Analysis for the Enhancement of Power System State Estimators

Report for the PSERC Project "Enhanced State Estimators" based on a Thesis by

Mark Jason Rice
Graduate Student
Arizona State University

PSERC Publication 07-08

April 2007

Information about this project

For information about this project contact:

Gerald T. Heydt, Ph.D.
Arizona State University
Department of Electrical Engineering
Tempe, AZ 85287
Phone: 480-965-8307
Fax: 480-965-0745
Email: heydt@asu.edu

Power Systems Engineering Research Center

This is a project report from the Power Systems Engineering Research Center (PSERC). PSERC is a multi-university Center conducting research on challenges facing a restructuring electric power industry and educating the next generation of power engineers. More information about PSERC can be found at the Center's website: http://www.pserc.org.

For additional information, contact:

Power Systems Engineering Research Center
Arizona State University
577 Engineering Research Center
Box 878606
Tempe, AZ 85287-8606
Phone: 480-965-1643
Fax: 480-965-0745

Notice Concerning Copyright Material

Acknowledgements

This report is a Ph.D. thesis based on research conducted in support of the PSERC project "Enhanced State Estmators." The author expresses appreciation for the support provided by PSERC industrial members and by the National Science Foundation under grant NSF EEC-0001880 received from the Industry / University Cooperative Research Center program. The author thanks the follow people for their technical assistance: Gary Strickler, Stephen. Sturgill, and Naim Logic, who are all with Salt River Project in Phoenix, Arizona. Useful comments on Phasor Measurement Units and the Eastern Interconnection Phasor Project (EIPP) were obtained from Floyd Galvan of Entergy and his colleagues at EIPP project meetings at Arizona State University.

Dr. Gerald Heydt of Arizona State University (ASU) served as advisor to this thesis. Useful advice was obtained from several ASU faculty, particularly Dan Tylavsky, Vijay Vittal, Raja Ayyanar, and Richard G. Farmer. Comments from Dr. Ali Abur of Northeastern University are also acknowledged.

Executive Summary

Most utilities have state estimators in the package of energy management systems. The main functions of state estimators are to represent steady state system voltage, currents, and power flows – utilizing mathematics to enhance the accuracy of measurements. In this report, the author examines how the new technology of *phasor measurement units* (PMUs) can be used to enhance state estimation in electric power systems.

A study and review of condition analysis for state estimation is presented in this report. Condition analysis is a linear algebra analysis of the sensitivity of the estimations error due to measurement error. The basis of the analysis is the evaluation of the error ellipsoid in the linear least squares formulation of the state estimator problem. The study reveals that decreasing the condition number of the gain matrix increases the accuracy of state estimates. Some other innovative concepts presented in this report include: *singular distance* – calculating the distance between matrix G and the closest singular matrix; *scaling factor* – viewing the largest singular value of matrix G as a condition indicator; and *measurement placement using eigenvectors* – the use of eigenvector of smallest eigenvalue to find placement of measurements. Linearized equations are developed to estimate the change in the condition indicators for the addition of a state measurement.

The analysis of condition indicators for PMU placement led to significant improvement of condition number of the gain matrix. Two test bed systems are used in this report: the IEEE 57 test bed and a representation of a power system in the southwest U.S. The test bed system representing the southwest U.S. power system is 180 buses, 245 transmission lines, and 748 measurements. An algorithm is developed to use condition indicators as an additive tool to other sensory placement strategies.

Table of Contents

Table of Contents (continued)

List of Tables

List of Figures

List of Figures (continued)

List of Figures (continued)

Nomenclature

A	Incidence matrix; a generalized dense matrix
a	Scalar used in Weibull distribution
A/D	Analog to digital
AGC	Automatic generation control
B	A square matrix
b	Scalar used in Weibull distribution
C	Clustering coefficient
c	Speed of light
c_i	Local clustering coefficient
CNP	Condition number placement
CT	Current transformer
d	Singular distance
d_{ij}	Shortest distance between to vertices
$diag$	A vector of the values on the diagonal of a matrix
$E(\bullet)$	Expected value
E	Error
e	Noise vector
EIPP	Eastern interconnect phasor project
EMS	Energy management system
F	Scaling factor
f	Frequency
$f_{nominal}$	The nominal frequency of the power system
FACTS	Flexible alternating current transmission systems
G	Gain matrix
GPS	Global positioning system
H	Process matrix
h	Non-linear process functions
Δh	Augmented row to H
HVDC	High voltage direct current
I	The identity matrix
IEEE	Institute of Electrical and Electronic Engineers
K	Residual correlation matrix
k	Number of buses with PMUs
K_1	Condition number using the 1st norm
K_G	Condition number of G using the 2nd norm
K_p	Condition number using p^{th} norm
L	Average path length
L_p	The p^{th} norm
LFC	Load frequency control

Nomenclature (continued)

m	Number of measurements
MCT	Monte Carlo trials
N	Number of samples
n	Number of buses
N/S	Noise to signal ratio
N_b	Number of buses
NE	Normalized error
N_l	Number of lines
P	Active power
P_{AB}	Power flow from bus A to bus B
P_b	Power flow vector
P_i	Cumulative probability of state i
p_i	Individual probability of state i
PMU	Phasor measurement unit
prob(●)	Probability of event (●)
PSS	Power system stabilizers
Q	Reactive power
q_i	Sensory outage rate
r	Residual
R_P	Power error variance
R_{rms}	RMS of residual
R_V	Voltage error variance
randn	Pseudorandom values with normal distribution
RTO	Regional transmission organization
RMS	Root mean square
S	Singular matrix
s	Number of states
SCADA	Supervisory control and data acquisition
SCDR	Symmetrical component distance relay
SOC	Second of century
t	Time
THD	Total harmonic distortion
TVE	Total vector error
V	Modal matrix; Voltage phasor
V_m	Voltage maximum
W	Weighting matrix
w	weight
WACS	Wide area control system

Nomenclature (continued)

WAMS	Wide area measurement system
x	State vector
X_{AB}	Reactance of line from A to B
x_{exact}	Exact solution of state variable x
$\hat{x}$	Estimated value of state variable x
z	Measurement vector
δ	Voltage phase angle
θ	Sampling angle of a PMU
λ	Eigenvalues of a matrix
μ	Added measurements to H
Π	Product
π_i	The reciprocal of q_i
σ	Singular value of a matrix
τ	Sample interval
Φ	RMS voltage phase angle error
$\{\Phi_i\}$	An ensemble of phase angle errors, i = sample number
Ω	Maximum voltage phase angle error
$\{\Omega_i\}$	An ensemble of maximum bus voltage phase angle errors, i = sample number
$\Delta\Omega$	Discrete Fourier transform frequency resolution (r/s)
$\cup$	Union

1 State Estimators and Phasor Measurement Units

1.1 Background and Motivation

The electric power industry is undergoing multiple changes and restructuring towards deregulation. Some electric power utilities are increasing the loads on the transmission grid to implement power marketing. The increased power exchange has a concomitant requirement for *situational awareness*. This refers to the need for system operators to know the operating states of the system.

Most utilities have state estimators in the package of energy management systems (EMS). Figure 1.1 is a pictorial of the major functions of an EMS. The main functions of state estimators are to represent steady state system voltage, currents, and power flows – utilizing mathematics to enhance the accuracy of direct measurements. Also, until recently it has been nearly impossible to measure voltage and current phase angles but state estimation algorithms allow one to calculate these phase angles from voltage magnitude, current magnitude, and power measurements. There are several topics in state estimation being studied to improve the accuracy of the state estimation in power systems. In this report, the author examines how the new technology of phasor measurement units, a global positioning system (GPS) technology, can be used to enhance state estimation in electric power systems.

Phasor measurement units calculate the phasors of voltage and current from secondary side of current transformers and potential transformers. A growing number of power system protective digital relays are being introduced to the market with the ability to be used as phasor measurement units in addition to their protective relaying function. As phasor measurement unit technology becomes widely available; the electric utilities may want to use this technology as direct measurements in state estimation. Present communication methods from the energy management system to the substations may not provide enough bandwidth for phasor measurement units to send all measurements to the control center. Utilities want to know the cost to benefit ratio of adding PMUs as part of an assessment of investment in upgrading substation communications.

This report addresses state estimation enhancements attributed to phasor measurement units and how to use certain properties of the linear algebraic formulations to assess the performance of proposed locations and number of added measurements.

1.2 State Estimation Literature Review

Schweppe was one of the first to formulate static state estimation for a power network based on the power flow model [1]. The idea is to estimate the electrical states of the power network, mainly voltage magnitudes and phase angles. These states might not be directly observable based on physical relationships between the measurements and the desired unknown states. References [2-5] are textbooks relating to state estimation in power engineering; references [6-9] are representative of solutions methods; and [10, 11] are case studies.

An important element in the field of state estimation accuracy is the use of a weight matrix to increase the accuracy of the results. Weighting is done to enhance the

"input" of accurate measurements, and de-emphasize the less accurate measurements. It can be shown that the maximum likelihood estimate utilizes weights that are based on the covariance of the measurement devices [12]. Weighting is the practice of accounting for the confidence in a measurement. Over time, the confidence in a measurement may change. A solution to this problem is to auto tune the weights of measurements. The suggested method of auto tuning the weights is to examine the recent statistical variances of the measurements and use these to recalculate the weights of measurements from a short history [13]. For the case of multivariable normal statistical distribution of measurement errors, this selection of weights is known to result in a maximum likelihood state estimate. References [2, 3, 5-8, 12, 14] further relate to weighting of measurements for power system state estimation. Table 1.1 presents weights used in power systems state estimation.

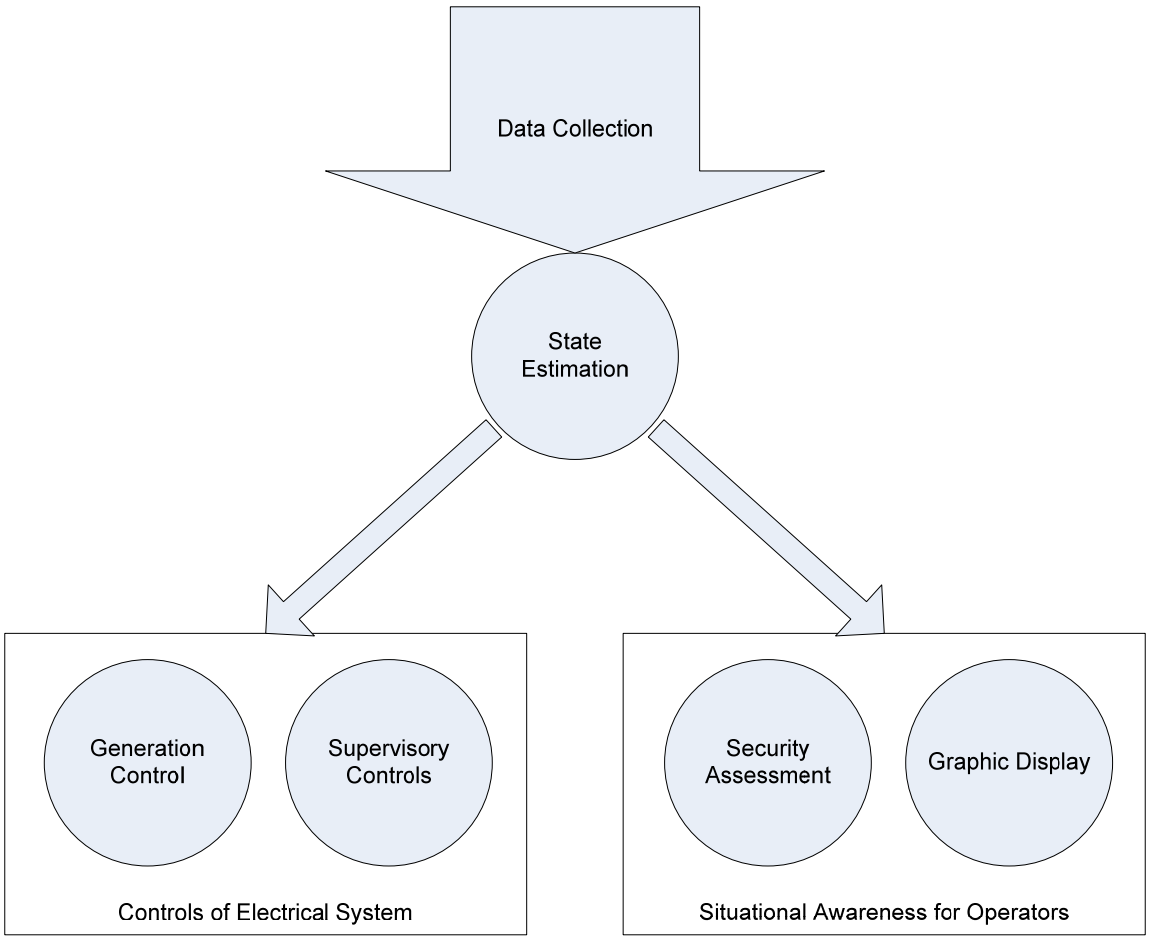

Figure 1.1 Main features of a modern EMS

Table 1.1 Typical weights for measurements used in power system state estimation

Type of Measurement	Typical Weights
Power flow and injections (P,Q)	10.00
Voltage Magnitude ($\|V\|$)	10.00
Current Magnitude ($\| I \|$)	0.001
Transformer Tap Settings	0.010

Measurement errors are typically assumed to be statistically distributed with a zero mean [15]. Due to increase use of technologies such as A/D converters, the zero mean assumption is not always true [15]. A suggested method of overcoming this problem is to combine measurement calibration [16-19] with state estimation. Calibration of the measurements can be done in parallel with state estimation by noting the error of measurement over several scans of the measurement. The calibration error will be a constant compared to measurement error which is normally distributed according to [19].

The process of overcoming measurement noise is inherent in taking physical measurements, but there are situations in which the data is grossly erroneous. One method for the detection of bad data, grossly erroneous data, is the examination of the measurements and if the measurements deviate from expected values by some preset threshold [10]. Another problem that causes state estimators inaccuracy is the power system model uncertainty. Generally the simple linear model $Hx=z$ is used where the H is the measurement model (process matrix), x is the state vector, and x is the measurements. The detection of both erroneous data in measurements and the process matrix uncertainty may be done by examining the residual of the equation $Hx=z$ [12]. Another 'error' in the process matrix is a result of linearization. Since the process matrix is truly a function of operating state, $H=h(x)$. The linearization of the problem results in the assumption of that $h(x)$ is simply a constant matrix H. As the iterative process of state estimation proceeds, $h(x)$ is linearized to Hx with fixed H within iterations. Matrix H is updated, however, from iteration to iteration.

1.3 The Pseudoinverse and Least-Squares Estimation

The commonly used model for a linear static system is

$$Hx+e=z \tag{1.1}$$

with H as the process matrix (m by s matrix), x is the state vector (dimension s), z is the measurement vector (dimension m) is over determined when m is larger than s, and e is the error vector (dimension m) which is assumed to have a mean zero and normal distribution for each measurement. References [2-5, 20] describe Equation (1.1). Equation (1.1) can be "solved" in the least-square sense by minimizing $||r||_2$,

$$r=Hx+e-z \tag{1.2}$$

where $\| \bullet \|_2$ refers to the 2-norm [4]. Properties of norms appear in [4] and Appendix B. It can be shown that $|| r ||_2$ is minimized when

$$x = \hat{x} = H^{+} z \,. \tag{1.3}$$

The notation $\hat{x}$ is the "estimate" of vector *x,* H^{+} pseudoinverse of *H*. References [2-5, 20] describe the properties of the pseudoinverse. Equation (1.3) is known as an unbiased least squares estimator.

Other methods of determining the state variables are under study. One such method is weighted least absolute value [21]. This method uses the infinite norm of the residual, $\| \bullet \|_\infty$; the maximum absolute value in the residual vector is used. Unlike weighted least squares, there is no explicit formula for the solution to linear weighted least absolute value. The weighted least absolute value is found by linear programming [21]. Another method suggested is to find the maximum agreement with measurements [14]. This method uses the 1-norm of the residual, $\| \bullet \|_1$. In the 1 norm the average absolute values in the residual vector is used [14].

The least squares method of state estimation requires the system to be observable. Observablity can be defined as: given a set of measurements and their locations (i.e., given *z* and *H*), then a unique estimate of the system state vector *x,* i.e. $\hat{x}$, can be found such that the 2-norm of the residual vector, $\|r\|_2$, is minimized. A basis of observability analysis is graph theory. To determine which states are unobservable, set the measurement vector, *z*, to zero,

$$H\hat{x} = 0 \,.$$

In the context of electric power systems, this yields a non-zero branch flow,

$$P_b = A\hat{x} \neq 0 \,.$$

The *A* matrix, i.e. the branch-bus incidence matrix, is used to determine P_b, the vector of branch flows. Because the measurement set *z* is set to zero, it is expected that no power flowing through the branches. A non zero branch flow indicates an *unobservable state* of $\hat{x}$ and those branches carrying nonzero power flows, will be referred to as *unobservable branches* [5]. The common technique in correcting the issue of unobservable areas is to provide an estimate of what the readings are in the unobservable areas to create an entire system model [22]. Other references discussing observability are [23-26].

Numerous other topics are discussed in the literature relating to state estimation in power systems including robustness [14, 27, 28], multiphase state estimation [29], and distributed computing [30].

1.4 Phasor Measurement Units Literature Review

Phasor measurement units (PMUs) are instruments that take measurements of voltages and currents and time-stamp these measurements with high precision. PMUs are equipped with Global Positioning System receivers. The GPS receivers allow for the synchronization of the several readings taken at distant points [31]. To accomplish synchronization of measurements taken at distant points, several measurements are taken, and the measurements are time stamped. Interpolation is used to obtain estimates of measurements at a given time within the time horizon of the measurements. PMUs were developed from the invention of the symmetrical component distance relay (SCDR). The

SCDR development outcome was a recursive algorithm for calculating symmetrical components of voltage and current [32]. Synchronization is made possible with the advent of the GPS satellite system [33]. The GPS system is a system of 36 satellites (of which 24 are used at one time) to produce time signals at the Earth's surface. GPS receivers can resolve these signals into (*x, y, z, t*) coordinates. The *t* coordinate is time. This is accomplished by solving the *distance= (rate) (time)* in three dimensions using satellite signals. The PMU records the sequence currents and voltages and time stamps the reading with time obtained by the GPS receiver. It is possible to achieve accuracy of synchronization of 1 microsecond or 0.021° for 60 hertz signal. This is well in the suitable range of measuring power frequency voltages and currents [32]. The basic distance-rate-time formulation of this problem is "solved" using state estimation. That is, a least squares problem formulation is used to find {*x, y, z, t*} which makes the distance-rate-time equations agree in the least squares sense. A minimum of four satellite readings are needed to obtain an observable problem to calculate {*x, y, z, t*}. Most PMUs have the ability to receive signals from at least ten satellites (i.e., *ten channel receivers*). Based upon the research done at Virginia Tech, the Macrodyne Company was able to begin production of PMU devices which led to the IEEE Standard 1344 "Sychrophasor" which defines the output data format of a PMU [32]. Figure 1.1 is a pictorial of PMU measurement system from [34].

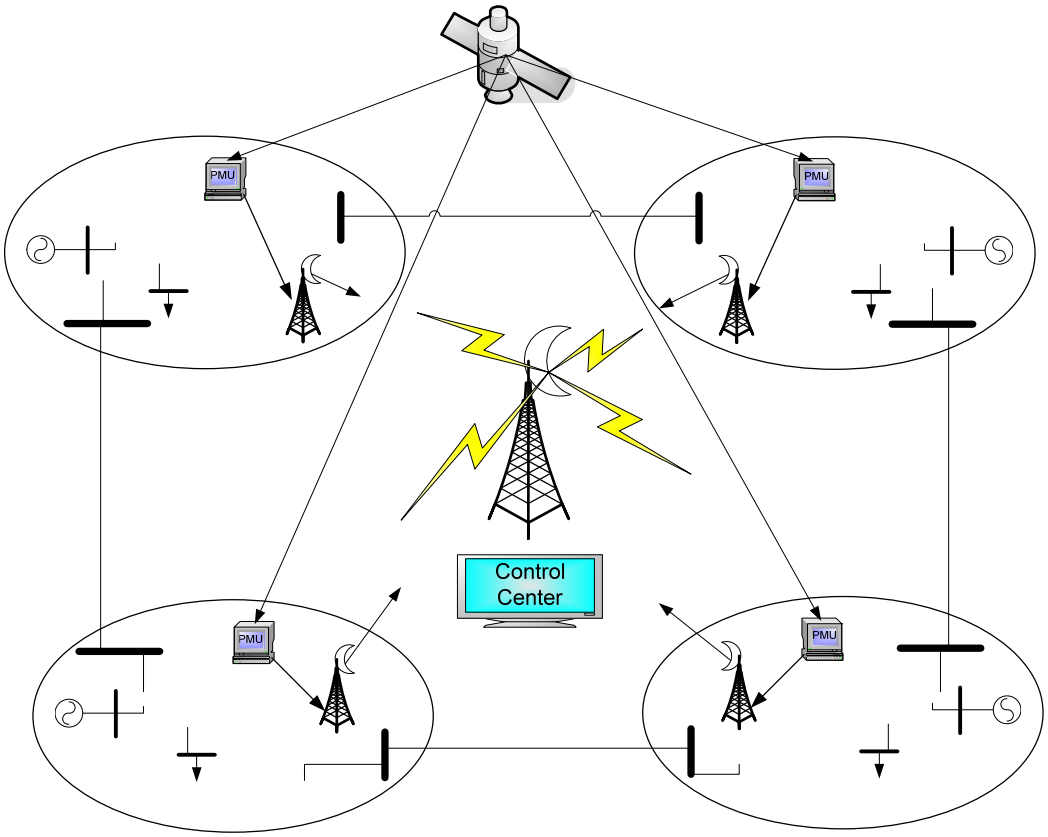

Figure 1.2 Conceptual diagram of a synchronized phasor measuring system redrawn from [34]

The calculation of the phasor measurement can be done using discrete Fourier transforms. A sinusoidal quantity representing voltage

$$v(t) = V_m \cos(\omega t + \delta)$$

has a phasor representation

$$V = \frac{V_m}{\sqrt{2}} e^{j\delta} .$$

By sampling $v(t)$ every τ seconds, the total duration of the ensemble of samples is $T=k\tau$. The discrete Fourier transform of $v(t)$ is

$$V(k\Delta\Omega) = \frac{1}{\sqrt{2}} \frac{2}{N} \left(\left(\sum_{i=1}^{N} v(i\tau) \cos(ik\tau\Delta\Omega) \right) - j \left(\sum_{i=1}^{N} v(i\tau) \sin(ik\tau\Delta\Omega) \right) \right)$$

where $\Delta\Omega=2\pi/N\tau$, and N is the number of samples in one period of the nominal power system frequency [35].

PMUs measure voltage and current with high accuracy at a rate of 2.88 kHz. It can calculate watts, vars, frequency, and phase angle 12 times per 60 hertz cycle. The actual sampling rate used to achieve this output is 1.4 MHz [36]. Some examples of uses of PMUs are fault recording, disturbance recording, and transmission and generation modeling [36].

PMUs are able to measure what was once virtually immeasurable: phase difference at different substations. With PMUs, the utilities are able to measure voltage phase angle.

The integration of PMUs could be into state estimation has been discussed in the literature [19, 37-45]. There is a school of thought that the measurements from the PMU are far superior of SCADA data used in traditional state estimation and should be collected and used separate from this data [46]. Others admit there is difference in the information and it is viable to use PMU measurements in with SCADA data [47]. Hydro-Quebec believes that the PMUs are accurate enough to not need correlation between PMU measurements. Their algorithm is to place the PMUs based on the buses which minimize the correlation between measurements between proposed PMU locations and present measurement locations [48]. An dramatic improvement in the state estimate has been seen by using a three-phase model and the use of GPS synchronized measurements [49].

With increased need for area multi-area of state estimation, there has been noted the possibility of the increased error in the state estimate as the size of systems grows [15]. PMUs are being investigated as a solution to this problem. The electric utilities in the regional transmission organization (RTO) would still do their state estimation. The RTO receives the results from the various state estimates of the areas under its control and PMU measurements from boundaries between electric utilities. The individual state estimators do not interact or exchange data with other state estimators. This allows for each estimator to have its own unique algorithm and not effect performance of other area estimators [41].

The Eastern Interconnect Phasor Project (EIPP) was created encourage the use of advanced metering technology in the eastern interconnect. The primary technology focused on is PMUs. The Eastern Interconnect Phasor Project (EIPP) is divided into two stages. The near term goal is to use the expertise and equipment developed with sponsorship from the U.S. Department of Energy to deliver immediate value to project participants in the eastern interconnect. Most of the existing expertise involves off-line analysis and is supportive of planning activities. The long-term goal is to add value to the interregional information system and measurement system using PMUs [50].

1.5 The IEEE Standard for Synchrophasors for Power Systems

The IEEE has recognized the need for standards for PMUs, also known as synchrophasors. The first standard for PMUs, IEEE 1344 [51], was written in 1995. The drafting of a standard for PMUs is, perhaps, documentation that PMUs are expected to occupy a significant role in power systems instrumentation. A working group was formed in January 2001 to create a new standard for PMUs, IEEE C37.118 [52]. The updated standard provides clarification for phasor and synchronized phasor definitions. The standard defines synchronized phasor measurements in substations so that the measurement equipment can be readily interfaced with associated systems. Table 1.2 lists the major contents of the updated standard.

To allow for integration of PMUs with other equipment, the standard provides common data format for exchanging information with PMUs. The data for time measurement shall consist of second-of-century (SOC) counts, fraction of second count, and a time status value. The SOC count is the number of seconds since the calendar time from midnight January 1, 1970. The accuracy of the time stamp required is ±1μs. The maximum phase time error allowable is 26 microseconds. Table 1.3 shows all the limitations imposed on the PMU.

1.6 The Migration from Wide Area Measurements to Wide Area Control

Wide area measurement systems (WAMS) are instrumentation infrastructures that span a wide geographic area (e.g. typically several control areas and potentially several operating companies). Under WAMS, the time required to transmit the sensory information (latency) back to the central control center is significant compared to the dynamics of the measurement. The latency for a measurement sent via satellite can be as high as 250 ms, and up to 100 ms for a signal sent using a 4800 bits/s modem [53].

Because of the latency issue under WAMS as well as in wider are control systems (WACS), PMUs offer time stamp measurements. PMUs allow several different state estimations to be integrated into a complete set of state estimates of an area [54]. In the deregulated market, the system operational conditions may change quickly and dynamic power flow patterns appear to the system operator [55]. Reference [56] discusses the ability to capture system dynamics using WAMS in the case of the North East blackout of August 14, 2003. A conclusion is that WAMS offer better characterization than digital fault recorders. The real need for capability to capture dynamic system data relates to *sys-*

tem control (i.e. WACS). Control signals need to be sent within one cycle of the disturbance to effectuate system control [57].

Table 1.2 Main contents of IEEE C37.118
(taken directly from [52])

Body of Standard	Appendices
• Synchrophasor measurement o Definition of phasor and synchrophasor o Measurement time tag o System time synchronization • Synchrophasor measurement requirements and compliance verification o Synchrophasor estimation o Accuracy limits o Compliance verification • Message format o Message application o Message framework o Data frame o Configuration frame o Header frame o Command frame	• Cyclic redundancy check codes • Time tagging and transient response • Message examples • Sources of synchronization • Time and synchronization communication • Benchmark tests • TVE evaluation and PMU testing • Synchrophasor message mapping into communications

Table 1.3 Influence quantities and allowable error limits for compliance levels 0-1
(taken directly from [52])

Influence quantity	Reference condition	Range of influence quantity change with respect to reference and maximum allowable TVE in percent (%) for each compliance level			
		Level 0		Level 1	
		Range	TVE (%)	Range	TVE (%)
Signal frequency	$f_{nominal}$	± 0.5 Hz	1	± 5 Hz	1
Signal magnitude	100 % rated	80 – 120% rated	1	10 – 120% rated	1
Phase angle	0 radian	± π radians	1	± π radians	1
Harmonic distortion	< 0.2 % THD	1% any harmonic up to 50th	1	10% any harmonic up to 50th	1
Our band of interfering signal, at frequency f_i, where $\|f_i - f_0\| > f_s/2$, f_s= phasor reporting rate, f_0=$f_{nominal}$	< 0.2 of input signal magnitude	1% of input signal magnitude	1	10% of input signal magnitude	1

Figure 1.3 is intended to depict the roles of measurements versus control. With WAMS becoming increasingly used, researchers have begun examining the concept of (WACS). Some potential elements of WACS are depicted in Figure 1.3. Such studies include the use of WAMS to control power system stabilizers [58, 59]. Other system stability controls are being researched also as seen in [35, 55, 60].

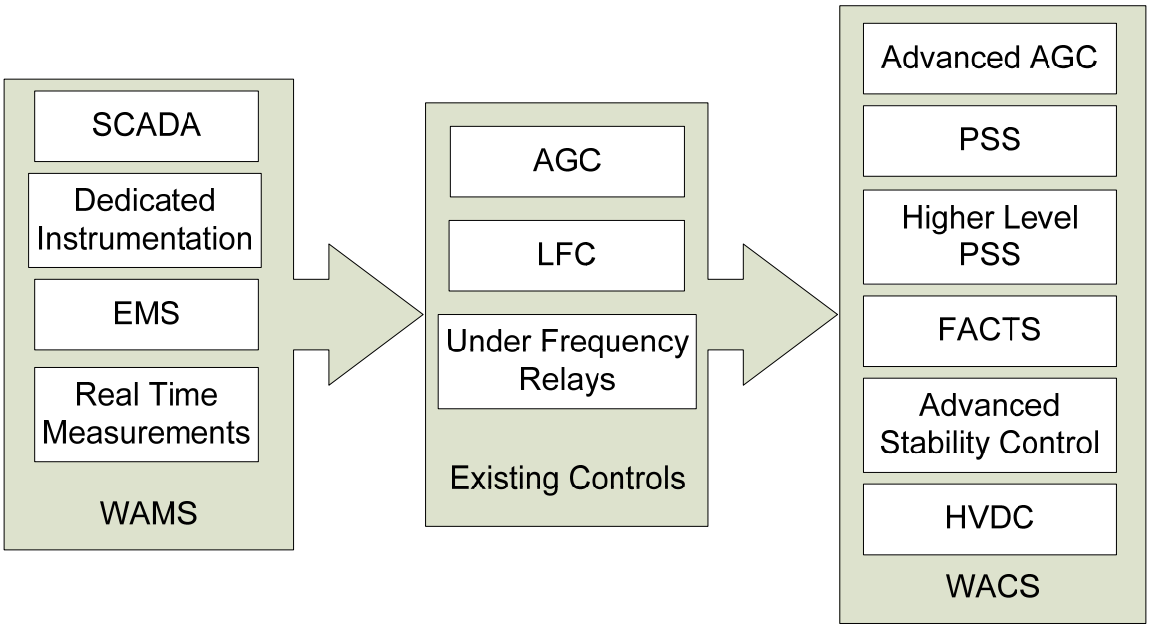

Figure 1.3 Pictorial of the transition of WAMS to WACS

1.7 Placement of Phasor Measurements

Power engineers have been looking at how to use PMUs to monitor and characterize the electrical transmission network. The PMUs have been implemented as a source of information to detect faults on transmission lines [33]. One method to examine locations to install PMUs is to make the system more observable. This starts with a spanning tree and looks for areas of the system which are unobservable [61]. In the approach presented in [61], the next step is to impose certain criteria on the search of the proper placement for the PMUs. In [62], three methods that have been examined are the modified simulated annealing method, direct combination, and the tabu search algorithm. All three were examined on the IEEE 14, 30, and 57 bus systems and the results show that the proposed methods can find the optimal solution in an efficient manner. Another method for determining the optimal placement of the PMU is to do a genetic algorithm search [63]. The authors of [64] suggest that a genetic search is the best because the two solution criteria may be in opposition to each other. In this case, criterion one is to maximize the redundancy and observable area of system. Criterion two is to minimize cost of the installation

[64]. Figure 1.2 is a pictorial that conceptualized the use of PMUs in state estimation measurements for increased observability. Another method suggested by [65] for finding optimal placement of PMUs for making the system observable is integer programming. Another paper [46] argues there should be more criteria added to the optimal placement of PMUs. These criteria include the examination of the placement of the devices to best observe the system stability.

Another index and general philosophy being used to find the optimal location of PMUs relates to the use of the condition number of the measurement matrix [66 - 68]. An algorithm for finding a measurement matrix with a small condition number was suggested by [66]. The algorithm creates a measurement matrix of all possible measurements. Subsequently each measurement is removed individually and the condition number of the measurement matrix is computed. The measurement removed this iteration is the measurement associated with the smallest condition number. This process is continued until the system is critically determined [66]. A later suggestion was to use the minimization of the condition number for harmonic state estimation [69].

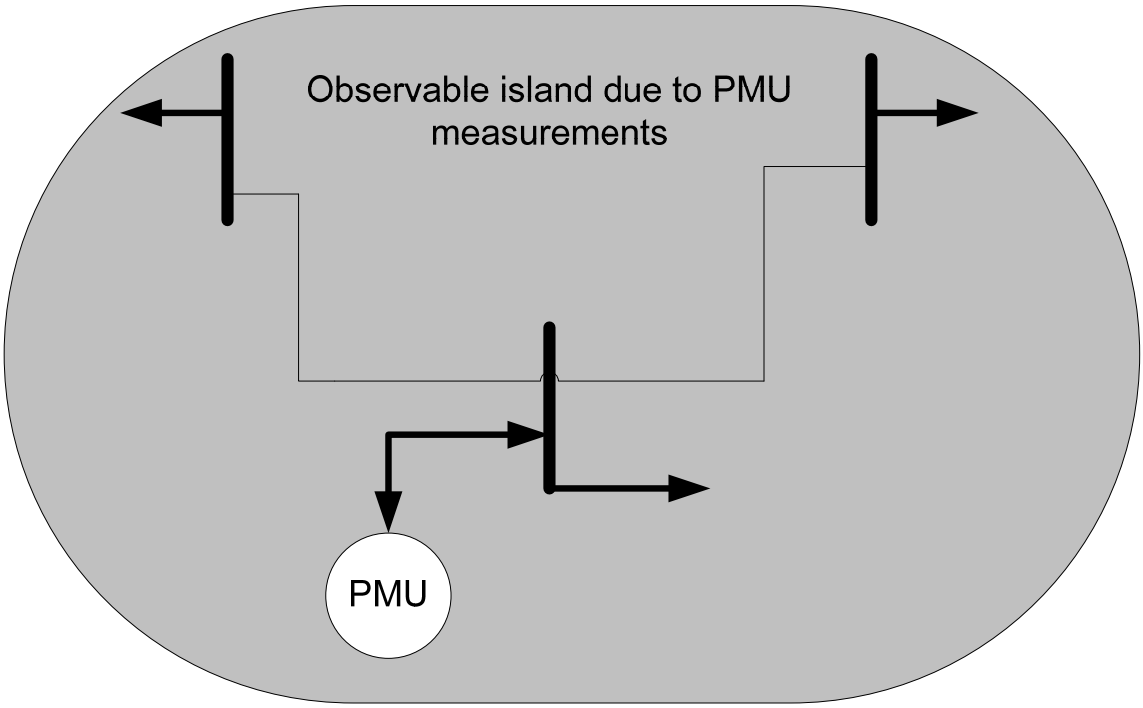

Figure 1.2 Pictorial expanded observability using PMU measurements

Measurement placement problems are not unique to PMUs. Another technology for placement algorithms relates to remote terminal units. One search method used for placement of remote terminal units is the heuristic search. Step one of a heuristic search is to create a measurement configuration that minimizes the number of measurements needed for the system to be observable. Then the configuration is optimized by minimizing the constrained number of remote terminal units used [70]. Another placement algo-

rithm for remote terminal units suggests that the system should be observable when one or two measurements are lost including remote terminal measurements [71].

1.8 Format of This Report

Chapter 1 is an introduction to state estimation and phasor measurement including literature review of recent advances in these fields of study. Chapter 2 contains the theoretical basis of sensory placement for state estimation. Chapter 3 contains case studies implementing theory presented in Chapter 2 about condition indicators. Chapter 4 contains a description of a novel tool to evaluate loss of measurements, the measurement outage table. Chapter 5 discusses case studies using utility operated electric power system. Chapter 6 contains conclusions and recommendations.

Appendices are used to supply supportive information:

Appendix A: Details of the examples used in this report
Appendix B: Examples of condition indicators on first iteration
Appendix C: Electrical connection data of System 2
Appendix D: Examples of Matlab script used in the research of this report
Appendix E: Results from Examples 11, 13, 14, and 16
Appendix F: The impact of weighting measurements on System 2.

2 The Foundations of State Estimation Sensory Placement

2.1 Phasor Measurement Units for Power System State Estimation

The increasing availability of PMU devices has caused increased interest in using PMUs as sensory input for state estimation. Not all PMUs installed can be used in state estimation because of system limitations (e.g., the bandwidth of the SCADA system measurements from remote substations and format and protocol inconsistencies). Further, company A may wish to place additional instrumentation in company B's system, and this issue may be problematic. When a power company is examining how to upgrade the system to allow for PMUs to be used for state estimation, one question that is asked is how incorporating this measurement into the state estimation affects the accuracy of the estimates. The answer relies on where the new PMU measurements are in the system. This report examines methods for determining the placement of PMUs for increasing the accuracy of the estimates.

2.2 The Method of Least Squares

A usual approach to the state estimation problem is to approximate $h(x)+e=z$ by the linear term in the Taylor series expansion,

$$z = h(x_0) + \left.\frac{dh(x)}{dx}\right|_{x_0} (x - x_0) + \ldots + e\,,$$

to

$$z = H(x-x_0) + z_o + e \tag{2.1}$$

H is the process matrix dimensioned (m x s), x is the state vector dimensioned (s), z is the measurement vector dimensioned (m), and e is the noise vector dimensioned (m). Equation 2.1 is the linearized form. In state estimation it assumed that the system is over determined, meaning there are more measurements than states. The problem becomes how to find the best fit between measurements $z+e$ and states x. In the least squares approach idea is minimize the difference L_2 norm of the residual,

$$r = z - H\hat{x} \tag{2.2}$$

$$|r|_2^2 = (Hx - z)^t (Hx - z). \tag{2.3}$$

To minimize Equation 2.3, take the derivative, which results in Equation 2.4. Then simple algebra is used to separate the best estimate of x, namely $\hat{x}$,

$$\left.\frac{\partial \mid r \mid_2^2}{\partial x}\right|_{x=\hat{x}} = 0 = H^t H\hat{x} - H^t z \tag{2.4}$$

$$H^t H\hat{x} = H^t z$$

$$\hat{x} = (H^t H)^{-1} H^t z\,. \tag{2.5}$$

The formulation in (2.5) is valid only when H^tH is nonsingular. There are two notable terms in Equation (2.5): the $(H^tH)^{-1}H^t$ term also known as the pseudoinverse and the gain matrix G,

$$G = H^t H \tag{2.6}$$

$$H^{+} = \left(H^{t} H\right)^{-1} H^{t} = G^{-1} H^{t}. \tag{2.7}$$

The notation H^{+} refers to the pseudoinverse [2-5].

A drawback of the least squares approximation is that the all the measurements are treated with the same weight. This procedure is unbiased. This implies that all the measuring tools are measuring with the same accuracy and precision. In power engineering, this is rarely the case. A term is added to the least squares formulation to provide emphasis for accurate measurements. The matrix W is m by m is used to weight or emphasize the accurate measurements. The weighted residual is $\sqrt{W}\left(Hx - Z\right)$. It can be shown that if, the measurement noise is Gaussian with zero mean and the W matrix is the inverse of the covariance matrix of the measurement noise, the maximum likelihood solution is obtained [3],

$$W = \begin{bmatrix} \sigma_1^{-2} & & & & \\ & \sigma_2^{-2} & & & \\ & & \ddots & & \\ & & & \ddots & \\ & & & & \sigma_m^{-2} \end{bmatrix} \tag{2.8}$$

$$r = \sqrt{W}\left(Hx - z\right) \tag{2.9}$$

$$\| r \|_2^2 = \left[\sqrt{W}\left(Hx - z\right)\right]^{t}\left[\sqrt{W}\left(Hx - z\right)\right]. \tag{2.10}$$

Equation (2.9) is the weighted residual equation. Moving the $\sqrt{W}$ inside the parenthesis, a formulation similar to the unbiased case is found. To find $\hat{x}$ that minimizes $\|r\|_2^2$, take the derivative,

$$\| \mathsf{r} \|_2^2 = \left(\sqrt{\mathsf{W}}\mathsf{H}\mathsf{x} - \sqrt{\mathsf{W}}\mathsf{z}\right)^{\mathrm{t}}\left(\sqrt{\mathsf{W}}\mathsf{H}\mathsf{x} - \sqrt{\mathsf{W}}\mathsf{z}\right)$$

$$H' = \sqrt{W} H$$

$$z' = \sqrt{W} z$$

$$\| r \|_2^2 = \left(H'x - z'\right)^{t}\left(H'x - z'\right) \tag{2.11}$$

$$\left.\frac{\partial \mid r \mid_2^2}{\partial x}\right|_{x=\hat{x}} = 0 = H''H'\hat{x} - H''^{t} z'$$

$$\hat{x} = \left(H''H'\right)^{-1} H'z'. \tag{2.12}$$

There is a caution in the use of the symbolism $\sqrt{W}$. Because there are several different matrices B that satisfy

$$B^{t} B = W$$

(i.e., there are several 'square roots' of the matrix W), the notation $\sqrt{W}$ is ambiguous. Let the term "symmetric positive definite matrix" refer to a symmetric matrix with all positive real eigenvalues. Since W is a covariance matrix, it is the form $E\left(zz^{t}\right)$, and all covariance matrices are positive definite [72], there are exists a unique symmetric posi-

tive definite B such that $B^t B = W$ [20]. Hence the notation $\sqrt{W}$ will refer to that unique symmetric positive definite B such that $B^t B = W$.

2.3 State Estimation Accuracy

The weighted least squares method of state estimation is as accurate at the measurements and the model used. The measurements are being projected onto the mathematical model of the system. If there is no error in the measurements, then the measurements lie on the surface described by the equations of the mathematical model of the system. When there are errors in the measurement then the weighted least squares solution minimizes the distance from the point of measurement to the surface as seen in Figure 2.1.

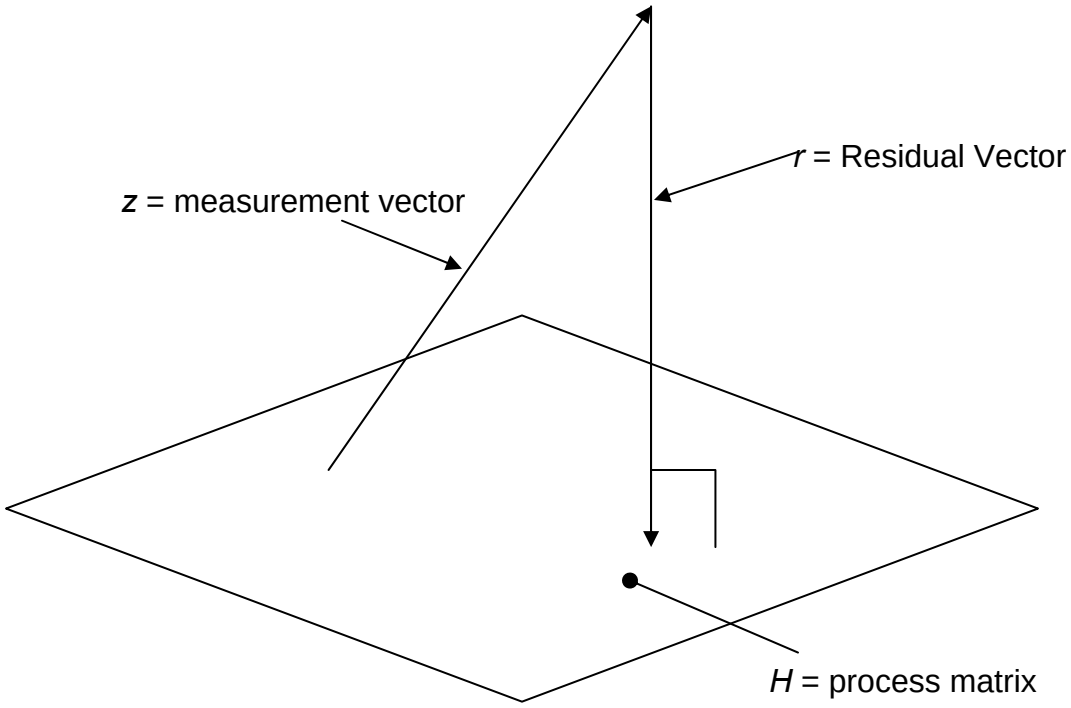

Figure 2.1 Projection of z onto H

The constraint given by [68] of the L_p norm of the residual is

$$\|r\|_p \le K_p(H)\|e\|_p \tag{2.13}$$

where are $\|r\|_p$ is the L_p norm of the residual and e is the vector of error in the measurements and $K_p(H)$ is the L_p condition number of the process matrix, H. The condition number of a square nonsingular matrix A is (2.14) and Table 2.1 is a list of properties of matrix norms, from which,

$$K_p(A) = \|A\|_p \|A^{-1}\|_p . \tag{2.14}$$

Table 2.1 Matrix norm properties
(taken from [73])

Eigenvalues of Matrix A	$\frac{1}{\left\|A^{-1}\right\|} \le \left\|\lambda\right\| \le \left\|A\right\|$	
L_p Norm of Matrix A	$\left\|A\right\| = Max\frac{\left\|Ax\right\|_p}{\left\|x\right\|_p}$	The task of computing a matrix norm is difficult if $p>1$. This is a nonlinear optimization problem with constraints.
Maximum Absolute Column Sum	$\left\|A\right\|_1 = \max_j \sum_{i=1}^{N}\left\|a_{i,j}\right\|$	
Spectral Norm	$\left\|A\right\|_2 = \sqrt{\max\left(\lambda\left(A^H A\right)\right)}$	
Maximum Absolute Row Sum	$\left\|A\right\|_\infty = \max_i \sum_{j=1}^{N}\left\|a_{i,j}\right\|$	
Note	$\left\|A\right\|_2^2 \le \left\|A\right\|_1\left\|A\right\|_\infty$	

The matrix H^tH is also called the gain matrix G. The gain matrix is of dimension s by s and G is symmetric. The calculation shown in (2.5) is closely related to the condition number of matrix G (the condition number K_G of G, using the 2-norm, is defined as the scalar $||G||_2||G^{-1}||_2$ where $||.||_2$ denotes the 2-norm [20]). As shown in [74], the sensitivity of the estimate of x to noise is improved (i.e., lessened) when K_G is small, and the sensitivity is worsened (increased) when K_G is large. Typical threshold values of K_G in state estimation applications, beyond which designers of the state estimator become concerned, are about 10^5.

The eigenvalues of G are equal to the singular values of G in this application when the G matrix is nonsingular; and the ratio of the largest to smallest eigenvalue of G is the condition number of G,

$$K_G = \frac{\lambda_s}{\lambda_1} = \frac{\sigma_s}{\sigma_1} \tag{2.15}$$

where λ, σ denote the eigenvalues and singular values of G respectively, and subscript s refers to the largest eigenvalue and singular value, and subscript 1 refers to the smallest values. Because G is symmetric, nonsingular, and real, the λ and σ values are all positive and real. The ordering of λ and σ is of ascending order. Throughout this report, the condition number based on the 2-norm shall be used because of its convenience and connection with the power engineering state estimation problem solved by minimum least squares; however, it is possible to use other norms (e.g., 1-norm and infinite norm).

2.4 The Singular Distance and Scaling Factor

The foregoing remarks focus on conventional thoughts in contemporary state estimation technology. As an example, the state estimation performance connection with

the condition number K_G has been discussed in the literature [20, 40, 74, 75]. At the juncture, the use of indicators such as K_G is expanded to several innovative measures.

It is clear that the gain matrix G has a substantial impact on the state estimator response to measurements and measurement noise and error. Inspection of (2.5) indicates that $G = H^t H$ should be as 'far from' singular as possible. With this as motivation, define the 'distance' from G to the nearest singular matrix S as d,

$$d = \min_S ||H^t H - S||_2$$

where the minimum is taken over all possible singular matrices S. Then d is the 'distance' from the gain matrix G to the nearest singular matrix, and this is termed here as the *singular distance.* It can be shown that the singular distance d is equal to the smallest singular value σ_1. Therefore

$$d = \frac{\sigma_s}{K_G} = \frac{\lambda_s}{K_G} = \sigma_1. \tag{2.16}$$

Again, recall that the eigenvalues and singular values are all positive and real, and ordered as $\lambda_1 \le \lambda_2 \le ... \le \lambda_s$ and $\sigma_1 \le \sigma_2 \le ... \le \sigma_s$. At the other end of the singular spectrum or eigenspectrum are the values σ_s, λ_s. These quantities may be interpreted as scaling factors which need to be reduced in order to decrease the generalized concept of gain from z to $\hat{x}$. For this reason, σ_s, λ_s are termed the scaling factor F,

$$F = \sigma_s = \lambda_s. \tag{2.17}$$

Then,

$$F = dK_G.$$

It is desired to make the singular distance as large as possible to improve the state estimator response. Similarly, it is desired to make the scaling factor as small as possible.

The condition indicators F, K_G, and d are proposed as tools to assess the number and placement of PMUs in a power system state estimation.

2.5 Augmenting State Estimation Software with PMU Hardware

PMUs use A/D converters to create measurements of time, active power, vars, frequency, current, and voltage. PMUs take as many as 12 measurements per 60 Hz cycle, and then approximating the best curve to fit the sample set. The PMU reads in data at the rate of 1.4 MHz [36]. Synchronous time signal received from GPS is accurate with in 1 microsecond or 0.0012° per 60 Hz cycle [32]. The accuracy of the PMU data is also dependent on the errors of current transformers and potential transformers [76 – 77]. The accuracy obtained of the measurements of PMU devices is at least five times greater than the accuracy of measurements obtained from SCADA devices measuring active and reactive power.

The process of finding the phase angle using a PMU is a set of state estimations. The determination of time using GPS is computed from the synchronized time signals being sent from the satellites. To determine time there must be at least four satellite signals being received because three other states (x,y,z) are also being determined. The GPS

unit receives time signals from the satellites and using distance equations shown in Figure 2.2. The receiver performs an iterative estimation process to determine the most likely (*x,y,z,t*).

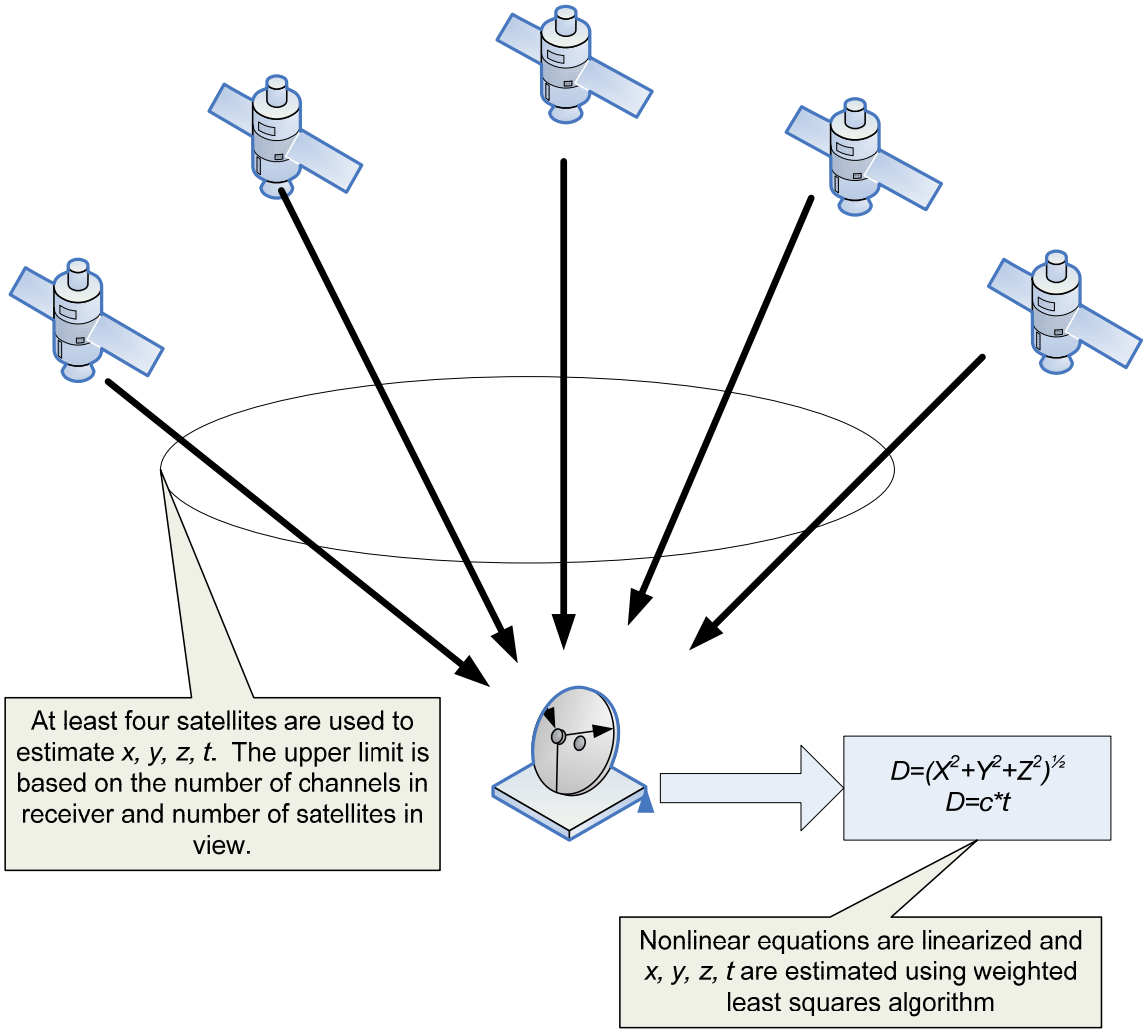

Figure 2.2 A representation of GPS system of a PMU

After an accurate time is calculated, a phase angle is determined by sampling the voltage or current signal. The PMU is able to record 2,880 measurements per second, 48 measurements a cycle, meaning measurements are estimated using only data samples from only part of the cycle as seen in Figure 2.3. The distance between samples is exaggerated for purpose of clarity.

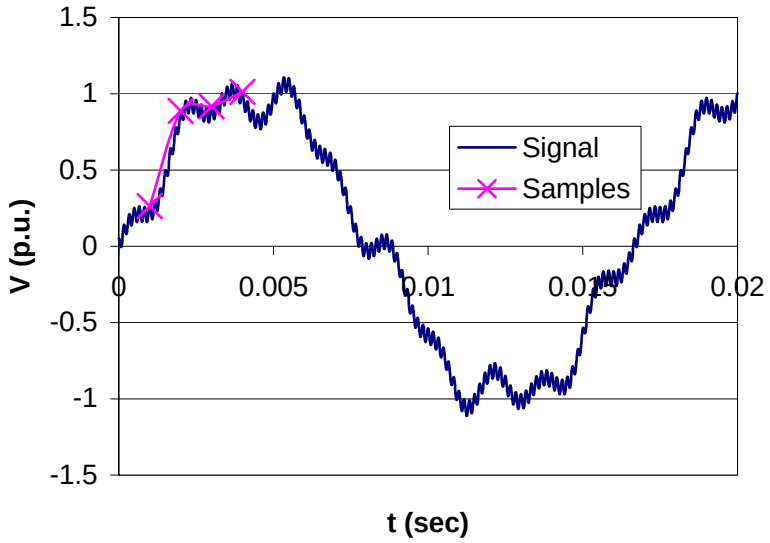

Figure 2.3 Illustrative noisy voltage signal and PMU samples

The measurements of voltage phase angles by PMUs are considered much more accurate than those made by other measurements in the system. Presently there are no other methods of directly measuring phase angle. Another advantage of PMU measurements over SCADA measurements is that PMU measurements have an accurate time stamp of when measurements were taken. This allows for synchronizing of PMU measurements that may be reported to EMS at different times and at diverse locations.

2.6 Location of PMUs

PMU placement can be done using several different criteria including security concerns, observability, and improvement in state estimation. In this report the criterion used to determine the location of PMUs will be improvements in the state estimator performance. The improvement in state estimation can be further broken down into two parts: increase in accuracy; and robustness of the state estimator.

The residual vector is typically used to determine the fit of the measurements to the model in power system state estimation. The residual is used because when state estimation is being conducted for an actual system, the 'true' values of the states are not known. The residual vector as discussed earlier is $r = z - H\hat{x}$. It is convenient to use the 2-norm of the r as an index of the agreement of the measurement equations,

$$\|r\|_2 = \sqrt[2]{r^t r} .$$

At the solution,

$$r = z - H\hat{x} .$$

In this study, it is possible to examine the deviation of $\hat{x}$ from the "exact" value of x. Normally this comparison is not possible but because of the use of test beds with a *known solution*, it is possible to use normalized error, *NE*, to assess the accuracy of $\hat{x}$,

$$NE = \frac{\left\| x_{exact} - \hat{x} \right\|_2}{\left\| x_{exact} \right\|_2}.$$

The normalized error has benefits for comparing direct substitution to weighted least squares. The normalization permits comparison of residual norms for residual vectors of different dimensions. Table 2.2 shows the various measurements of error.

Table 2.2 List of various measurements of error in the state vector

Normalized Error	$NE = \frac{\left\| x_{exact} - \hat{x} \right\|_2}{\left\| x_{exact} \right\|_2}$
Norm of the Residual	$\left\| r \right\|_2 = \left\| z - H\hat{x} \right\|_2$
Weighted Residual Norm	$\left\| r_w \right\|_2 = \left\| \sqrt{W} z - \sqrt{W} H\hat{x} \right\|_2$
RMS of Residual	$R_{rms} = \frac{1}{\sqrt{m}} \left\| z - H\hat{x} \right\|_2$

As discussed in Section 2.3 the minimization of the condition number of the G matrix can provide a location for PMU placement. Having a G with a smaller condition number will result in state estimator that will provide more accurate results when noise is present in the measurement vector. The work done in [78] resulted in a determination of the condition number for a radial system with only power flow measurements and lines of unit reactance. The condition number can then be computed as

$$K_1(H) = 2n(n+1) \tag{2.18}$$

where n is the number of buses in the system and $K_1(H)$ is the condition number of the H matrix using the 1-norm. Thus, as the number of buses in the system increases, so does the condition number. Reference [78] also presents a method for finding the condition number of radial system with only power injection measurements.

Another paper, [74], examines what would happen to condition number as power measurements are replaced by PMU measurements in the radial case. The results of [74] were that with proper weighting of the measurements, the condition number could be determined as function of number of PMUs and number of buses. The weight given to power measurements is the inverse of power error variance, R_p. The weight given to voltage measurements including PMU measurements is the inverse of voltage error variance, R_v. Let μ be the number of PMU buses, n be the number system of buses. If

$$\frac{4}{R_p} < \frac{1}{R_v}$$

and

$$R_v < \frac{R_p(n-\mu)(n-\mu+1)}{2},$$

then the condition number is

$$K_1(H) = \frac{R_p(n-\mu)(n-\mu+1)}{2R_v}. \tag{2.19}$$

Note that the foregoing focused on the radial system configuration. Figure 2.4 is a graphic that depicts the "spectrum" or the degree of networking of a system. The fully networked case (i.e., all the buses connected to all other buses) is shown to the right of Figure 2.4 and fully radial systems are to the far left of Figure 2.4. "Real" networks lie in between these extremes.

It can be shown that a similar equation to (2.18) is valid for the fully networked system. Equation 2.20 give the condition number of the fully networked system as it relates to the number of buses in the system,

$$K_1(H) = 2n - 3. \tag{2.20}$$

Note that (2.20) is linear compared to the quadratic form in (2.18) and that the fully networked system condition number is always smaller than the radial system of the same size (for systems of unit line reactance). The condition number of a "real" system will be in between values found using (2.18) and (2.20).

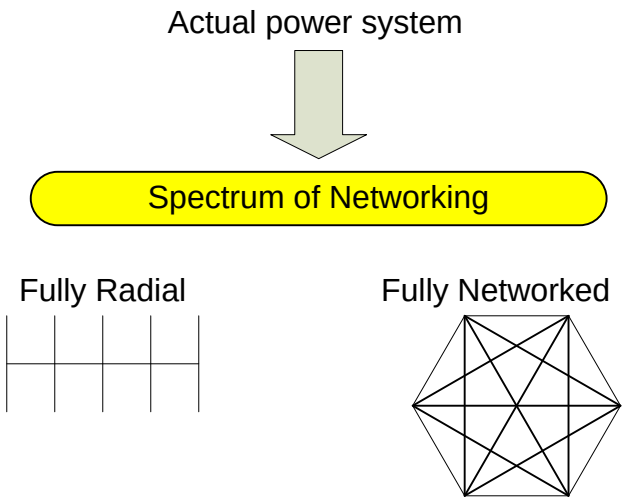

Figure 2.4 "Spectrum" of the networking extremes of electric power systems

2.7 Small World Theory

A small world network is a network of graph for which most nodes are not neighbors to one and another, but destination nodes can be reached by following a small number of branches. To be classified as a small world network the network must be sparse,

$$Edges << \frac{Nodes(Nodes+1)}{2}.$$

The system must not be considered fully networked [79]. The system nodes must all be connected by at least one path. Structural properties of small world networks are path length, *L(p)*, and clustering coefficient, *C(p)* [79]. The global average path length is

$$L(Global) = \frac{1}{Nodes(Nodes-1)} \sum_{i,j \in G, i \neq j} d_{ij} ,$$

where d_{ij} is the shortest path between 2 nodes. The average clustering coefficient for the entire network is

$$C(Global) = \frac{1}{Nodes} \sum_{i \in G} C_i ,$$

where C_i is the ratio of the number edges connecting bus *i* to neighbors to the number of possible edges connecting to neighbors of bus *i*. The western area power system is studied to see if it was a small world network [80]. Table 2.3 displays the small world measures of the Western Electricity Coordinating Council (WECC). The random case used for comparisons is using the same amount of nodes, i.e. buses, and same amount of branches connected to each bus, but randomly choosing the nodes that the branches connect [80]. The power grid shows small world characteristics of average length, *L*, of path being larger than the random length of path and clustering coefficient, *C*, being much larger than the random clustering coefficient.

Table 2.3 Small world properties of the WECC system

	Actual grid	Randomly connected nodes
L(G)	18.7	12.4
C(G)	0.080	0.005

Other famous small world networks include neural network of a worm, spread disease, and telecommunication networks [79, 80]. In all of the examples of small world networks studied, including the western area power system, the system was found to be robust to the failure of a vertex. The probability of catastrophic events in the system being caused by the loss of a single vertex is minimal [80].

The power system is monitored by a network of sensors traditionally measuring voltage magnitude and power. The communication between the sensors on the system and the control center can be either by wireless communications or dedicated wired communication channels, e.g., dedicated phones lines or fiber optic cables. Assuming, the wired communications paths follow the transmission paths. Then communications network of sensors using wired communication channels can be considered a small world network. It is stated in [80] that small networks are:

- less subjected to signal congestions
- more robust in cases of path failures.

If these characteristics are true, a sensory signal communications network that generally follows the WECC electric power network would be less subjected to signal congestion and more robust in the case of communication path failure.

2.8 The Sensitivity of Condition Indicators to Added State Measurements

Added measurements to an existing system which already contains m measurements causes the process matrix H to augment with added rows. State estimator design is often considered for an existing system with a previously designed set of measurements. Consider the case of μ added measurements to a system with m measurements already in place. Further, let the added measurements be direct measurements of states (i.e., entries of the state vector x). The addition of added state measurements is pertinent due to the interest in the utilization of phasor measurement units (PMUs) or synchrophasor measurements [35, 81] because PMUs can measure phase angles of bus voltages. Then H becomes a $m+\mu$ by s matrix,

$$H_{augmented} = \begin{bmatrix} & H & \\ 0 \quad \ldots & 1 & \ldots \quad 0 \end{bmatrix} \begin{matrix} \\ \} \Delta h \end{matrix}$$

but the dimension of G remains s by s. Consider further the case that the added measurements are direct measurements of μ states. Then the added rows of H consist of all zero entries except in μ columns which may be collectively called columns k where the non-zero entries are $\Delta h_{k1}, \Delta h_{k2}, ..., \Delta h_{k\mu}$. The gain matrix G experiences the addition of $+(\Delta h_{k1})^2, +(\Delta h_{k2})^2, ..., (\Delta h_{k\mu})^2$ in the $\{k_1,k_1\}$, $\{k_2,k_2\}$, … , $\{k_\mu,k_\mu\}$ diagonal positions. Thus the condition indicators of G will change due to the added measurements. The change in eigenstructure of a matrix due to the change of elements of that matrix is well known. For example, the sensitivity of the eigenvalue λ_j of G to a single diagonal entry $G_{i,\,i}$ is given by [75],

$$\frac{\partial \lambda_j}{\partial G_{i,i}} = (V_{i,j})^2 \tag{2.21}$$

where V is the s by s matrix of eigenvectors of G arranged column-by-column, and the eigenvectors are of unit length. The matrix V is called the modal matrix of G. The sensitivity of λ_j to several changes of entries on the diagonal of G, namely $+(\Delta h_{k1})^2, +(\Delta h_{k2})^2, ..., +(\Delta h_{k\mu})^2$ in the positions $\{k_1,k_1\}$, $\{k_2,k_2\}$, … , $\{k_\mu,k_\mu\}$ is found using (2.17) and superimposing (adding) the several sensitivities corresponding to $i = k_1, k_2, \ldots, k_\mu$. Addition is presumed possible if the Δh entries are small and the formulation is assumed nearly linear locally. Because the condition indicators are intimately related to the eigenvalues of G, it is possible to 'design' (i.e., locate, and assign measurement weights) the added state measurement entries with a view of improving the several condition indicators.

For purposes of discussion, the condition analysis of added state measurements is now confined to the addition of one measurement at state k, *i.e.*, $\mu = 1$. The generalization to the case of many added state measurements is discussed below. If the added measure-

ment of state k results in Δh_{k1} in the H matrix, and $(\Delta h_{k1})^2$ is sufficiently small, (2.21) may be used to estimate the condition indicators using

$$\Delta\lambda_j \approx \frac{\partial \lambda_j}{\partial G_{i,i}} \Delta G_{i,i}.$$

The results are

$$\Delta d = V_{k1}^2 (\Delta h_{k1})^2 \tag{2.22}$$

$$\Delta K_G = \frac{V_{ks}^2 - K_G V_{k1}^2}{\lambda_1 + V_{k1}^2 (\Delta h_{k1})^2} (\Delta h_{k1})^2 \tag{2.23}$$

$$\Delta f = V_{ks}^2 (\Delta h_{k1})^2. \tag{2.24}$$

Note that in (2.22 – 2.24), the difference condition indicator terms are given by, for example, $\Delta d = d_{new} - d_{old}$. For the case that $(\Delta h_{k1})^2$ is small, the following approximation may be used in place of (2.23),

$$\Delta K_G = \frac{V_{ks}^2 - K_G V_{k1}^2}{\lambda_1} (\Delta h_{k1})^2. \tag{2.25}$$

2.9 Summary of Proposed Innovative Concepts

The in and review of condition analysis for state estimation revealed a correlation between decreasing the condition number of the gain matrix and increasing the accuracy of state estimates. Some other innovative concepts presented in Chapter 2 include:

- *Singular distance* – calculating the distance between matrix A and the closest singular matrix.
- *Scaling factor* – viewing the largest singular value of matrix A as a condition indicator.
- *Measurement placement using eigenvectors* – the use of eigenvector of smallest eigenvalue to find placement of measurements.

Also, the observation that the WECC electrical network in the United States is "small world" and it is conjectured that sensory communications paths are in parallel with electric power paths result in a communications infrastructure that is less subject to congestion and more robust in cases of path failure.

3 Illustrative Applications of Condtion Indices Based Approaches to State Estimatior Design

3.1 The Spectrum of Condition Indicators in State Estimator Applications

As a quick illustration of the usual order of magnitude of some singular distances, scaling factors and condition numbers in this power engineering application, see Table 3.1. For convenience, the collective reference to K_G, d, and f shall be *condition indicators*. The study of the condition indicators will be termed *condition analysis*.

Table 3.1 Condition indicators of some illustrative power systems*

		Radial system of N_b buses	Fully networked system of N_b buses (all buses connected to all other buses)
Impedances of lines		All unity	All unity
Number of buses		N_b	N_b
Number of lines		N_b -1	$\frac{N_b}{2}(N_b-1)$
Number of line P measurements		N_b -1	$\frac{N_b}{2}(N_b-1)$
Number of line Q measurements		N_b -1	$\frac{N_b}{2}(N_b-1)$
Number of bus $\|V\|$ measurements		N_b	N_b
Number of injection measurements		*0*	*0*
Number of measurements, m		$3N_b$ -2	$N_b^{\,2}$
Number of states, s		$2N_b$ -1	$2N_b$ -1
Condition indicators	K_G	$2N_b^{\,2}$	N_b+1
	d	$2.5/N_b^{\,2}$	1
	F	5	N_b+1

* 2-norms are used for the condition indicators. Representative results are shown for the cases indicated. All bus voltages measured, all line P, Q measured; unbiased estimates, at the first iteration. Values shown are for large N.

3.2 Two Test Beds for Condition Analysis

The two previous examples are of the extremes of the "spectrum" of networking, engineering intuition indicates that the IEEE 57 test bed [82] lies somewhere in between. Figure 3.1 is a one line diagram of the IEEE 57 test bed system. The IEEE 57 bus test bed

(System 1) has 30 buses in which there are 2 lines connected to the bus (i.e. similar to a radial system) and 1 bus that has one line connected to the bus. System 1 has 26 buses in which there are 3 or more lines connected and there are 80 lines total in the system. Table 3.2 shows these bus connection data comprising the two systems being studied. Note that in Table 3.2 the notation $\delta(a)$ is the discrete dirac delta function which is zero everywhere except when $a=1$ where $\delta(a)=1$.

Table 3.2 Topology characteristics of Systems 1 and 2

System	N_b	N_l	Number of Buses at which only 1 line incident	Number of Buses at which 2 lines incident	Number of buses at which ≥3 lines incident
Radial	N_b	N_b-1	*2*	N_b -2	*0*
System 1*	57	80	1	30	26
System 2**	180	254	12	103	65
Fully Networked	N_b	$N_b(N_b-1)/2$	$2\delta(N_b-2)$	$3\delta(N_b-3)$	N_b

* IEEE 57 bus test bed

** Representative power system in the southwest US

The H matrix for the IEEE 57 bus test bed has varying admittance values this will influence the condition number of the H matrix. The measurement set for the H matrix is all the real and reactive power flows and real and reactive power injections at buses 1, 2, 3, 6, 7, 9, 12, 25, 53, 18 for Example 1. The reactance of the lines in System 2 ranges from 0.0152 p.u. to 1.355 p.u. or two orders magnitude.

The other system to be studied in this report is representative of the power system in the southwest US (System 2). System 2 contains 180 buses, and 254 lines. The system has impedances from $1x10^{-5}$ to 0.4787 per unit on a 100 MVA base. The measurement set is 239 power flow measurements, 236 reactive power flow measurements, 99 power injection measurements, 99 reactive power injection measurements, and 75 bus voltage measurements. Table 3.3 is list of *condition indicators* for both System 1 and 2.

3.3 Description of the Iterative State Estimator Used

The state estimator used for this report was written by Xiaolin Mao, a postdoctoral researcher at Arizona State University [83]. The properties of the state estimator are:

- Uses conventional measurements: real and reactive power flow and injection measurement, and voltage magnitude measurements
- Accepts in IEEE common data format information for topology
- Accepts excel files as inputs for measurements
- The limit of iterations is 50
- The tolerance for convergence is 0.0001.

Table 3.3 Condition indicators of System 1 and System 2

		System 1	System 2
Impedances of lines		Actual line impedances used	Actual line impedances used
Number of buses		*57*	*180*
Number of lines		*80*	254
Number of line *P* measurements		*80*	239
Number of line *Q* measurements		*80*	236
Number of bus $\|V\|$ measurements		*0*	75
Number of injection measurements		*24*	*198*
Number of measurements, *m*		*184*	748
Number of states, *s*		*113*	*359*
Condition indicators	K_G	24,593	$6.9x10^{10}$
	D	0.4633	1.1648
	F	11,368	$8.0019x10^{10}$

* IEEE 57 bus test bed

** Representative power system in the southwest US

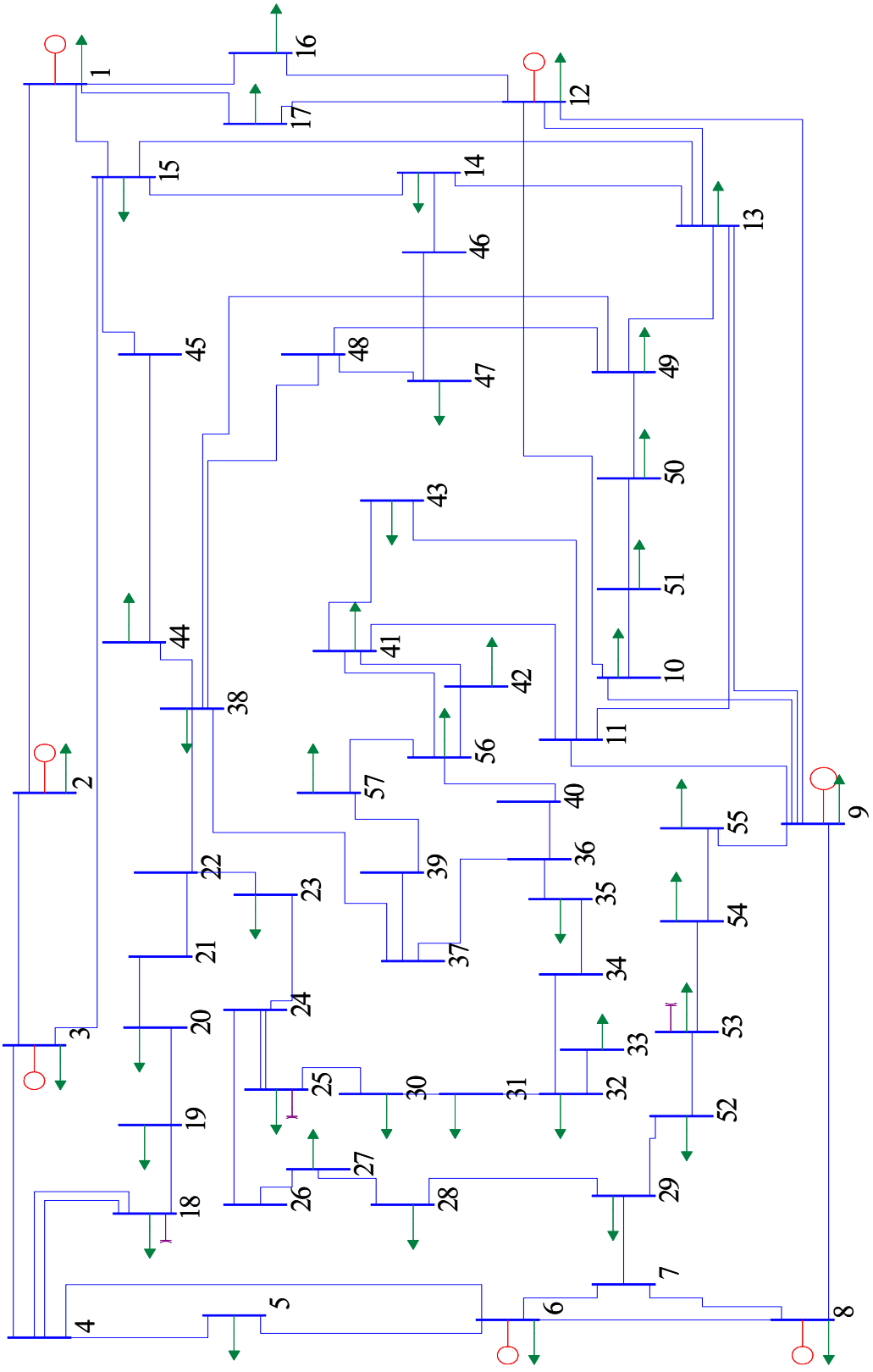

Figure 3.1 One line diagram of the IEEE 57 test bed case study (System 1)
(redrawn from [82])

3.4 Linearized Approximations of Singular Distance Using the Iterative State Estimator

Example 1 is constructed to explore if the linearized approximations of the condition indicators presented in (2.22-2.25) are valid when using an iterative state estimator to solve the nonlinear power equations. The details of all examples appear in Appendix A. In example 1, System 1 is used. The procedure for Example 1 was to solve the state estimation from a flat start based on a set of measurements with no PMUs added, and find the predicted change to d for each of the iterations. Then to solve the state estimation from flat start with previous measurements augmented with a single PMU measurement. The state estimator converged in 4 iterations for both. Figure 3.2 is a plot of the smallest eigenvalue, d, as state estimator converges on a solution. The predicted value for d is close to the actual value of d with the placement of PMUs.

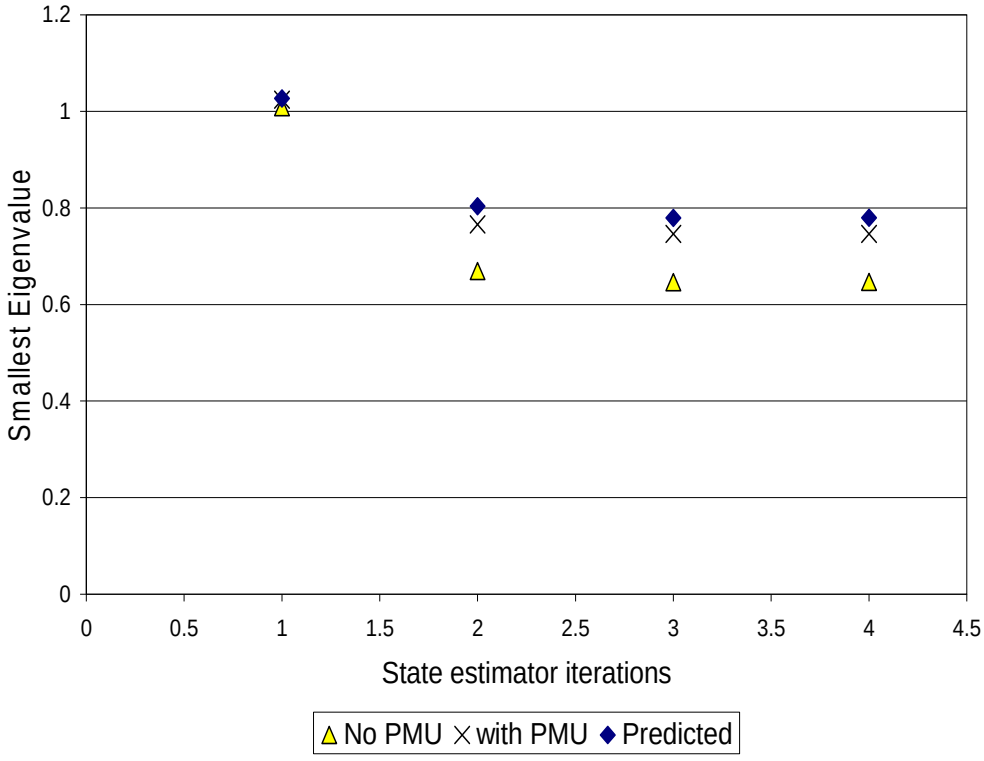

Figure 3.2 Impact on singular distance of placement of a PMU at bus 32 (Example 1)

3.5 An Algorithm for Condition Analysis

The condition analysis concepts above are proposed for the following applications:

- Application to an existing system in which the SE has a valid G matrix. The system is under study for added measurements.

- The condition analysis is a tool used in connection with other placement techniques. It is assumed that the system is observable.
- A "sanity check" for proposed measurement placement.

In these applications, it was found that the impact of measurement noise on state estimation is attenuated. This point is illustrated in the subsequent example. Also, it is found that the condition analysis of the placement of the proposed measurements agrees with redundancy analysis – also illustrated below.

Figure 3.3 is a conceptual depiction of how conditional analysis might be integrated into a design search algorithm for measurement placement.

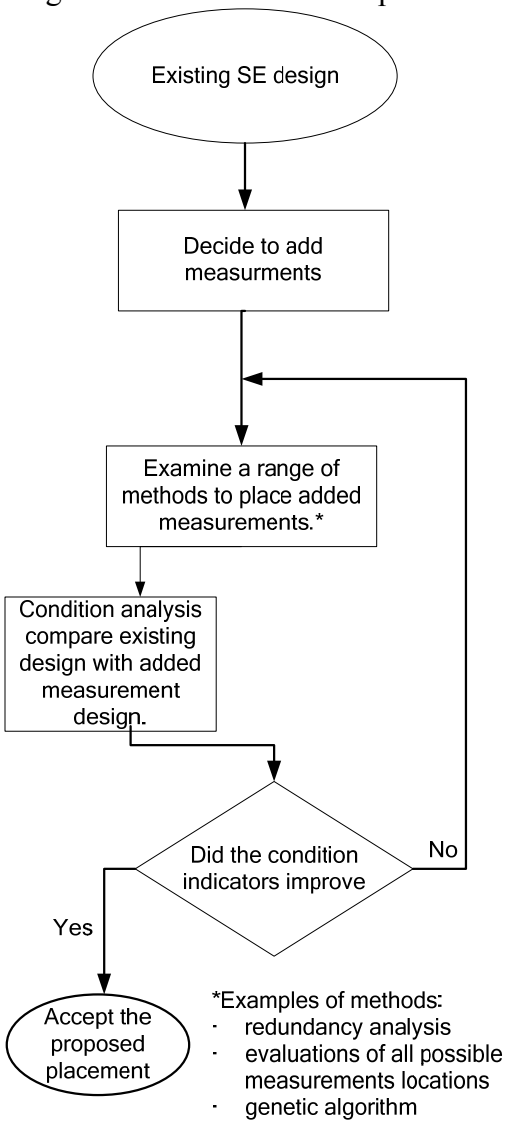

Figure 3.3 An algorithm for the use of condition analysis in conjunction with other measurement placement methods

3.6 Illustration of State Estimation Design Based on Condition Indicators

The foregoing implies that the condition indicators d, K_G, and f may be used to assist in the selection of the locations of additional power system SE measurements. Using the difference formulations (2.22-2.25), one might select k to correspond to the largest value of $(V_{k1})^2$ (i.e., increase d); select k to correspond to the smallest $(V_{ks})^2$ (i.e., decrease f); or select k to result in the smallest value of $(V_{ks})^2 - K_G(V_{k1})^2$ (to decrease K_G).

For purposes of illustration the IEEE 57 bus test bed will be used; Figure 3.1 is a one line diagram of the system. The example illustrates the effects of adding direct measurement of bus voltage phase angle using PMUs. Three cases are studied:

- Example 2: addition of no phasor measurements
- Example 3: addition of 1 phasor measurement
- Example 4: addition of 5 phasor measurements.

The criterion used in placement of the phasor measurements is to maximize the reduction of the condition value using the linearized approximation in (2.23).

The values for ΔK_G and Δd given in Table 3.4 (unlike Table 3.3) are calculated using the *solved* solution gain matrix (i.e. the final gain matrix calculated by state estimator). Note, the accuracy of the prediction of the change in condition number (2.23) and the change in singular distance (2.22) are greater in Example 3 than in Example 4 measurements.

The state estimation was performed with weight of unity given to all measurements including bus voltage phase angle. The traditional measurements (real and reactive power flows, real and reactive power injections, and bus voltage magnitudes) were polluted with noise. The signal to noise ratio was 10. The noise was created using Matlab function *randn*, which creates pseudorandom numbers with mean of zero and standard deviation of 1, Gaussian distributed pseudorandom numbers. The bus voltage phase angle measurements were not contaminated with noise. The tolerance of the state estimator was set to 10^{-4} with a maximum iteration count of 50. Note that the error in the state vector, $\hat{x}$, is shown as error in voltage magnitude, $|V|$, and as error in phase angle, δ.

The error in $\hat{x}$ is determined by finding the difference between $\hat{x}$ and the actual value of x. The actual value of x is known due to the fact the analyses were performed on the IEEE 57 bus test bed where the bus voltage magnitude and bus voltage phase angles are known. The error values in Table 3.4 represent the mean of the norm of the error in the bus voltage magnitude and bus voltage phase angle. The number of trials performed is 10,000. Note that there is little improvement in the error in $|V|$, and small improvement seen in the error in δ.

At this point, Example 5 is introduced as an example, using the IEEE 57 bus test bed, and using several state measurement weights. Figure 3.4 is a graph showing varying weights applied to a phasor measurement (w_{SM}) on bus 33 for Example 5. The weight matrix used in Example 5 is

$$W = \begin{bmatrix} I & 0 \\ 0 & w_{SM} I \end{bmatrix},$$

where I is the identity matrix. Note the linear growth in the predicted singular distance and the leveling off of the actual singular distance. Note the change predicted using (2.22) and weight of 1 is an increase in d of 97%, and the actual change seen is 58%. The linearization equations for the change in condition indicators are for small changes, not for such significant changes as seen in Example 5. The singular distance is the smallest singular value of the gain matrix (i.e., the denominator of the condition number of the gain matrix). As the singular distance increase the condition number decreases and the gain matrix is further from the closest singular matrix.

Table 3.4 Comparison of three test cases using the IEEE 57 bus test bed

		Example 2: No PMUs added	Example 3: 1 PMU added	Example 4: 5 PMUs added
Location of PMU using (8)		N/A	33	25, 30, 31, 32, 33
Final iteration k_G‡		36,163	22,920	14,682
ΔK_G	Predicted using (8)	N/A	-17,828	-29,015
	Actual value on solution G	N/A	-13,243	-21,481
Final iteration d‡		0.2897	0.4570	0.7130
Δd	Predicted using (7)	N/A	0.2817	1.1760
	Actual value on solution G	N/A	0.1673	0.4233
Error in $\hat{x}$	in $\|V\|$ of all buses*	0.1319	0.1312	0.1321
	in δ of all buses*	6.4059	6.1048	5.6289
	in δ at bus 33	0.6655	0.2998	0.0581
	in δ at buses 25, 30, 31, 32, 33*	2.9076	2.3816	0.9589

* 2-norm is used in error calculations

‡ "Final Iteration" refers to the converged solution of the nonlinear SE problem.

3.7 Condition Analysis in the Examples 4 and 6

The examples using *condition analysis* described above are discussed further here. The issue of whether added measurements (e.g., 5 PMUs in Example 4 above) should be analyzed *one-at-a-time* or *all-at-once* was studied. Recall that Example 4 is the

case of five state measurements added at once. The addition of state measurements one-at-a-time is denoted as Example 6. Table 3.5 shows the effects of adding PMUs one-at-a-time predicting the change in condition number and singular distance. In the case of one-at-a-time addition of measurements, the gain matrix G after adding one measurement was used to identify the impact of the second added measurement. The subsequent gain matrix is used to find the impact of the third addition, and so on. The PMUs were added to buses in the following order: (1st) 32, (2nd) 30, (3rd) 31, (4th) 33, and (5th) 25.

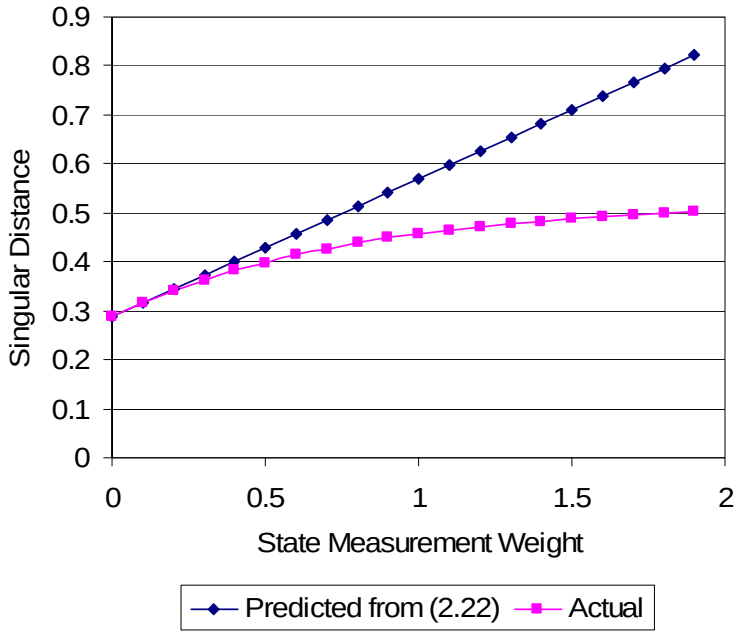

Figure 3.4 Impact of state measurement weight on singular distance using the IEEE 57 bus test bed (singular distance of H^tWH is depicted at the SE solution, Example 5)

Table 3.5 contains a comparison of predicted (P) versus actual (A) changes in the condition number and singular distance of the SE gain matrix G. Two cases are depicted. In the case of one-at-a-time design, five different ΔK_G and Δd values are tabulated for the sensitivity based predictions (P) entries in Table 3.5 are readily compared to actual (A) changes. The error due to the sensitivity-based approximations is assessed by observing the error depicted as $|P\text{-}A|$. Three observations are made:

- The error both in the ΔK_G and Δd, due to the sensitivity-based approximations generally decreases as measurements are added one-at-a-time.
- The improvement (i.e., decrease in ΔK_G and increase in Δd) decreases as measurements are sequentially added one-at-a-time.
- The errors $|P\text{-}A|$ for the one-at-a-time calculations are significantly less then the error for the five added at once calculations.

Table 3.5 Comparison of predicted values from (2.22, 2.23) to actual values (Examples 4 and 6)

		ΔK_G			Δd		
		P	*A*	|*P-A*|	*P*	*A*	|*P-A*|
One-at-a-time	1st	-17828	-13243	4585	0.2817	0.1673	0.1144
	2nd	- 8106	- 6182	1924	0.2501	0.1686	0.0815
	3rd	- 2970	- 1396	1574	0.1349	0.0569	0.078
	4th	- 956	- 483	473	0.0453	0.0221	0.0232
	5th	- 616	- 176	440	0.0305	0.0085	0.022
5 added at once		-29015	-21481	7534	1.1760	0.4233	0.7527

P = Predicted from (2.22, 2.23) *A = Actual value*

Figure 3.5(a) is a depiction of how eigenvalues of *G* migrate when measurements are added. Note that the smallest eigenvalue of *G* can "overtake" the second smallest eigenvalue as in Figure 3.5(b). It is possible to define a second condition number of *G*

$$K_G^{(2)} = \frac{\lambda_s}{\lambda_2} \tag{3.1}$$

and notice that (2.23) can be rewritten as

$$\Delta K_G^{(2)} = \frac{V_{ks}^2 - k_G^{(2)} V_{k2}^2}{\lambda_2 + V_{k2}^2 (\Delta h_k)^2} (\Delta h_k)^2 \tag{3.2}$$

Then it is desired to minimize some measure of K_G and $K_G^{(2)}$. For example:

- Minimize max $\{K_G, K_G^{(2)}\}$
- Minimize $K_G + \alpha K_G^{(2)}$

where α is a suitable constant, e.g., α = (0.1). A need for such a function has been observed as in the case of placing five PMUs all at once, Example 4. In Example 4, the eigenvalue migration depicted in Figure 3.5 (b) occurred.

3.8 Redundancy Analysis of the Example

The foregoing is an analysis of the placement and effectiveness of state measurements based on *condition indicators*. An improvement was seen in the condition number of the gain matrix, and improvement was observed in the accuracy of the state estimation. Another measure of improvement in state estimation relates to the *robustness* of the measurements. An indicator of robustness of a measurement set is the redundancy of measurements.

References [84, 85, 86] are a sampling of methods used to identify a critical measurement and critical sets (e.g., a critical measurement couple or a critical measurement triple). In reference [86], the redundancy is determined with respect to the *integer local redundancy* (i.e., the number of measurements needed to be removed to make the measurement a critical measurement) and the *non-integer redundancy* (i.e., a study of the sensitivity matrix coefficients) by studying the residual sensitivity matrix, *S,*

$$S = I - \left(HG^{-1}H^t W\right). \tag{3.3}$$

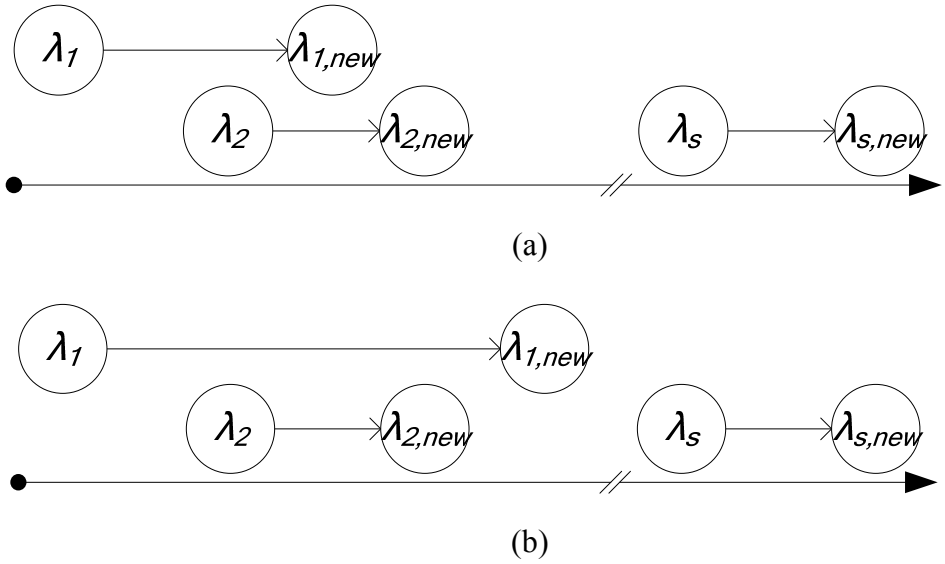

Figure 3.5 Pictorial of movement of eigenvalues upon addition of a measurement: (a) migration of eigenvalues as measurements are added, (b) example in which eigenvalue λ_1 'overtakes' λ_2

Local redundancy of a specific measurement is expressed as the number of measurements which have connection to a given measurement point [87]. Reference [88] categorizes the redundancy of a measurement as:

- *Not redundant* if it is a critical measurement;
- *Singly redundant* if it is a member of a critical measurement couple (two measurements are a critical couple if elimination of one makes the other critical);
- *Multiply redundant* if the measurement is not a critical or a singly redundant measurement.

To identify the critical measurements, the sensitivity matrix, *S,* is formed. When the diagonal element of the sensitivity matrix *S* is 0, the corresponding measurement is a critical measurement. According to [86], to obtain the local redundancy, the residual correlation matrix is formed

$$K = diag(S)^{-1/2}(S)diag(S)^{-1/2}. \tag{3.4}$$

where '*diag*' refers to a diagonal matrix of entries S_{ii}. The largest off-diagonal element in the i^{th} row corresponds to the largest correlated measurement of measurement *i*. The most correlated measurement of measurement *i* is eliminated until measurement *i* becomes non-redundant (i.e. the measurement being studied becomes a *critical* measurement). Each of the measurement eliminations is counted as one local redundancy.

Using the foregoing redundancy evaluation, Table 3.6 shows the redundancy level of the IEEE 57 bus test bed with the given measurements set. It is observed that four critical measurements are identified in Example 2 (i.e., no phase measurements added); the addition of one phase measurement at bus 33 in Example 3 eliminates two critical

measurements and the addition of phasor measurements at buses 25, 30, 31, 32, 33 in Example 4 eliminates all critical measurements identified in Example 2.

Inspection of Table 3.6 indicates that in Example 2, all four indicated measurements are critical. In Example 3, the condition analysis identified bus 33 as a desired location of a state measurement. This identification is consistent with the appearance of the redundancy index of two for lines that terminate at bus 33. That is, redundancy analysis shows that if a measurement is placed in line 32-22, redundancy increases. In the Example 4 column of Table 3.6, it is noted that addition of five PMU identified using condition analysis further improves the measurement redundancy (note the appearance of redundancy two and redundancy 3 in Example 4 in Table 3.6). These remarks indicate the consistency between redundancy analysis and condition analysis. For all cases studied, the analysis of condition indicators is found to be consistent with redundancy analysis, and for this reason, condition analysis is offered as an additional tool in the assessment of placement of measurements.

Table 3.6 Redundancy indices for the IEEE 57 bus test bed

Line flow measurements	Example 2 No PMUs	Example 3 1 PMU	Example 4 5 PMUs
P32 33	1	2	2
Q32 33	1	2	2
P37 39	1	1	3
Q37 39	1	1	3

P = Active power measurement *Q = Reactive power measurement*

3.9 Conclusions

It appears it is possible to "engineer" the eigenspectrum of G (sensor placement in H) using linearized analysis. An innovative way to place measurements using condition indicators is presented. The placing of measurements by optimizing condition indicators is recommended to be used in conjunction with other measurement placement strategies (e.g., observability analysis or contingency analysis). An illustration was given showing placement of bus voltage phase measurements with regard to impacts on the condition indicators. The sensitivity-based formulas for condition indicators give an assessment of the effects of added measurements on the eigenvalues of the gain matrix. The accuracy of the sensitivity-based calculations of condition indicators decreases as the number of measurements increases. Placement of added state measurements using a condition indicator philosophy appears to be consistent with placement using redundancy analysis.

The condition analysis concepts above are proposed for the following applications:

- Application to an existing system in which the SE has a valid G matrix. The system is under study for added measurements

- The condition analysis is a tool used in connection with other placement techniques. It is assumed that the system is observable.
- A "sanity check" for proposed measurement placement.

In these applications, it was found that the impact of measurement noise on state estimation is attenuated. Also, it is found that the condition analysis of the placement of the proposed measurements agrees with redundancy analysis.

- The error both in the ΔK_G and Δd, due to the sensitivity-based approximations generally decreases as measurements are added one-at-a-time.
- The improvement (i.e., decrease in ΔK_G and increase in Δd) decreases as measurements are sequentially added one-at-a-time.
- The errors $|P\text{-}A|$ for the one-at-a-time calculations are significantly less then the error for the five added at once calculations

4 The Measurement Outage Table

4.1 The Construction of a Measurement Outage Table

A "measurement outage table" is a tabulation of possible failure status scenarios versus their probability of occurrence. The measurement outage table is analogous to the generation capacity outage tables described in [89]. In the example capacity outage table seen in Table 4.1, states of the availability of generators versus the probability of occurrence of those states are tabulated. The capacity outage table is used in various applications in generation sufficiency analysis such as calculation of the loss of load probability, the calculation of expected available generation, and then calculation of generating margin [89 – 92].

Table 4.1Sample capacity outage table
taken directly from [84]

Unit 1 (5 MW)	*Unit 2 (3 MW)*	*Unit 3 (3 MW)*	*Capacity out of service (MW)*	*Individual probability*	*Cumulative probability*
1	1	1	0	0.941192	1.000000
1	1	0	3	0.019208	0.058808
1	0	1	3	0.019208	0.039600
0	1	1	5	0.019208	0.020392
1	0	0	6	0.000392	0.001184
0	1	0	8	0.000392	0.000792
0	0	1	8	0.000392	0.000400
0	0	0	11	0.000008	0.000008

Status 1 = in service
Status 0 = out of service

The measurement outage table uses the probability of a measurement failure. Table 4.2 is the proposed measurement outage table from Rice [93,94]. Rows of Table 4.2 correspond to a specific measurement failure. The measurement outage table is offered as a potential tool to analyze state estimation sensory impacts. For example, using the right most columns of Table 4.2, it is possible to statistically evaluate the condition indicators. In Table 4.2, q_i is the sensory outage rate of sensor i and π_i is used at the "reciprocal" of q_i,

$$\pi_i = 1 - q_i.$$

Note that π_i is the probability of measurement i being in service. The individual probability of the state occurring is p_s and P_s is the cumulative probability, (i.e. the sum of all rows prior and including row s),

$$P_s = \sum_{i=1}^{s} p_i = P_{s-1} + p_s .$$

It is conjectured that it is possible to identify where a phasor measurement can be placed to increase the robustness of the state estimator design, (i.e., the entire system is still observable after a measurement failure). The performance indicators used in the table should not only detect if a measurement outage produces an unobservable island, but

should also detect how "well conditioned" the process matrix, H, is, and the impact of measurement failure on state estimator expected error.

Table 4.2 A measurement outage table

		Sensor Outage State							Individual Probability	Cumulative Probability	State Estimator Performance		
	State	1	2	3	4	…	m-1	m	(p_s)	(P_s)	K_G	λ_1	f
1sensor failure	1	1	1	1	1	…	1	0	(a)	P_1	The state estimation performance indicators might include: expected condition number, singular distance, and scaling factor.		
	2	1	1	1	1		0	1	(b)	$P_1 + P_2$			
	…	…					…		…	…			
	m-1	1	0	1	1		1	1	…	…			
	m	0	1	1	1	…	1	1	(c)	$\sum_{i=1}^{m} P_i$			
2 sensors failure	m+1	1	1	1	1	…	0	0	(d)	$\sum_{i=1}^{m+1} P_i$			
	…	…					…		…	…			
	(e)	0	0	1	1	…	1	1	(f)	$\sum_{i=1}^{m+\frac{1}{2}m(m-1)} P_i$			
for "N-3," "N-4," … cases													

(a) $\left(\prod_{i=1}^{m-1}\pi_i\right)q_m = P_1$ (b) $\left(\prod_{\substack{i=1\\ i\neq m-1}}^{m}\pi_i\right)q_{m-1} = P_2$ (c) $\left(\prod_{i=2}^{m}\pi_i\right)q_2 = P_m$

(d) $\left(\prod_{i=1}^{m-2}\pi_i\right)q_m q_{m-1} = P_{m+1}$ (e) $m + \frac{m(m-1)}{2}$ (f) $\left(\prod_{i=3}^{m}\pi_i\right)q_1 q_2 = P_{m+\frac{1}{2}m(m-1)}$

4.2 Sensor Outage Rate

The forced outage rate of generators is documented by [92, 95-96]. However in the literature little appears relating to sensor outages. This section contains a discussion about calculating sensor outage rates used in the measurement outage table.

A failure curve is formed by a piecewise function,

$$p(t) = \begin{cases} C_0 - C_1 t + \lambda & 0 \le t \le T_1 \\ \lambda t & T_1 < t \le T_2 \\ C_2(t - T_2) + \lambda & T_2 < t \end{cases},$$

or series of Weibull functions

$$p(t) = \underbrace{ab(at)^{b-1}}_{Weibull\_1} + \underbrace{\left(\frac{a}{b}\right)(at)^{(1/b)-1}}_{Weibull\_2}.$$

Both functions resemble a bathtub. The probability density function is broken into three parts. The large percent failure in the time from 0 to T_1 is due to defective products. This interval may be termed representative of "infant mortality." Time T_2 is the predicted end

of life of the asset. A low percent of failures can be observed from T_1 to T_2. Time beyond T_2 is after predicted life of the product. Figure 4.1 is a probability density function of a Weibull distribution. The dotted line is the piecewise function

$$p(t) = \begin{cases} 0.2 - 0.114t + 0.12 & 0 \le t \le 1.75 \\ 0.12 & 1.75 < t \le 11.5 \\ 0.123(t - 11.5) + 0.12 & 11.5 < t \end{cases}.$$

The solid line is the continuous function of two Weibull functions

$$p(t) = \underbrace{0.065(15)(0.065t)^{15-1}}_{Weibull\_1} + \underbrace{\left(\frac{0.065}{15}\right)(0.065t)^{(1/15)-1}}_{Weibull\_2}.$$

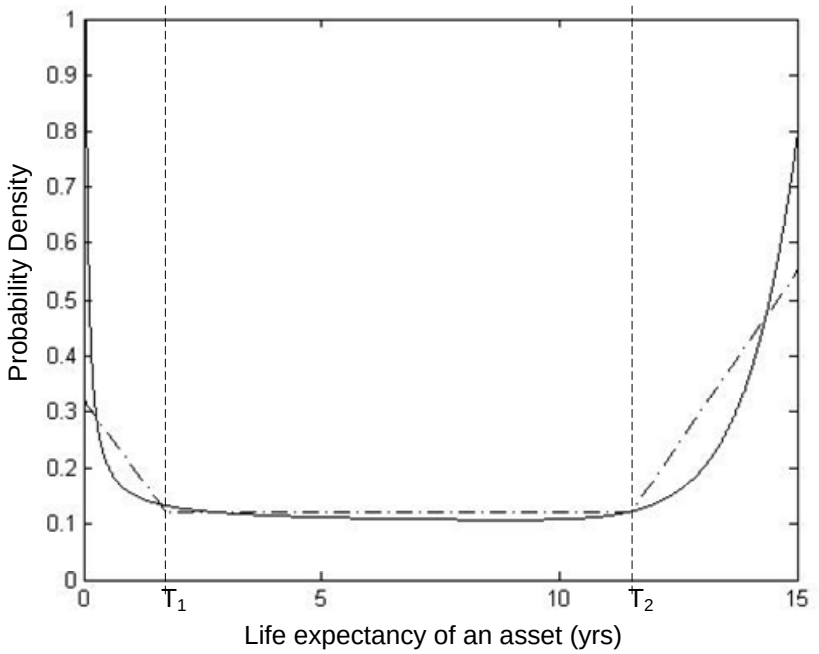

Figure 4.1 Probability density piecewise (dotted line) and continuous (solid line) Weibull models failure rates

The Canadian Electrical Association has a database of most equipment ("assets") failures in Canada since at least 1988. Reference [98] contains a summary of the Canadian Electrical Association benchmarking report for equipment failure from 1988 to 1992. The data in [98] will be used in determining a sensor outage rate to be used in a measurement outage table. Table 4.3 is a summary of terminal related forced outages. Figure 4.1 is a plot of kilometer years and outages versus voltage class. Note the two largest voltage classes are the 100 – 149 kV and 200 – 299 kV and largest number of outages occurred in these two voltage classes. Figure 4.2 is a plot of mean and median repair time versus voltage class. Note the large difference between the mean and median, which infers a small number of outages that may have taken much longer to repair than most outages. Table 4.3 is taken directly from the literature [98] and Figure 4.2 and Figure 4.3 are interpretations inferred from Table 4.3. Note that "km.a" in Table 4.3 refers to "kilometer-years."

Table 4.3 Summary of transmission line statistics for terminal-related sustained forced outages (taken directly from [98])

	Voltage Class (kV)					
Statistic	100 – 149	150 – 199	200 – 299	300 – 399	500 – 599	600 – 699
Kilometer years (km.a)	9,583	627	5,263	1,147	606	539
Number of outages	1,574	82	991	150	186	153
Total time (h)	16,352	619	8,618	3,889	8,887	3,949
Frequency (1/ km.a)	0.1642	0.1307	0.1883	0.1307	0.3069	0.2394
Mean duration (h)	10.4	7.0	8.7	25.9	47.8	25.8
Median duration (h)	0.05	0.30	0.22	0.37	0.64	1.70

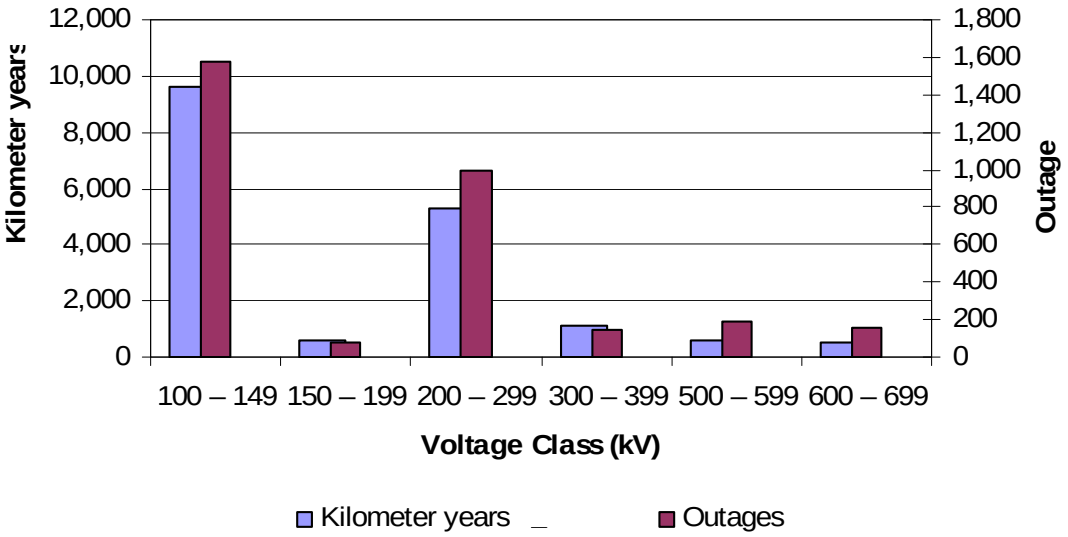

Figure 4.2 Number of outages and kilometer years versus voltage class for transmission lines in Canada

Reference [98] separates terminal related outages by type including: control and protection equipment, surge arrester, bus, disconnect, circuit switcher, current transformer (free standing), potential devices, wave traps, other, and unknown. Table 4.4 shows the percentage of terminal related line outages from subcomponent failure. Note, the large percentage of outages associated with unknown causes.

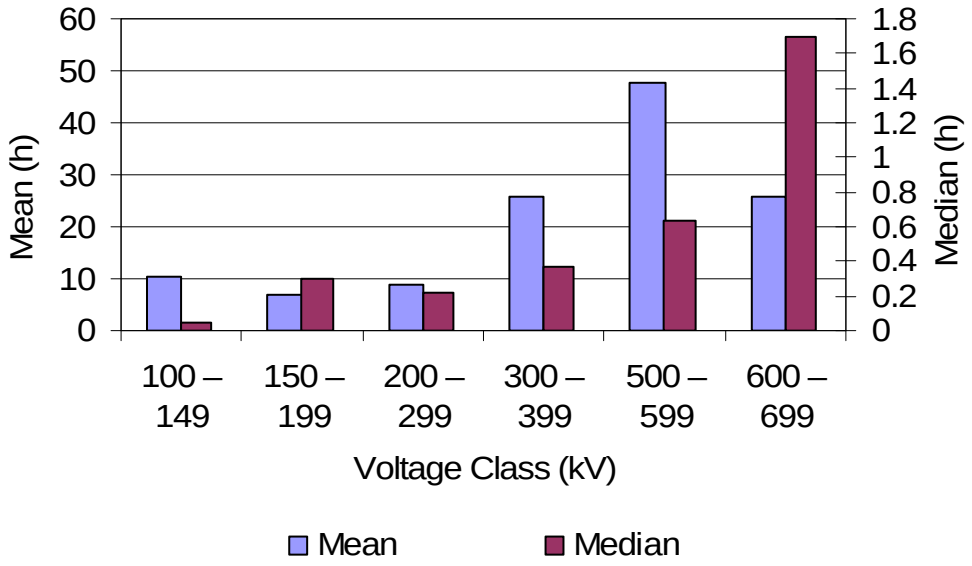

Figure 4.3 Hours of outage versus voltage class for electrical transmission system in Canada

Table 4.4 Percent of terminal related sorted by voltage class and subcomponent failure (created from [98])

	Voltage Class (kV)					
Cause	100 – 149	150 – 199	200 – 299	300 – 399	500 – 599	600 – 799
Control and protection equipment	42.02	26.66	58.05	42.69	53.24	38.55
Surge arrester	0.85	0	0.42	0	0	0.67
Bus	2.13	0	2.02	0.69	9.16	3.26
Disconnect	6.52	3.67	7.49	14.00	7.01	36.59
Circuit switcher	0.12	0	0.69	1.3	3.23	0.67
Current transformer (free standing)	0.3	0	0.69	0	6.45	1.96
Potential device	2.92	2.45	7.86	15.3	3.23	7.18
Wave traps	0	0	0	0.69	0.55	0
Other	5.79	1.22	5.26	3.98	5.38	8.48
Unknown	39.34	65.88	17.58	21.35	11.83	2.63

For the sensory outage rate used in the following section, only the statistics for the current transformers and potential devices are used. The statistics of control and protection equipment failures are not used because the control and protection equipment category includes failures in the mechanical workings of circuit breakers (e.g. leaks in the gas tanks). Since the end objective is to find a time-to-failure of voltage and current sensors, the circuit breaker data are omitted. For the IEEE 57 bus test bed system, an aggregate of all voltage classes in Table 4.4 will be used. Table 4.5 is the calculation of outages in the four year study.

Table 4.5 Subcomponent failure in the four year study

	Voltage class (kV)						
	100 - 150	150 - 199	200 - 299	300 - 399	500 - 599	600 - 799	Total
Number of potential devices outages	46	2	78	23	6	11	166
Number current transformer outages	5	0	7	0	12	3	27
Potential device outage (h)	2.3	0.6	17.16	8.51	3.84	18.7	51.11
Current transformer outage (h)	0.25	0	1.54	0	7.68	5.1	14.57

To determine the hours of outages the median was used instead of the mean due to disparity between the data. Note that the median is much smaller than the mean. The median was multiplied by the number of outages attributed to the subcomponent failure. The total hours of outage for potential devices is 51.11 hours and for current transformers is 14.57 hours for the four year study. By logic, the sensor outage rate for potential devices is $1.46\text{x}10^{-4}$ and for current transformers $4.16\text{x}10^{-5}$,

$$PT_{fail} = \frac{PT_{outage}}{StudyLength} = \frac{51.11h}{4yrs\left(\frac{365.25days}{1yr}\right)\left(\frac{24h}{1day}\right)} = \frac{51.11h}{35064h}$$

$$CT_{fail} = \frac{CT_{outage}}{StudyLength} = \frac{14.57h}{4yrs\left(\frac{365.25days}{1yr}\right)\left(\frac{24h}{1day}\right)} = \frac{14.57h}{35064h}.$$

The power measurements rely on the operative status of both the current transformers and potential devices. Thus power measurement failure rate is

$$PowerMeasure_{fail} = CT_{fail} \cup PT_{fail} = 1 - \left(\left(1 - prob\left(CT_{fail}\right)\right)\left(1 - prob\left(PT_{fail}\right)\right)\right).$$

Therefore the failure rate of power measurement sensors is $1.87\text{x}10^{-3}$.

4.3 IEEE 57 Bus Test Bed

A measurement outage tables were created for the IEEE 57 bus test bed in three examples:

- Example 7 - 0 PMUs
- Example 8 - 1 PMU
- Example 9 - 5 PMUs.

As described in Chapter 3 System 1, the IEEE 57 bus test bed system, will be used with a voltage measurement at all buses, real and reactive power flows of all transmission lines and ten pairs of real and reactive power injections. Each of the measurements were removed individually from the measurement set, creating a new set of measurements $z_{N\text{-}1}$. State estimator solved using $z_{N\text{-}1}$. Then using the final iteration gain matrix of the state estimator the condition number, singular distance, and scaling factor were calculated. In Examples 7 - 9, in the *N-1* cases no cases were found to make the gain matrix singular (i.e. the condition number equal to zero). Table 4.6 is a sample of a measurement outage table for Example 7. The failure rate of the voltage phase and magnitude measurements use the potential device failure rate calculated in the prior section.

Table 4.6 was obtained from a calculation of K_G, d, and F using their definitions (2.15, 2.16, 2.17). It is also possible to calculate the expected K_G, d, and F. From Table 4.6,

$$E(K_G) = \frac{\sum_{i=0}^{237} (p_i)(K_G)_i}{P_{237}} = 36411.06$$

$$E(d) = \frac{\sum_{i=0}^{237} (p_i)(d)_i}{P_{237}} = 0.28814$$

$$E(F) = \frac{\sum_{i=0}^{237} (p_i)(F)_i}{P_{237}} = 10464.71.$$

These are "exact" expectations as obtained from full analysis of 238 gain matrices (each of which is 113 by 113). Note that P_{237} refers to the cumulative probability summed over the state 0, 1, 2, … , 237. The expectations can also be estimated from ΔK_G, Δd, and ΔF formulas (2.22, 2.23, 2.24). These estimates result in

$$E(K_G) = P_{237}(K_G)_0 + \sum_{i=1}^{237} (p_i)(\Delta K_G)_i = 36211.10$$

$$E(d) = P_{237}(d)_0 + \sum_{i=1}^{237} (p_i)(\Delta d)_i = 0.28932$$

$$E(F) = P_{237}(F)_0 + \sum_{i=1}^{237} (p_i)(\Delta F)_i = 10462.64.$$

The difference between the "exact" expected K_G and the estimated is 0.549%. The differences in d and F between the "exact" expected values and the estimated are 0.410% and 0.020% respectively.

Table 4.6 Samples of measurement outage table of IEEE 57 bus test bed with 0 PMUs, Example 7

State	Lost Measure-ment Location	Type	Failure Rate	Probability of State (p_s)	K_G	p_s*K_G	d	p_s*d	F	p_s*F
0	Base case no measurement lost			0.656706	36163.21	23748.6	0.289701	0.190248	10476.51	6879.989
1	1	Active Injection	0.001873	0.001232	35107.44	43.2529	0.288361	0.000355	10123.62	12.47247
2	2	Active Injection	0.001873	0.001232	35342.23	43.5422	0.289434	0.000357	10229.24	12.60259
3	3	Active Injection	0.001873	0.001232	35972.06	44.3182	0.289703	0.000357	10421.23	12.83913
…	…	…	…	…	…	…	…	…	…	…
18	25	Reactive Injec-tion	0.001873	0.001232	36356.6	44.7919	0.288278	0.000355	10480.81	12.91254
19	53	Reactive Injec-tion	0.001873	0.001232	36161.52	44.5516	0.28981	0.000357	10479.98	12.9115
20	18	Reactive Injec-tion	0.001873	0.001232	36163.22	44.5537	0.289696	0.000357	10476.34	12.90702
21	1	Active Flow	0.001873	0.001232	35567.17	43.8193	0.289694	0.000357	10303.6	12.6942
22	15	Active Flow	0.001873	0.001232	36179.75	44.574	0.289291	0.000356	10466.47	12.89486
…	…	…	…	…	…	…	…	…	…	…
179	75	Reactive Flow	0.001873	0.001232	36169.61	44.5615	0.289648	0.000357	10476.47	12.90718
180	77	Reactive Flow	0.001873	0.001232	36177.95	44.5718	0.289581	0.000357	10476.44	12.90715
181	1	Voltage Mag	0.001458	0.000959	36193.44	34.696	0.289509	0.000278	10478.33	10.04479
182	2	Voltage Mag	0.001458	0.000959	36193.45	34.696	0.289557	0.000278	10480.05	10.04645
183	3	Voltage Mag	0.001458	0.000959	36196.38	34.6988	0.289356	0.000277	10473.65	10.04031
…	…	…	…	…	…	…	…	…	…	…

Note: p_s = probability of state s

Table 4.7 is summary of the measurement outage tables completed in the illustrations. Only the *N-1* cases were performed (i.e. *N-1 sensors* are in service). That is, the *N-k*, $k \geq 2$ cases are deemed to be of low probability and these are omitted. Note the improvement in all of the condition indicators and in both extremes and expected values as the number of PMUs goes from zero to one to five. The main observations are:

- The system study had no critical measurements (i.e. none of N-1 cases studies resulted in gain matrix, *G*, being singular).
- Table 4.7 shows that largest condition number for a single measurement failure decreases significantly for the addition of a single PMU.
- The expected of condition number of the gain matrix, K_G, decreases linearly as voltage phase angle measurements are added.
- The linearized formulas for ΔK_G, Δd, and ΔF (2.22, 2.23, 2.24) estimate the expected values of the condition indicators within 1%.

Table 4.7 Summary of measurement outage tables for System 1

	Example 7: 0 PMUs	Example 8: 1 PMU	Example 9: 5 PMUs
Cumulative Probability	0.9331	0.9327	0.9310
Max (K_G)	90892	36163	27115
E(K_G)	36411.06	23019.91	14813.92
E(K_G) calculated using (2.23)	36211.10	22918.44	14680.10
Min (d)	0.115267	0.289701	0.386095
E (d)	0.28814	0.45493	0.70776
E(d) calculated using (2.22)	0.28932	0.45644	0.71221
Max (F)	10560.46	10558.34	10551.53
E (F)	10464.71	10462.98	10457.41
E(F) calculated using (2.24)	10462.63	10460.93	10455.73

4.4 Conclusions

The measurement outage table uses the probability of a measurement failure. This is analogous to the probability of loss of generation in a generation capacity outage table. The measurement outage table is offered as a potential tool to analyze state estimation sensory impacts. For example, it is possible to statistically evaluate the condition indicators. It is possible to identify where a phasor measurement can be placed to increase the robustness of the state estimator design, (i.e., the entire system is still observable after a measurement failure).

The maximum condition number in the gain matrix decreases substantially more for the first PMU added compared to the addition of the next four PMUs. The smallest singular distance in the measurement outage table increases significantly more for the addition of first PMU than the addition of the next four PMUs.

The main conclusions of this chapter are that it is possible to calculate the expected values of the condition indicators for the measurement outage table using the lin-

earized formulas (2.22, 2.22, 2.24), and that the addition of PMU measurements decreases expected condition numbers of the state estimator during failure scenarios. Assuming reasonable measurement failure rates, the expected condition number drops by a factor of nearly three for the addition of five PMUs.

5 Application of the State Estimation Conditional Analysis to a Utility Operated Electric System

5.1 Test Bed: A Utility Operated Electric System

System 2 is representative of a US power system in the southwest in summer 2005. Table 5.1 contains basic descriptions of System 2. This system is approximately 3 times the size of System 1. Appendix D contains the system data. This system does not lend itself to depiction on a printed page, but Figure 5.1 shows the 230 kV and 500 kV portions of the system alone. Figure 5.1 is a conceptual drawing of the electrical connections of System 2 to display of complexity of the system. The entire system contains buses in the voltage classes 69 kV – 500 kV.

Table 5.1 Summary of System 2 parameters

Number of Buses	180
Number of Transmission Lines	254
Number of States	359
Number of Measurements	748

5.2 Impact of Adding PMUs to the Utility Operated Electric System: Example 10

In Example 10 a study the impact of adding PMUs to test System 2 is examined. The objectives of the study include the impact of the PMUs on condition indicators. In Example 10, the measurements are created from a power flow performed on System 2. The locations of active and reactive power measurements and voltage magnitude measurements are from a local utility. The voltage phase angle measurements are from the solved power flow.

The condition number of gain matrix for final iteration of state estimation for System 2 is 6.456×10^{10}. The condition number of the gain matrix is this size due to the scale difference of branch impedances. The system has branches that have impedances from 1×10^{-5} to 0.4787 per unit on a 100 MVA base. The singular distance is 1.267 and the scaling factor is 8.182×10^{10}. The number of actual buses in System 2 is 150 and 30 buses are virtual buses for sectionalized lines.

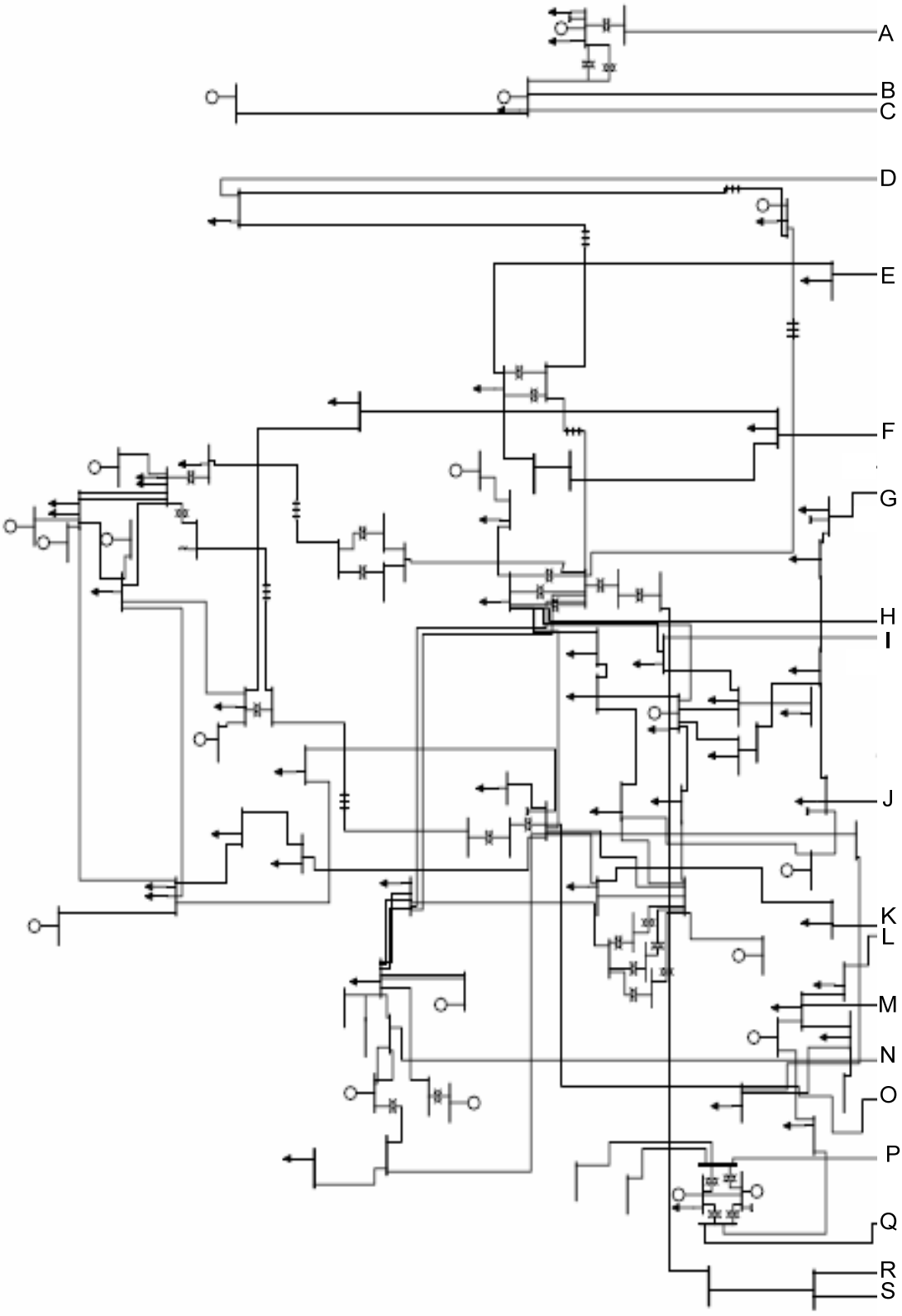

Figure 5.1a East side of the 230 – 500 kV portions of test System 2

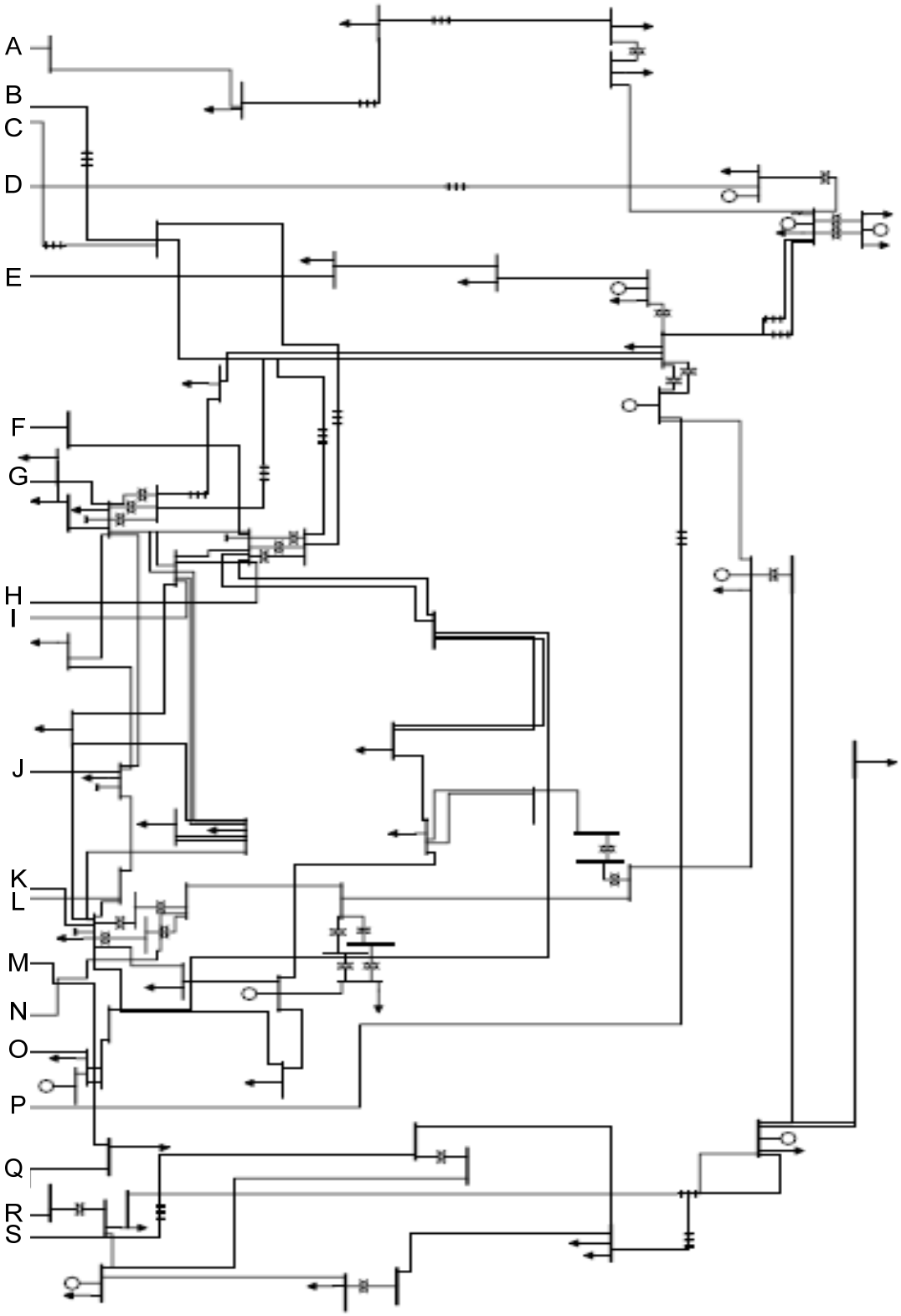

Figure 5.1b West side of the 230 – 500 kV portions of test System 2

Figure 5.2 depicts the condition number of G as the PMUs are added one at a time to decrease the gain matrix as described by (2.23). A quadratic trend line is added to Figure 5.2 to show the behavior of K_G with number of added PMUs. In Figure 5.3 the predicted change in condition number of the gain matrix is plotted. Equation 2.23 is used to predict the change in the singular distance of the gain matrix for each PMU measurement added. Note, that

$$\Delta K_G = \frac{V_{ks}^2 - K_G V_{k1}^2}{\lambda_1 + V_{k1}^2 (\Delta h_{k1})^2} (\Delta h_{k1})^2$$

$$\Delta K_G = \sum_{k=0}^{150} \frac{V_{ks}^2 - K_G V_{k1}^2}{\lambda_1 + V_{k1}^2 (\Delta h_{k1})^2} (\Delta h_{k1})^2$$

$$\Delta K_G = -8.26 x 10^9 .$$

This prediction can be compared to the change in condition number of the gain matrix observed in Figure 5.2, namely -7.56 x 10^9. The slope of the trend line of Figure 5.2 is quadratic and the slope of the Figure 5.3 is linear. Thus, these observations show the relationship between predicted and calculated (actual) change in condition number of the gain matrix.

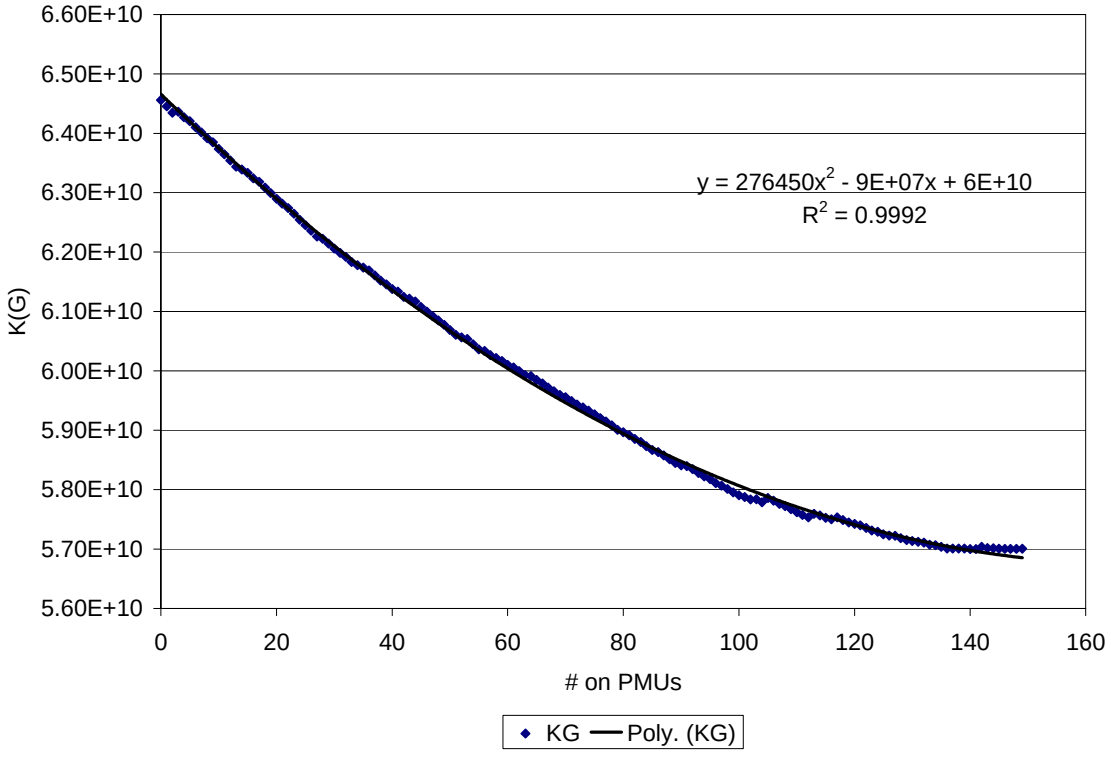

Figure 5.2 Condition number of the solved gain matrix for System 2 as PMUs are added (Example 10)

The singular distance of the gain matrix, d, is plotted versus the addition of measurements from PMUs in Figure 5.4. The trend line is quadratic with high component with a linear coefficient. In Figure 5.5 the predicted change in singular distance is plotted. Equation 2.22 is used to predict the change in the singular distance of the gain matrix for each PMU measurement added. Note, that

$$\Delta d = V_{k1}^2 \left(\Delta h_{k1}\right)^2$$

$$\Delta d = \sum_{k=1}^{150} V_{k1}^2 \left(\Delta h_{k1}\right)^2$$

$$\Delta d = 0.196 .$$

This prediction can be compared to the change in d observed in Figure 5.4. The change in d from zero PMUs in the system to 150 PMUs in Example 10 is 0.185. The slope of the trend line of Figure 5.4 is quadratic and the slope of the characteristic in Figure 5.5 is linear. Thus, these observations show the relationship between predicted and calculated (actual) change in d.

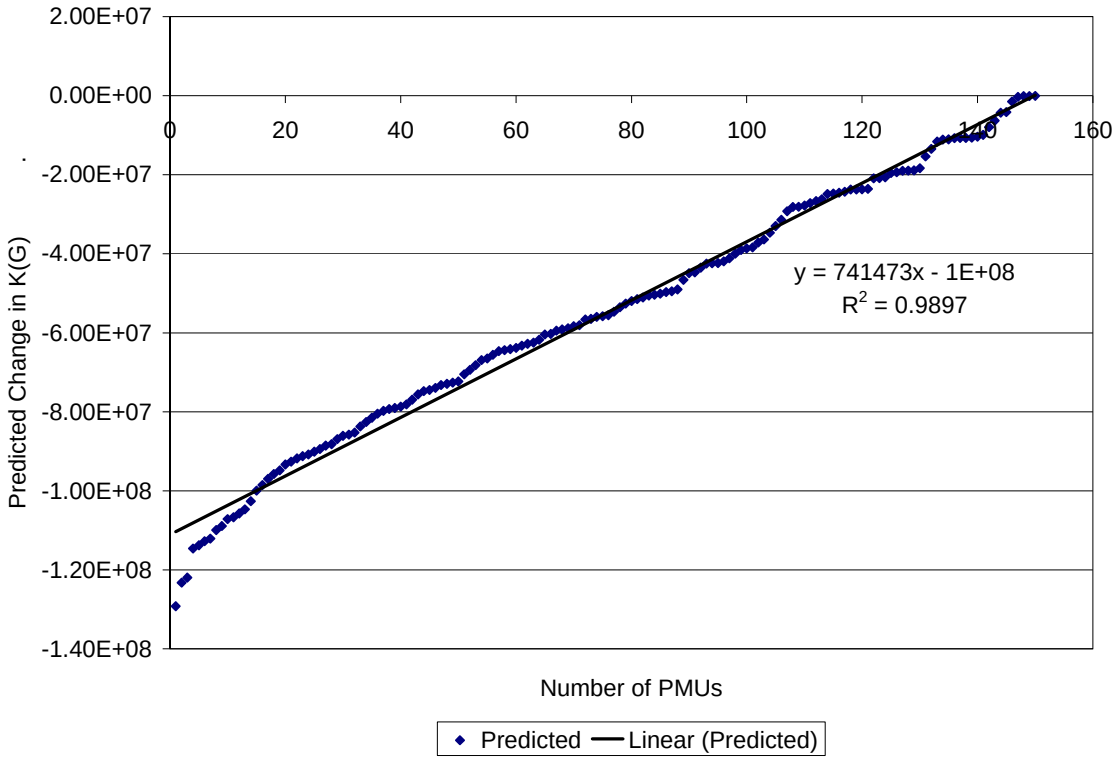

Figure 5.3 Predicted change in the gain matrix of the System 2 using (2.23) for the addition of PMUs (Example 10)

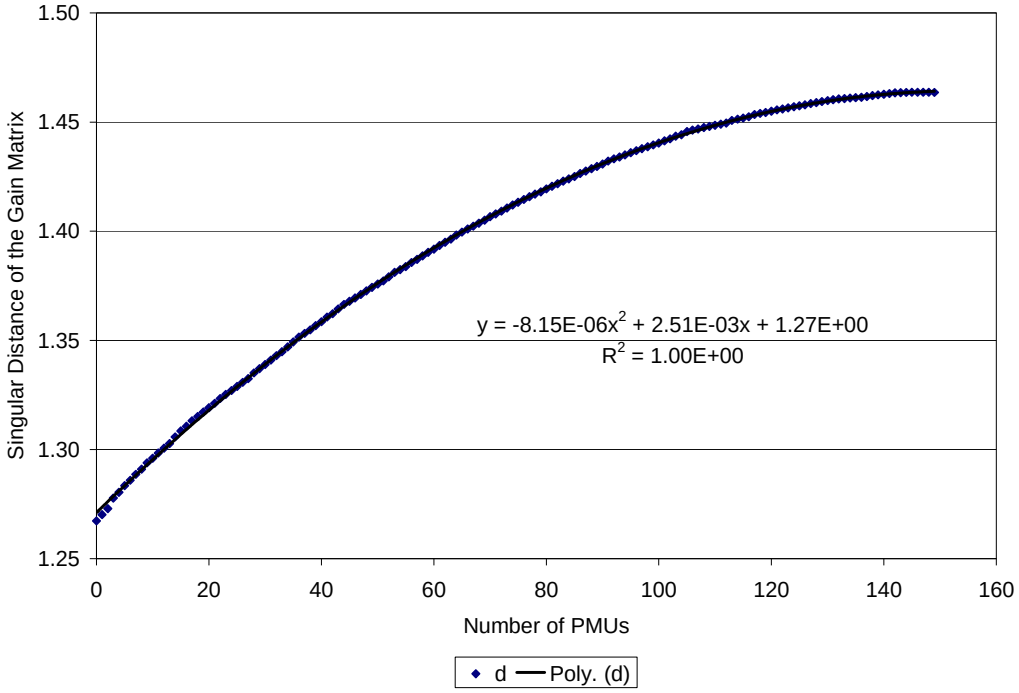

Figure 5.4 Singular distance of the gain matrix of System 2 as PMUs are added one at a time (Example 10)

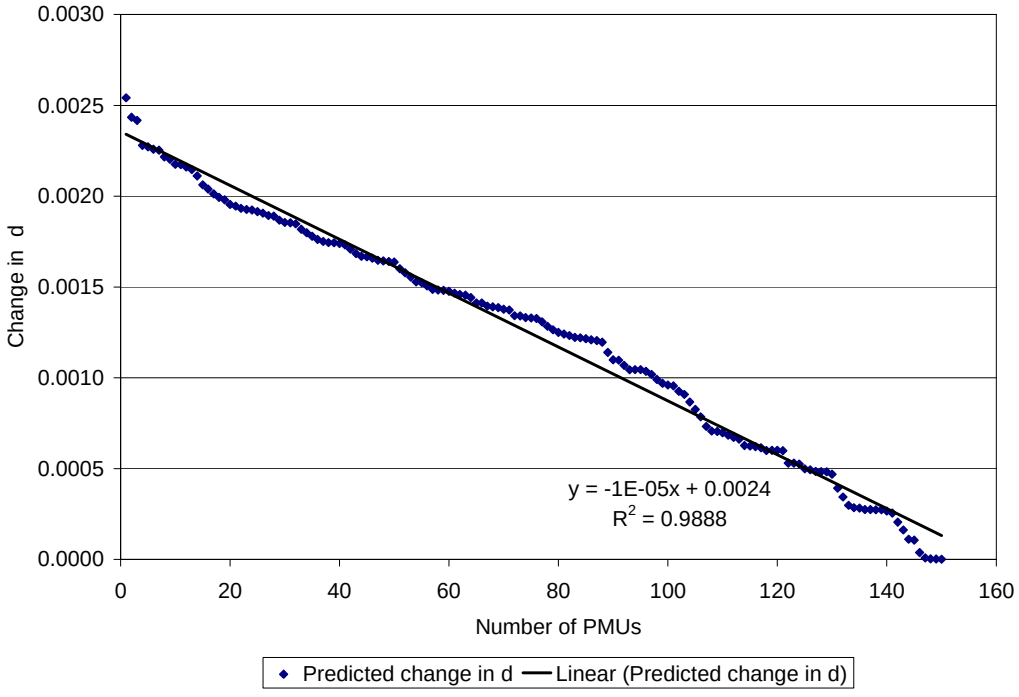

Figure 5.5 The predicted change using (2.21) in singular distance of the gain matrix for System 2 as PMUs are added one at a time (Example 10)

5.3 Impact on State Estimation of Utility Owned System by Addition of PMUs

System 2 is tested using pseudorandom Gaussian distributed noise inserted in the power and voltage magnitude measurements at levels of 5%, 10%, and 15%. The PMU measurements are modeled with 0.5% and 1% noise. The state estimator solves 1,000 trials each with 0, 15, 30, 45, 60, 75, 90, 105, 120, 135, and 150 PMUs. The PMUs are located using the ranking done as described in Section 5.2. The PMUs are added in the order of rank. Table 5.2 is the organization of Examples 11 - 16.

Table 5.2 Summary of examples of SE simulations performed with System 2

SCADA Noise Level	PMU Noise Level	
	0.5%	1.0%
5%	Example 11	Example 12
10%	Example 13	Example 14
15%	Example 15	Example 16

5.4 Results of Example 12

Examples 12 and 15 are chosen to for illustration below. The results from Example 11 – 16 are best presented graphically. For purposes of terminology of the graphical results, note that the subsequent figures are labeled:

- *Maximum voltage angle error* is the largest absolute difference between the voltage phase angle from the solved power flown and estimated voltage phase angle from the converged state estimator.
- *RMS voltage angle error* is the root mean square of the difference between all voltage phase angles estimates and that of the power flow.
- *Maximum voltage magnitude error* is the largest absolute difference between the voltage magnitude from the solved power flown and estimated voltage phase angle from the converged state estimator.
- *RMS voltage magnitude error* is the root mean square of the difference between all voltage magnitudes estimates and that of the power flow.

For clarity some definitions are given of the terminology used on the Figures 5.7 – 5.18. The data points are:

- *Max* data points are of the largest maximum error in all 1000 trials with a given number of PMUs, e.g. 15 PMUs.
- *Min* data points are the smallest maximum voltage phase angle error of the trials performed with a given number of PMUs.
- *Mean* data points are mean of all 1000 trials for a given number of PMUs.

The maximum bus voltage phase angle error, Ω, is evaluated (maximized) over the 150 buses in the system to create 1000 data points. Each of the 1000 data points corresponds to one trial in the Monte Carlo study. Thus $\Omega_1, \Omega_2, \ldots, \Omega_{1000}$ is an ensemble denoted $\{\Omega\}$. The maximum of $\{\Omega_i\}$, $i = 1, \ldots, 1000$ is plotted as "Max" in Figure 5.7. Further, the minimum of $\{\Omega_i\}$, $i = 1, \ldots, 1000$ is plotted as "Min." And the mean of the ensemble $\{\Omega_i\}$, $i = 1, \ldots, 1000$ is plotted as "Mean." This notation is depicted in Figure 5.6, where each circled row corresponds to a trial. The notation *e* stands for the error between bus voltage phase angle estimated and bus voltage phase angle from the power flow.

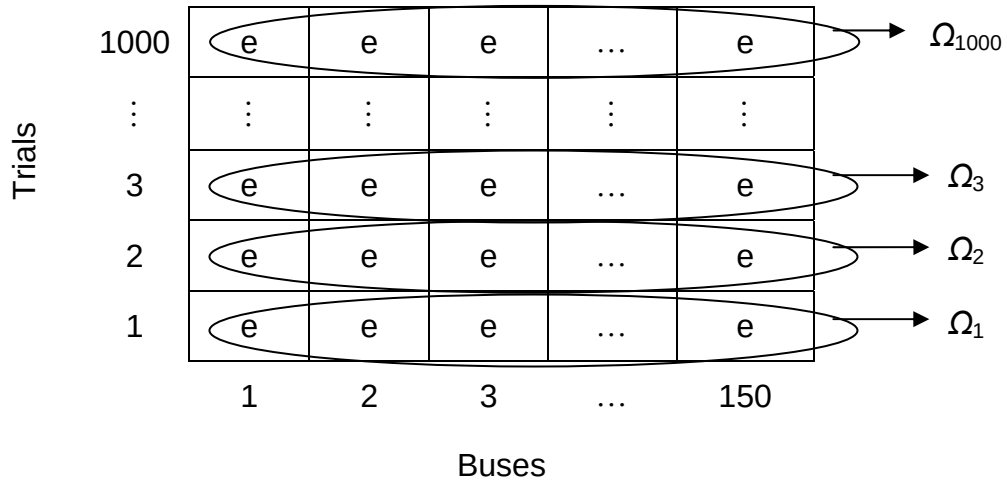

Figure 5.6 Notation used for the statistical study of maximum bus voltage phase angle error

Example 12 is a 1,000 Monte Carlo trials simulation with SCADA measurement noise level of 5% and 1% noise in PMU phase angle measurements. Figure 5.7 displays the maximum phase angle error of Example 12 as voltage phase angles are added. The *max* line decreases 0.093 degrees from 0 PMUs to 150 PMUs, and *min* line decreases 0.001 degrees from 0 PMUs to 150 PMUs. The *mean* of maximum voltage phase angle error decreases 0.032 degrees from 0 PMUs to 150 PMUs. Small changes are seen in voltage phase angle errors in Examples 11 – 16. In these Examples the weight of the PMU measurement is same as SCAD measurements. Example 17 presented in Appendix F is of the state estimation with weighting the PMU 10 times greater than the SCADA measurements. In Example 17, the mean of the maximum phase angle error is reduced by half by adding 135 PMUs.

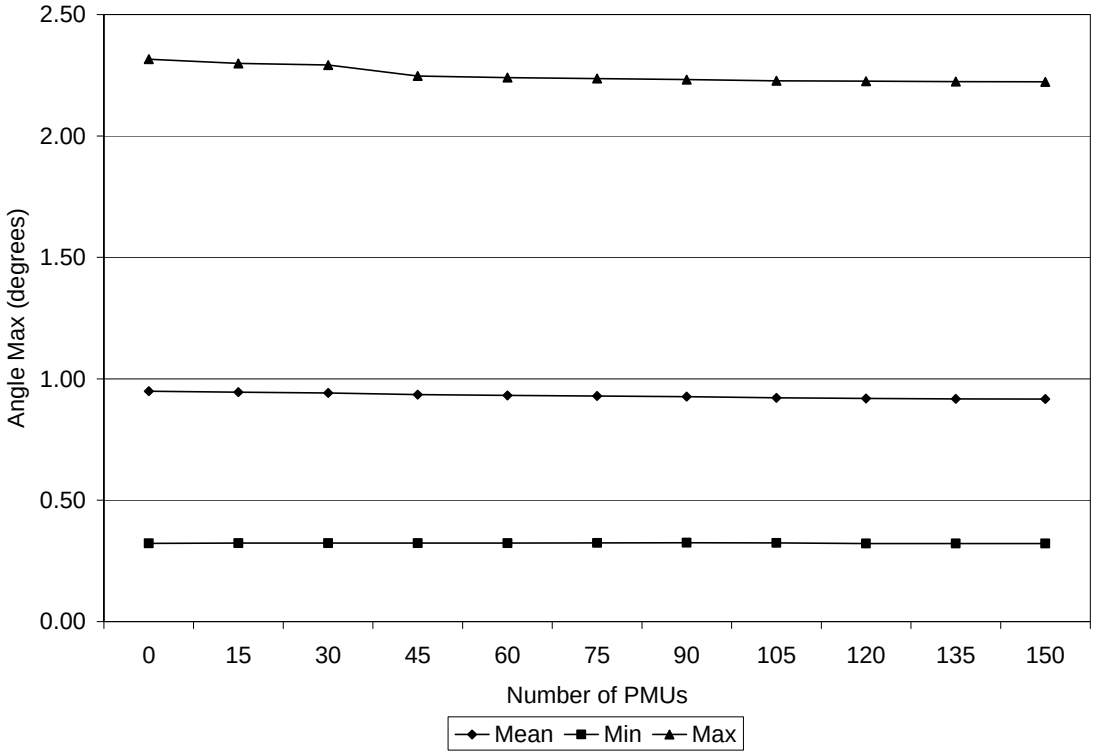

Figure 5.7 Maximum voltage angle error for SCADA noise 5% and PMU noise 1% on System 2 (Example 12)

Similar to the maximum phase angle error the RMS bus voltage phase angle error, Φ, is evaluated over the 150 buses in the system to create 1000 data points. Each of the 1000 data points correspond to one trial in the Monte Carlo study denoted $\{\Phi\}$. Thus Φ_1, Φ_2, ... , Φ_{1000} is an ensemble of RMS bus voltage phase angle error. The maximum of $\{\Phi_i\}$, $i = 1, \ldots, 1000$ is plotted as "Max" in Figure 5.9. Further, the minimum of $\{\Phi_i\}$, $i = 1, \ldots, 1000$ is plotted as "Min." And the mean of the ensemble $\{\Phi_i\}$, $i = 1, \ldots, 1000$ is plotted as "Mean."

Figure 5.8 depicts RMS phase angle error of Example 12. The *max* line decreases 0.013 degrees from 0 PMUs to 150 PMUs, and the *min* decreases 3.62×10^{-5} degrees from 0 PMUs to 150 PMUs. Note, the quadratic shape of the *max* voltage phase angles measurements. The *mean* of RMS voltage phase angle error in Example 12 decreases 0.002 degrees from 0 PMUs to 150 PMUs.

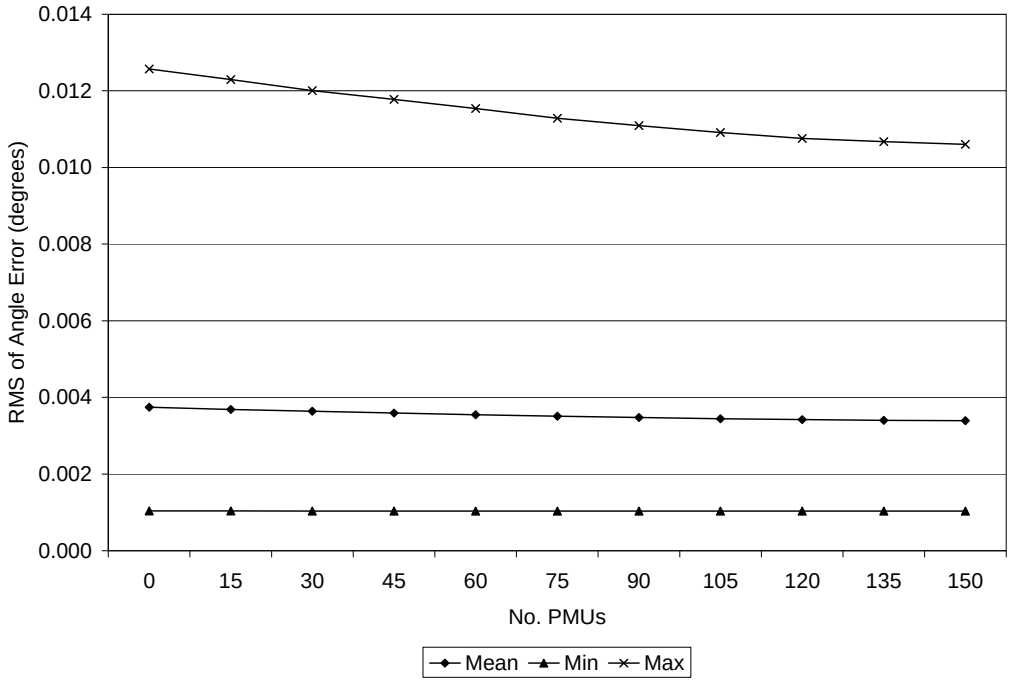

Figure 5.8 RMS voltage angle error for SCADA noise 5% and PMU noise 1% on System 2 (Example 12)

As in the case of maximum bus voltage phase angle error, Ω, the maximum voltage magnitude error is evaluated (maximized) over the 150 buses in the system to create 1000 data points. Each of the 1000 data points in the ensemble corresponds to one trial in the Monte Carlo study. The maximum of the ensemble is plotted as "Max" in Figure 5.9. Further, the minimum of the ensemble is plotted as "Min." And the mean of the ensemble is plotted as "Mean."

Figure 5.9 depicts the maximum voltage magnitude error of Example 12. The *max* decreases 7.2 x 10^{-4} p.u. from 0 PMUs to 150 PMUs. The *min* decreases 1.4 x 10^{-4} p.u. from 0 PMUs to 150 PMUs. The *mean* shows a decrease in maximum voltage magnitude error of 1.9 x 10^{-5} p.u. from 0 PMUs to the addition of 150 PMUs. Plots of *min*, *max* and *mean* for Example 12 show no significant changes as phase angle measurements are added. This is attributed to weak coupling between voltage phase angle state and voltage magnitude state in the state estimation algorithm.

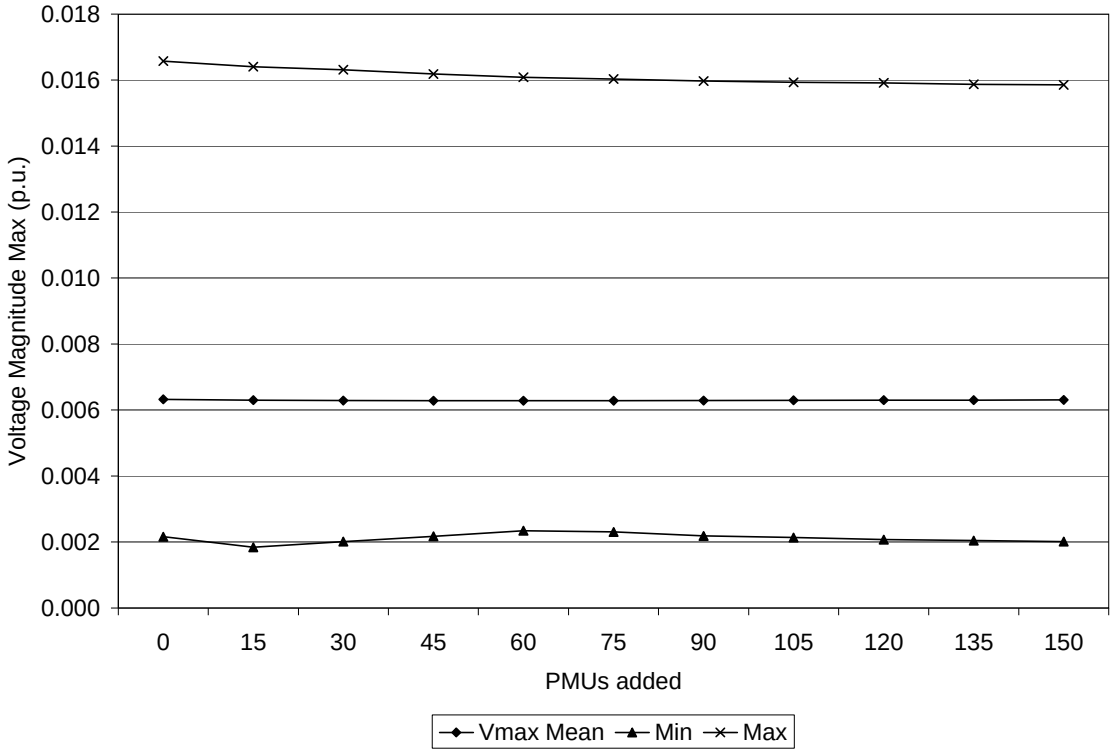

Figure 5.9 Maximum voltage magnitude error for SCADA noise 5% and PMU noise 1% on System 2 (Example 12)

The RMS bus voltage magnitude error is evaluated over the 150 buses in the system to create 1000 data points. Each of the 1000 data points in the ensemble corresponds to one trial in the Monte Carlo study. The maximum of ensemble is plotted as "Max" in Figure 5.10. Further the minimum of ensemble is plotted as "Min." And the mean of the ensemble is plotted as "Mean."

Figure 5.10 shows RMS voltage magnitude error of Example 12. The *max* line increases 3 x 10^{-5} p.u. from 0 PMUs to 150 PMUs, and the *min* line decreases 3 x 10^{-8} p.u. from 0 PMUs to the addition of 150 PMUs. The *mean* shows a decrease in RMS voltage magnitude error of 2 x 10^{-6} p.u. from 0 PMUs to the addition of 150 PMUs. The slight increase in error in both the *max* data and *mean* is due to the fact that the phase angle measurements can "push" the error away from those state estimates and into other states estimates, e.g. the error is "pushed" away from the voltage phase angle states to voltage magnitude states.

Figure 5.11 displays the condition number of the converged iteration gain matrix, K_G, of the state estimator with noise in the SCADA measurements of 5% and 1% noise in PMU phase angle measurements, Example 12. Note, mean of K_G in Example 12 is the same as in Example 10, System 2 with no measurement noise. Figure 5.12 depicts the singular distance of the converged iteration of the gain matrix, in Example 12. The plot of the *mean* of *d* for Example 12 agrees with Example 10.

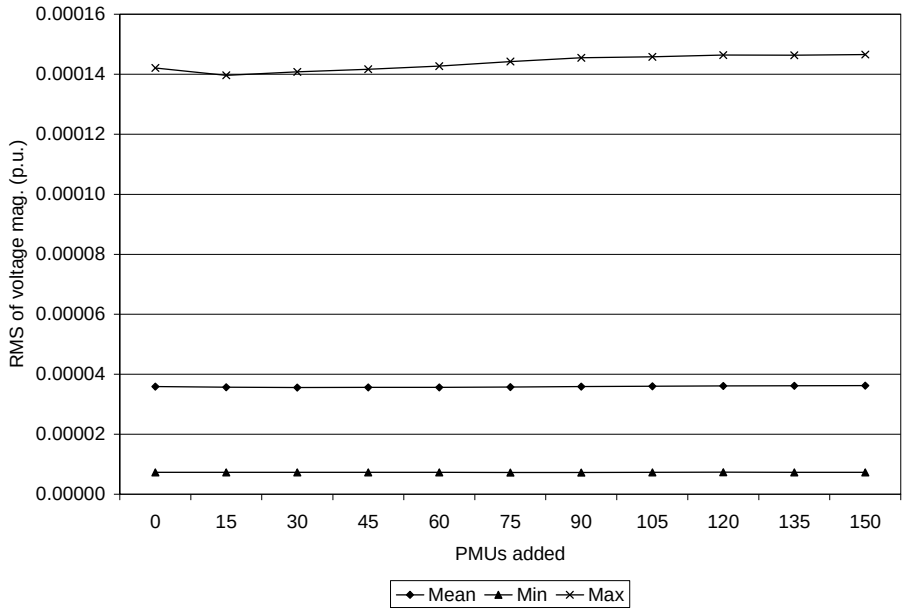

Figure 5.10 RMS voltage magnitude error for SCADA noise 5% and PMU noise 1% on System 2 (Example 12)

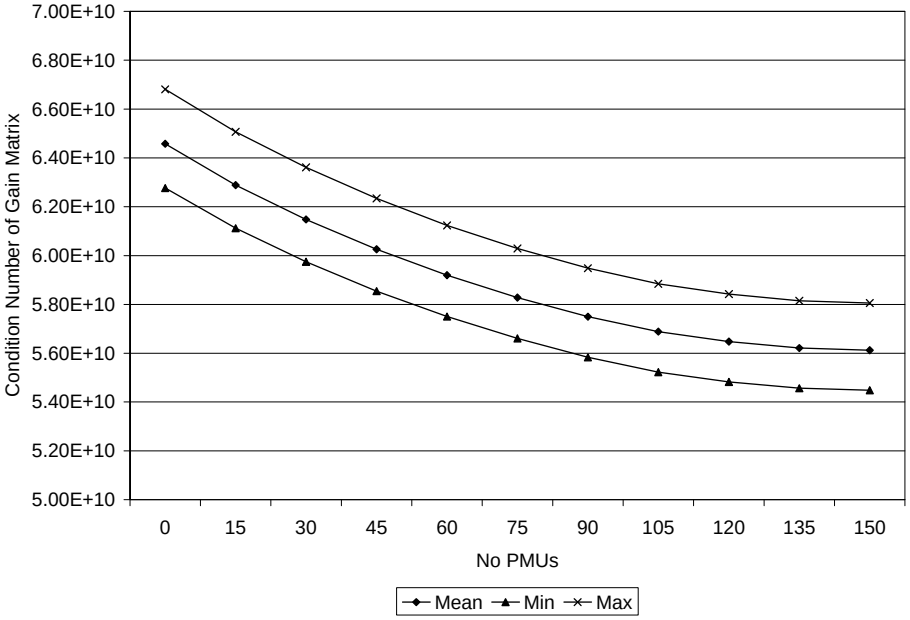

Figure 5.11 K_G for solved iteration of System 2 with SCADA noise 5% and PMU noise 1% (Example 12)

The full calculations shown above (i.e., 1000 Monte Carlo trials, each finding the K_G and d for the ~ 360 by 360 G matrix) are now compared to linear approximations found from (2.23), (2.22). In Example 10, the linear approximations are used and Figure 5.11 could be "overlaid" with Figure 5.2. Thus the general observation for Example 10 also applies to Example 12: the ΔK_G can be predicted using the simple linearized formulas and the result is accurate to within 2.2% of the actual change in K_G. Similarly, Δd can be predicted using the simple linearized formulas and the result is accurate to within 3.0% of the actual change in d.

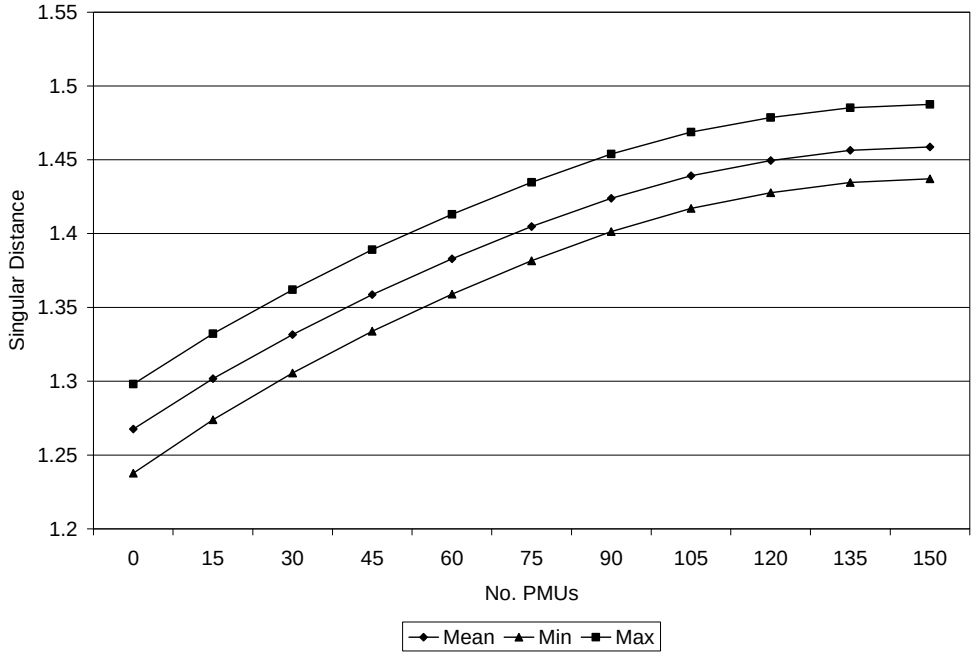

Figure 5.12 Parameter d for solved iteration of System 2 with SCADA noise 5% and PMU noise 1% (Example 12)

5.5 Results of Example 15

Example 15 is a 1,000 Monte Carlo trials simulation with SCADA measurement noise level of 15% and 0.5% noise in PMU voltage phase angle measurements. Figure 5.13 shows the maximum voltage phase angle error of Example 15. Table 5.2 is of the change in the *min, max,* and mean of maximum voltage phase angle in Example 15 as PMUs are added. Note that the changes in the *min, max,* and *mean* all decrease in nonlinear fashion. That is the decrease in the maximum voltage phase angle error is greater for the first 45 PMUs placed on the system than the last 45 PMUs. The decrease in *min* and *max* of maximum voltage phase angle as PMU measurements are added in Example 15 is an order of magnitude larger than that in Example 12, 1% PMU noise and 5% SCADA noise. The decrease in *mean* of maximum voltage phase angle in Example 15 is twice as observed in Example 12.

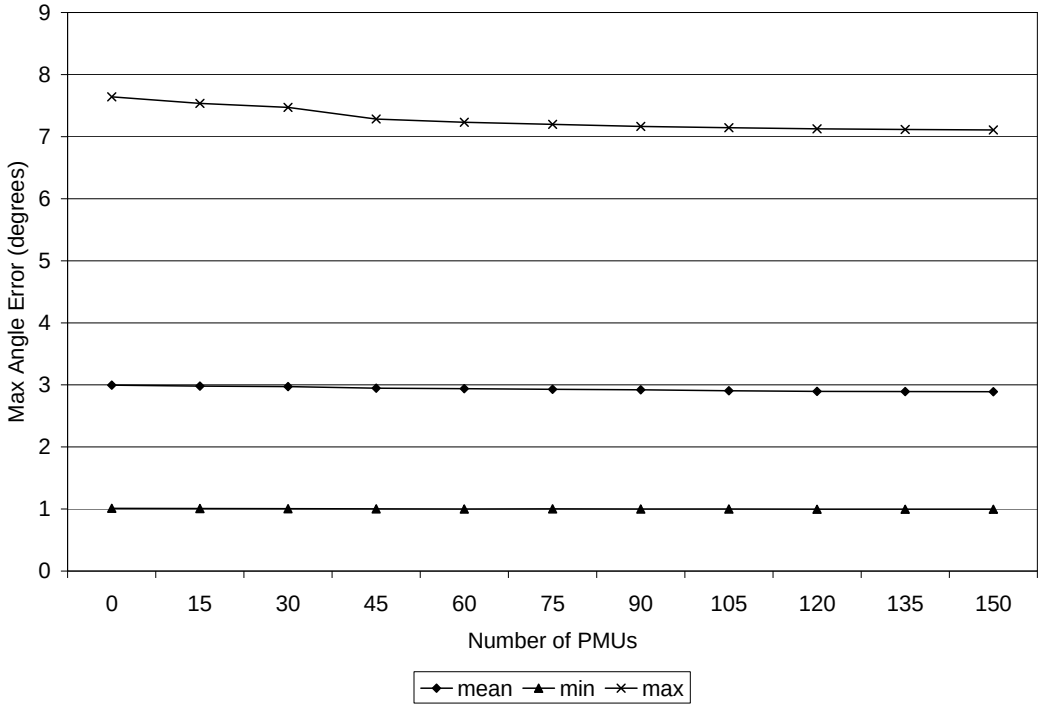

Figure 5.13 Maximum voltage angle error for SCADA noise 15% and PMU noise 0.5% on System 2 (Example 15)

Table 5.3 Change in min, max, and mean of maximum voltage phase angle for Example 15

PMUs Added	Δ Min	Δ Max	Δ Mean
0 to 45th PMU	0.00765°	0.35659°	0.04780°
45th PMU to 105th	0.00402°	0.14049°	0.04381°
105th PMU to 150th	0.00426°	0.03847°	0.01557°

Figure 5.14 depicts the RMS phase angle error Example 15, noise in the SCADA measurements of 15% and 0.5% noise in PMU phase angle measurements. The *max* decreases 0.035 degrees from 0 PMUs to 150 PMUs. Note, the quadratic shape of the *max* as voltage phase angles measurements are added to the measurement set. The *min* and *mean* show a slight decreases in RMS voltage phase angle error. Note that the change in the *min* and *mean* lines are also quadratic in shape. Thus the improvement in RMS voltage phase angle error is greater for the addition of first PMU than the subsequent PMU. Also note, the decrease in *max* and *mean* of RMS phase angle error in Example 15 is three times that in Example 12, 1% PMU noise and 5% SCADA noise.

Figure 5.15 shows the maximum voltage magnitude error in Example 15. The *max* decreases 3.1 x 10^{-4} p.u. from 0 PMUs to 150 PMUs. The *min* decreases 3.2 x 10^{-4} p.u. from 0 PMUs to 150 PMUs. The *mean* data shows a decrease in RMS voltage magnitude error of 1.9 x 10^{-4} p.u. from 0 PMUs to the addition of 150 PMUs. A decrease in *min*, *max*, and *mean* of maximum voltage magnitude error as 150 phase angle measurements are added only occurs in Examples 15 and 16, SCADA noise of 15%.

Figure 5.16 displays the RMS voltage magnitude error in Example 15, noise in the SCADA measurements of 15% and 0.5% noise in PMU phase angle measurements. The *max* increases linearly 2.4 x 10^{-4} p.u. from 0 PMUs to 150 PMUs. The *min* data increases 3.8 x 10^{-6} p.u. from 0 PMUs to 150 PMUs. This increase from start to end does not follow any trend line. The *mean* data shows a decrease in RMS voltage magnitude error of 1.1 x 10^{-5} p.u. from 0 PMUs to the addition of 150 PMUs. The mean line has negative slope until the addition of 75th PMU then the slope of the mean line is positive. That is the mean has a minimum point at 75th PMU addition. The slight increase in error the *max* data is due to the fact that the phase angle measurements can "push" the error away from those state estimates and into other states estimates.

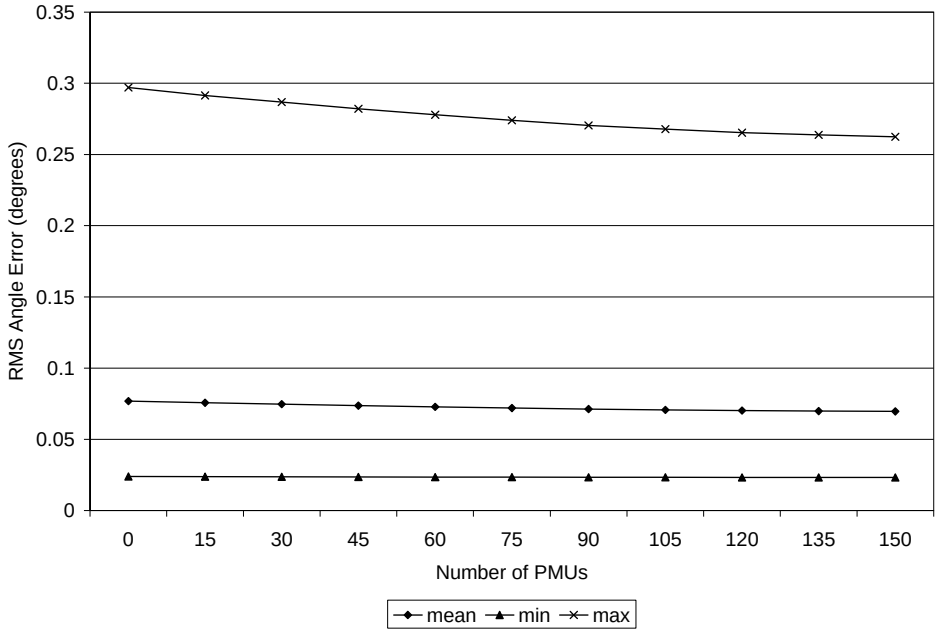

Figure 5.14 RMS voltage angle error for SCADA noise 15% and PMU noise 0.5% on System 2 (Example 15)

Figure 5.17 depicts of the condition number of the converged iteration gain matrix, K_G, of the state estimator with noise in the SCADA measurements of 15% and 0.5% noise in PMU phase angle measurements (Example 15). The plot of *mean* agrees K_G of Example 10, zero noise, and Example 12, 5% noise in SCADA and 1% noise in PMUs, to two places of accuracy. The *max* plot in Figure 5.19 is approximately 2 x 10^9 larger than previous *max* plots of K_G in Examples 11 - 14. Figure 5.19 is of the singular distance of the converged iteration of the gain matrix, *d*, in Example 15. The plots of *min*, *max*, and

mean data points agree with singular distance calculated in Example 10 and Example 12 to two places of accuracy.

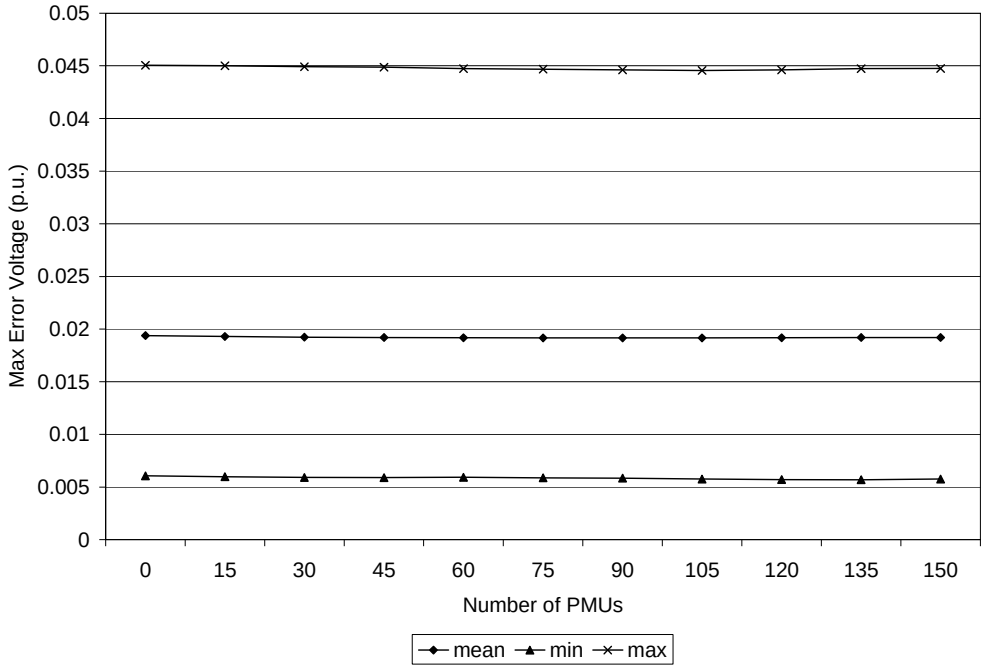

Figure 5.15 Maximum voltage magnitude error for SCADA noise 15% and PMU noise 0.5% on System 2 (Example 15)

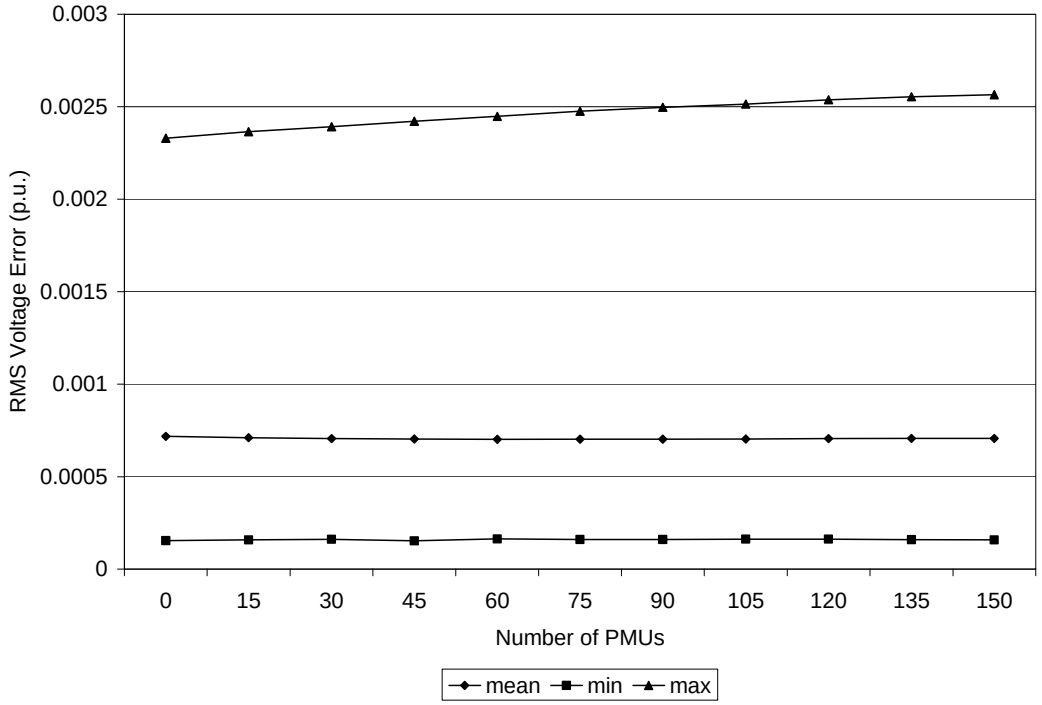

Figure 5.16 RMS voltage magnitude error for SCADA noise 15% and PMU noise 0.5% on System 2 (Example 15)

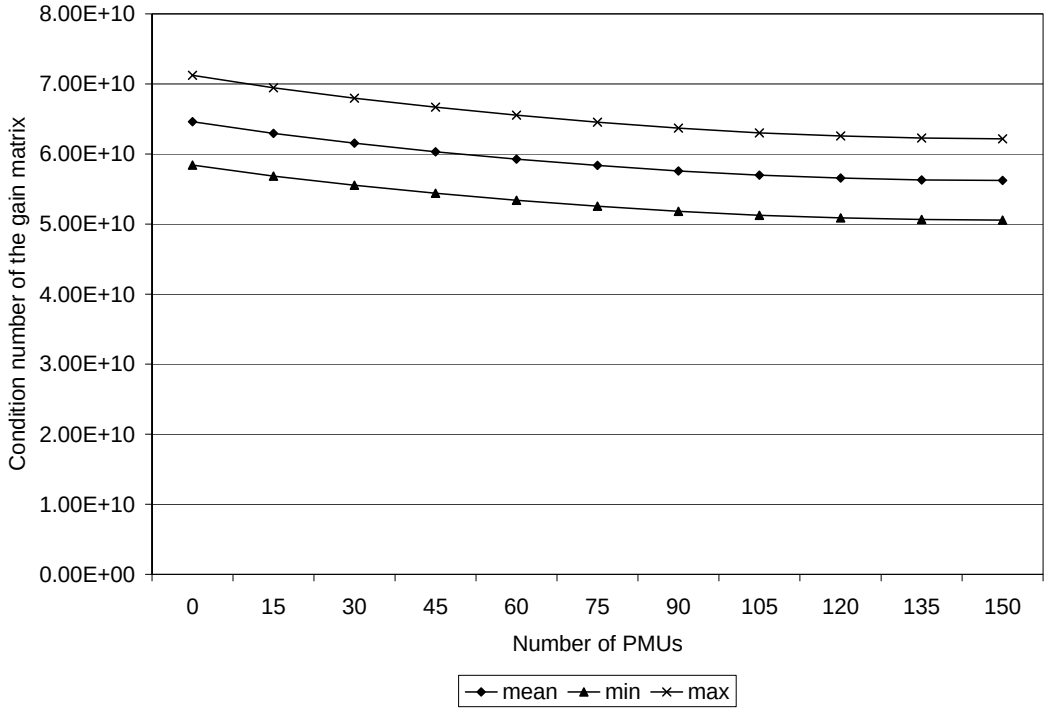

Figure 5.17 K_G for solved iteration of System 2 with SCADA noise 15% and PMU noise 0.5% (Example 15)

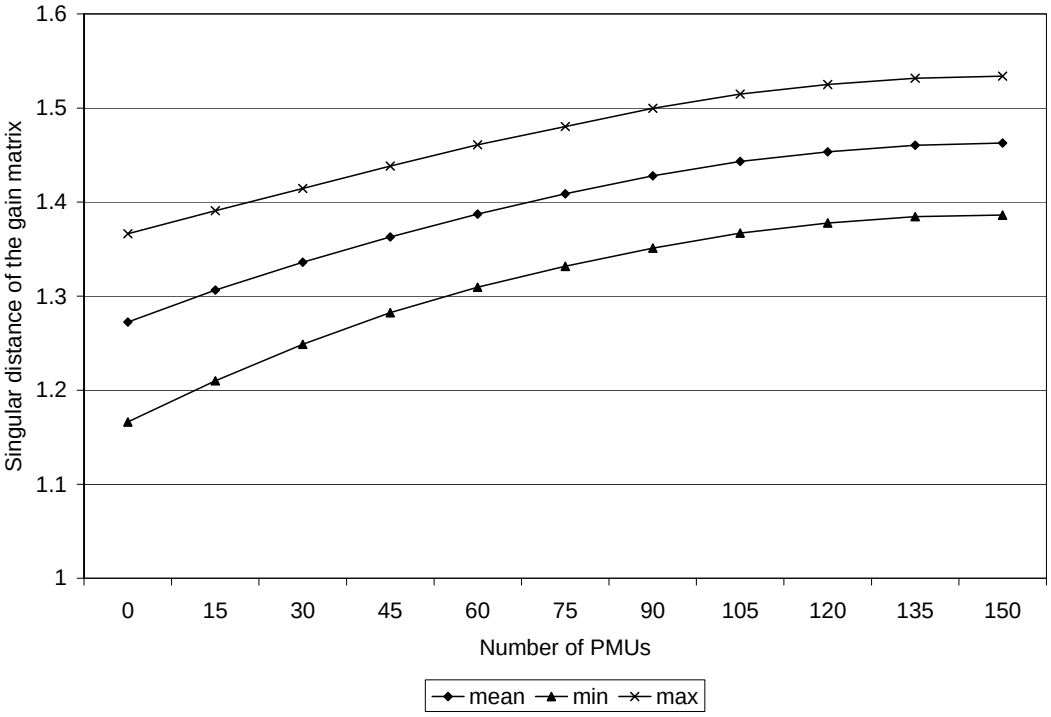

Figure 5.18 Parameter *d* of the solved iteration of System with SCADA noise 15% and PMU noise 0.5% (Example 15)

In Example 15, 1000 Monte Carlo trials are performed. For each trial the condition number and singular distance of the converged gain matrices (G is of the size 359 by 359) are calculated. The mean of K_G in Example 15 is the same as the K_G calculated in Example 10. The change in the mean of K_G is compared to the linear approximation of ΔK_G calculated in Example 10 using (2.23), and the simple linearized approximations of ΔK_G are within 1.8% of the observed change in K_G. Similarly, the change in d can be predicted using the linearized formula (2.22) and is found to be within 2.6% of the change observed in Example 15.

5.6 Summary of Examples 11 - 16

Examples 11, 13, 14, and 16 are shown in Appendix E. These examples are included in the summaries below. The improvement in mean of the voltage phase bus angle error increased as the noise level of the SCADA measurements increased for the addition of 150 PMU phase angle measurements. Table 5.4 shows the change in mean of the maximum phase angle. Note in Table 5.4, the change is not dependent on the noise level in PMU phase angle measurements. This could imply that the improvement is more from the direct measurement of the state, than the accuracy of the phase angle measurement. Table 5.5 shows the change in the error of the mean of RMS voltage phase angle error. The change in mean of RMS phase angle error increases in size as the SCADA noise levels increase, but changing the noise level in the voltage phase angle appears to have no effect on the improvement in the accuracy. The change in RMS error is an order of magnitude smaller than the change in maximum voltage phase angle.

Table 5.4 The decrease in the *mean* of *maximum voltage angle error* data from 0 PMUs to 150 PMUs in the measurements (Examples 11 – 16)

SCADA noise level	PMU noise level	
	0.5%	1.0%
5%	0.033°	0.032°
10%	0.065°	0.072°
15%	0.107°	0.107°

The improvement in mean of voltage magnitude error increased as the noise level of the SCADA measurements increased for the addition of 150 PMU measurements. Table 5.6 contains the change in mean of the maximum voltage magnitude. Note in Table 5.6 the mean of maximum voltage magnitude increases for noise level of 5% SCADA and 0.5% PMUs. This could imply that error was pushed from the voltage phase angle state to the voltage magnitude states, however, this phenomenon is only seen in this case and the change is insignificantly small.

Table 5.5 The decrease in the *mean* of *RMS voltage angle error* data from 0 PMUs to 150 PMUs in the measurements (Examples 11 – 16)

SCADA noise level	PMU noise level	
	0.5%	1.0%
5%	0.002°	0.002°
10%	0.005°	0.005°
15%	0.007°	0.007°

Table 5.6 The change in the *mean* of *maximum voltage magnitude error* data from 0 PMUs to 150 PMUs in the measurements (Examples 11 – 16)

SCADA noise level	PMU noise level	
	0.5%	1.0%
5%	1.5×10^{-4} p.u.	-1.9×10^{-5} p.u.
10%	-8.7×10^{-5} p.u.	-1.3×10^{-4} p.u.
15%	-1.9×10^{-4} p.u.	-2.0×10^{-4} p.u.

Table 5.7 shows the change in the mean of RMS voltage magnitude error in Examples 11 - 16. The change in the mean of RMS voltage magnitude error increases in size as the SCADA noise levels increase but changing the noise level in the voltage phase angle measurements appears to have no effect on the improvement in the accuracy. The change in RMS error is an order of magnitude smaller than the change in maximum voltage magnitude error. The noise levels used in Examples 11 -16 had little effect on the condition indicators of K_G and d. That is the condition indicators are not dependent on the noise in the measurements. This observation appears to be intuitively evident because K_G and d are functions of G only – not functions of noise. However, because the ultimate gain matrix G is derived at the solution, and G is obtained from linearization (see 2.1 –

2.2), the point of linearization *does* depend on noise. The impact of noise on K_G or d is evident Figures 5.11, 5.12, 5.17 and 5.18 due to the three unique lines for *min*, *max*, and *mean*.

Table 5.7 The change in the *mean* of *RMS voltage magnitude error* data from 0 PMUs to 150 PMUs in the measurements (Examples 11 – 16)

SCADA noise level	PMU noise level	
	0.5%	1.0%
5%	-1.8×10^{-6} p.u.	-2.0×10^{-6} p.u.
10%	-4.7×10^{-6} p.u.	-7.3×10^{-6} p.u.
15%	-1.1×10^{-5} p.u.	-1.1×10^{-5} p.u.

In Examples 11 – 16 improvement was seen in both the RMS and maximum of voltage phase angle in all cases. The improvement seen in both RMS and maximum voltage phase angle is not linear. Rather, the improvement in accuracy of phase angle estimates for each PMU measurement added diminishes as more PMUs are added.

5.7 Conclusions

In this study, the impact of adding PMUs to test System 2 is examined. In Chapter 5 System 2, a representation of a power system in the southwest US, was used approximately three times the size of IEEE 57 bus test bed, System 1. The condition indicators, condition number of the gain matrix (K_G) and singular distance of the gain matrix (d), and linear approximations of the change in the condition indicators (2.22, 2.23) were calculated using System 2. The change observed when phase angle measurements were added was as predicted using the linear approximations for change of condition indicators. In Examples 11 – 16, the level of noise in either the SCADA measurements or PMU measurements did not significantly alter the condition indicators of the gain matrix.

An improvement in state estimation accuracy was distinguished as PMUs were added to System 2 for all noise levels studied. The noise level of the SCADA measurements had an impact on the improvement of the accuracy as PMUs were added. In Examples 11 – 16, if the PMU noise level is in the S/N ration range of 10 to 20, the impact of noise in the PMU voltage phase angle measurements has low impact on the improvement of accuracy in state estimation.

6 Conclusions and Future Work

6.1 Research Contributions

The research contributions of this report have been in the area of state estimation of large scale power systems. The research contributions in this report are summarized in Table 6.1.

Table 6.1 Summary of the main research contributions in this report

Major Contributions	• Definition of condition indicators • Utilization of condition indicators for state estimation design • Formulas describing the linear behavior of condition indicators up the addition of measurements • The use of condition indicators to assess placement of PMUs • Definition of a measurement outage table • Utilization of a measurement outage table to asses robustness state estimator design • Formulations of probability of measurement outage
Secondary Contributions	• Case studies performed to test the performance of condition indicators on a large scale power system • Calculation of the probability of measurement out of service using reliability statistics • The use of linearized formulas of the condition indicators to find expected values for the measurement outage table

The study and review of condition analysis for state estimation using a least squares method revealed a correlation between decreasing the condition number of the gain matrix, G, and increasing the accuracy of state estimates. Some other innovative concepts and contributions include definition and use of:

- *Singular distance* – calculating the distance between matrix A and the closest singular matrix.
- *Scaling factor* – viewing the largest singular value of matrix A as a condition indicator.

Further contributions are:

- *Measurement placement using eigenvectors* – the use of eigenvector of smallest eigenvalue to find placement of measurements.

- *Linear approximations for the change in condition indicators* - the use (2.21 – 2.23) in predicting the change in the condition indicators.

It appears it is possible to "engineer" the eigenspectrum of G (sensor placement in H) using linearized analysis. Illustrations were given showing placement of bus voltage phase measurements with regard to impacts on the condition indicators. The sensitivity-based formulas for condition indicators give an assessment of the effects of added measurements on the eigenvalues of the gain matrix. The accuracy of the sensitivity-based calculations of condition indicators decreases as the number of measurements increases. Placement of added state measurements using a condition indicator philosophy appears to be consistent with placement using redundancy analysis.

The condition analysis concepts above are proposed for the following applications:

- Application to an existing system in which the SE has a valid G matrix. The system is under study for added measurements
- The condition analysis is a tool used in connection with other placement techniques. It is assumed that the system is observable.
- A "sanity check" for proposed measurement placement.

In these applications, it was found that the impact of measurement noise on state estimation is attenuated. This point is illustrated in the examples shown in the report. The examples included a 180 bus system. In addition, it is found that the condition analysis of the placement of the proposed measurements agrees with redundancy analysis:

- The error both in the ΔK_G and Δd, due to the sensitivity-based approximations generally decreases as measurements are added.
- The improvement (i.e., decrease in ΔK_G and increase in Δd) decreases as measurements are sequentially added.

An additional contribution relates to the construction and use of a measurement outage table. The measurement outage table uses the probability of a measurement failure. This is analogous to the probability of loss of generation in a generation capacity outage table. The measurement outage table is offered as a potential tool to analyze state estimation sensory impacts. For example, it is possible to statistically evaluate the condition indicators. It is possible to identify where a phasor measurement can be placed to increase the robustness of the state estimator design, (i.e., the entire system is still observable after a measurement failure). The performance indicators used in the table not only detects if a measurement outage produces an unobservable island, but also detects how "well conditioned" the process matrix, H, is, and the impact of measurement failure on state estimator expected error. The main conclusions of about the measurement outage table are:

- It is possible to calculate the expected values of the condition indicators for the measurement outage table using the linearized formulas (2.22, 2.22, 2.24); and
- The addition of PMU measurements improves the condition indicators (i.e., the condition number decreases and singular distance increases) of the state estimator during failure scenarios.

6.2 Present Status of the EIPP Project

The Eastern Interconnect Phasor Project, EIPP, is advancing toward the goal of widespread geographic penetration of PMUs in the eastern interconnect. The location of PMUs is decided by the utility installing, all of which have different criteria for placement.

The reference bus is a virtual bus calculated from three PMU measurements near a nuclear power plant in southeast Tennessee owned by Tennessee Valley Authority. The frequency, voltage phase angle, and voltage magnitude is broadcast to the Tennessee Valley Authority control room in real time and stored in a super phasor data concentrator. The information from all PMUs reporting to the super phasor data concentrator is then broadcast to all participating utilities in near real time via fiber optic cable links.

Members of EIPP are now preparing their energy management software (EMS) to include PMU measurements in the measurement set for state estimation. A software vendor specializing in EMS is working with the members to include the use of PMU measurements in state estimation and improve the metrics applied to the solved solution of the state estimator. Metrics that are being used to show improvement in accuracy of the state estimator are:

- *Variance of state* – the inverse of the solved gain matrix, the smaller the values on the diagonal the closer to the actual state
- *Critical measurements* – the local redundancy procedure outlined in this report is performed
- *Condition number of the gain* matrix – is used to determine the robustness of the state estimator for current topology and measurement set

Other characteristics will be collected during a six month trial will be performed with the vendors state estimator using PMU measurements operating in parallel to an operative state estimator. The operative state estimator does not use PMU measurements. The trial period is expected to be six months long. Some of the statistics being collected on both state estimators are:

- The number of converged solutions
- Power flow mismatch at the buses
- Accuracy of state estimation on congested transmission lines
- Accuracy of critical bus voltages.

6.3 Future Work and Recommendations

This report has focused on improving the state estimator of large scale power systems by including voltage phase angle measurements from PMUs. Future work and recommendations are:

- *Western EIPP* – The Western Electricity Coordinating Council (WECC) was one of the first promoters of the use PMUs in protective relaying. Several utilities in the WECC have remedial action schemes based on PMU measurements. The WECC has far fewer PMUs online than in the eastern interconnect and infrastructure needed for a super phasor data concentrator is still emerg-

ing. A concerted effort needs to be made by the utilities in the western United States to follow the example of the EIPP and push for advanced metering technologies use on the WECC system.

- *Correlation with redundancy* – In Examples 2 – 4 local redundancies are calculated. Improvements in local redundancy are observed in Examples 3 and 4, when PMUs are added to improve the condition indicators. Further investigation in this phenomenon needs to be performed.
- *Experience with PMUs* – The examples presented in this report models PMUs as described in journal articles. There is still much to be learned about actual performance of PMUs operated on utility owned electric system.
- *Use of PMUs in WACS* – The research done in this report focused on the use of PMUs for state estimation. The speed and quality of the data from PMUs could make WACS more feasible. The location of PMUs to have the most significant impact on WACS needs to be studied. The time delay between measurements from PMU and control signals being sent needs to be studied.

References

[1] J. W. F. Shweppe, D. Rom, "Power system static state estimation: part I, II, and III," in *Power Industry Computer Conference*, 1969.

[2] A. Monticelli, *State estimation in electric power systems: a generalized approach*. Boston: Kluwer Academic Publishers, 1999.

[3] A. J. Wood and B. F. Wollenberg, *Power generation, operation, and control*, 2nd ed. New York: J. Wiley & Sons, 1996.

[4] F. C. Schweppe, *Uncertain dynamic systems*. Englewood Cliffs, N.J.,: Prentice-Hall, 1973.

[5] A. Abur and A. Gómez Expósito, *Power system state estimation : theory and implementation*. New York, NY: Marcel Dekker, 2004.

[6] A. Monticelli, "Electric power system state estimation," *Proceedings of the IEEE,* vol. 88, pp. 262-282, 2000.

[7] O. Alsac, N. Vempati, B. Stott, and A. Monticelli, "Generalized state estimation," *IEEE Transactions on Power Systems,* vol. 13, pp. 1069-1075, 1998.

[8] J. B. Carvalho and F. M. Barbosa, "A modern state estimation in power system energy," *PowerTech Budapest International Conference on Electric Power Engineering,* p. 270, 1999.

[9] I. O. Habiballah, "Modified two-level state estimation approach [for power systems]," *IEE Proceedings - Generation, Transmission and Distribution,* vol. 143, pp. 193-199, 1996.

[10] M. E. El-Hawary, "Bad data detection of unequal magnitudes in state estimation of power systems," *IEEE Power Engineering Review,* vol. 22, pp. 57-60, 2002.

[11] M. V. F. Pereira and N. J. Balu, "Composite generation/transmission reliability evaluation," *Proceedings of the IEEE,* vol. 80, pp. 470-491, 1992.

[12] P. Zarco and A. G. Exposito, "Power system parameter estimation: a survey," *IEEE Transactions on Power Systems,* vol. 15, pp. 216-222, 2000.

[13] S. Zhong and A. Abur, "Auto tuning of measurement weights in WLS state estimation," *IEEE Transactions on Power Systems,* vol. 19, pp. 2006-2013, 2004.

[14] S. Gastoni, G. Granelli, and M. Montagna, "Robust state-estimation procedure based on the maximum agreement between measurements," *IEEE Transactions on Power Systems,* vol. 19, pp. 2038-2043, 2004.

[15] A. P. S. Meliopoulos and G. K. Stefopoulos, "Characterization of state estimation biases," *International Conference on Probabilistic Methods Applied to Power Systems,* pp. 600-607, 2004.

[16] M. M. Adibi, K. A. Clements, R. J. Kafka, and J. P. Stovall, "Remote measurement calibration," *IEEE Computer Applications in Power,* vol. 3, pp. 37-42, 1990.

[17] M. M. Adibi, K. A. Clements, R. J. Kafka, and J. P. Stovall, "Integration of remote measurement calibration with state estimation-a feasibility study," *IEEE Transactions on Power Systems,* vol. 7, pp. 1164-1172, 1992.

[18] J. G. Moreno, J. L. M. Vigil-Escalera, and R. S. Alvarez, "Statistical measurement calibration based on state estimator results," *IEEE Transmission and Distribution Conference,* vol. 1, pp. 184-189, 1999.

[19] S. Zhong and A. Abur, "Combined state estimation and measurement calibration," *IEEE Transactions on Power Systems,* vol. 20, pp. 458-465, 2005.
[20] G. H. Golub and C. F. Van Loan, *Matrix computations*. Baltimore: Johns Hopkins University Press, 1983.
[21] R. A. Jabr and B. C. Pal, "Iteratively reweighted least-squares implementation of the WLAV state-estimation method," *IEE Proceedings -Generation, Transmission and Distribution,* vol. 151, pp. 103-108, 2004.
[22] B. Gou and A. Abur, "An improved measurement placement algorithm for network observability," *IEEE Transactions on Power Systems,* vol. 16, pp. 819-824, 2001.
[23] E. Castillo, A. J. Conejo, R. E. Pruneda, and C. Solares, "State estimation observability based on the null space of the measurement Jacobian matrix," *IEEE Transactions on Power Systems,* vol. 20, pp. 1656-1658, 2005.
[24] R. F. Nuqui and A. G. Phadke, "Phasor measurement unit placement techniques for complete and incomplete observability," *IEEE Transactions on Power Delivery,* vol. 20, pp. 2381-2388, 2005.
[25] E. Castillo, A. J. Conejo, R. E. Pruneda, and C. Solares, "Observability analysis in state estimation: a unified numerical approach," *IEEE Transactions on Power Systems,* vol. 21, pp. 877-886, 2006.
[26] B. Gou, "Jacobian matrix-based observability analysis for state estimation," *IEEE Transactions on Power Systems,* vol. 21, pp. 348-356, 2006.
[27] S. Pajic and K. A. Clements, "Power system state estimation via globally convergent methods," *IEEE Transactions on Power Systems,* vol. 20, pp. 1683-1689, 2005.
[28] P. Ristanovic, "State estimation based real-time markets - challenges and practical solutions," *IEEE Power Engineering Society General Meeting,* vol. 3, pp. 2849-2850, 2005.
[29] A. V. Jaen, P. C. Romero, and A. G. Exposito, "Substation data validation by a local three-phase generalized state estimator," *IEEE Transactions on Power Systems,* vol. 20, pp. 264-271, 2005.
[30] S. S. Lin and C. Huay, "An efficient algorithm for solving distributed state estimator and laboratory implementation," *Proceedings of 11th International Conference on Parallel and Distributed Systems,* vol. 1, pp. 689-694, 2005.
[31] K.-S. Cho, J.-R. Shin, and S. H. Hyun, "Optimal placement of phasor measurement units with GPS receiver," *IEEE Power Engineering Society Winter Meeting,* vol. 1, 2001, pp. 258-262, 2001.
[32] A. G. Phadke, "Synchronized phasor measurements-a historical overview," *IEEE/PES Transmission and Distribution Conference and Exhibition: Asia Pacific,* vol. 1, pp. 476-479, 2002.
[33] W. Lewandowski, J. Azoubib, and W. J. Klepczynski, "GPS: primary tool for time transfer," *Proceedings of the IEEE,* vol. 87, pp. 163-172, 1999.
[34] X. Dongjie, H. Renmu, W. Peng, and X. Tao, "Comparison of several PMU placement algorithms for state estimation," *Eighth IEE International Conference on Developments in Power System Protection,* vol. 1, pp. 32-35, 2004.

[35] A. G. Phadke, B. Pickett, M. Adamiak, M. Begovic, G. Benmouyal, R. O. Burnett, Jr., T. W. Cease, J. Goossens, D. J. Hansen, M. Kezunovic, L. L. Mankoff, P. G. McLaren, G. Michel, R. J. Murphy, J. Nordstrom, M. S. Sachdev, H. S. Smith, J. S. Thorp, M. Trotignon, T. C. Wang, and M. A. Xavier, "Synchronized sampling and phasor measurements for relaying and control," *IEEE Transactions on Power Delivery,* vol. 9, pp. 442-452, 1994.

[36] R. O. Burnett, Jr., M. M. Butts, and P. S. Sterlina, "Power system applications for phasor measurement units," *Computer Applications in Power, IEEE,* vol. 7, pp. 8-13, 1994.

[37] H. Bai, S. Zhou, and Z. Guo, "Innovation network graph state estimation based PMUs," *IEEE/PES Transmission and Distribution Conference and Exhibition: Asia and Pacific,* pp. 1-6, 2005.

[38] J. Chen and A. Abur, "Improved bad data processing via strategic placement of PMUs," *IEEE Power Engineering Society General Meeting,* vol. 1 pp. 509-513, 2005.

[39] D. Junce and C. Zexiang, "Mixed Measurements State Estimation Based on Wide-Area Measurement System and Analysis," *IEEE/PES Transmission and Distribution Conference and Exhibition: Asia and Pacific,* pp. 1-5, 2005.

[40] C. Rakpenthai, S. Premrudeepreechacharn, S. Uatrongjit, and N. R. Watson, "An Improved PMUs Placement Method for Power System State Estimation," *The 7th International Power Engineering Conference, IPEC,* pp. 1-4, 2005.

[41] L. Zhao and A. Abur, "Multi area state estimation using synchronized phasor measurements," *IEEE Transactions on Power Systems,* vol. 20, pp. 611-617, 2005.

[42] E. Price, "Practical considerations for implementing wide area monitoring, protection and control," *59th Annual Conference for Protective Relay Engineers,* pp. 12, 2006.

[43] M. Rice and G. T. Heydt, "Power Systems State Estimation Accuracy Enhancement Through the Use of PMU Measurements," *IEEE PES Transmission and Distribution Conference and Exposition*, Dallas, TX, May 2006.

[44] M. Rice and G. T. Heydt, *Phasor Measurement Unit Data in Power System State Estimation,* PSerc Intermediate Project Report for "Enhanced State Estimators," April 2005.

[45] M. Rice, *Phasor Measurement Unit Data in Power System State Estimation,* Masters Thesis, Dec. 2004.

[46] G. B. Denegri, M. Invernizzi, and F. Milano, "A security oriented approach to PMU positioning for advanced monitoring of a transmission grid," *Proceedings of International Conference on Power System Technology, vol. 2*, pp. 798-803, 2002.

[47] R. Zivanovic and C. Cairns, "Implementation of PMU technology in state estimation: an overview," *IEEE AFRICON 4th*, vol. 2, pp. 1006-1011, 1996.

[48] I. Kamwa and R. Grondin, "PMU configuration for system dynamic performance measurement in large, multiarea power systems," *IEEE Transactions on Power Systems,* vol. 17, pp. 385-394, 2002.

[49] S. B. M. Ingram, S. Matthews, A. P. Meliopoulos, G Cokkinides, "Use of phasor measurements, SCADA and IED data to improve the state estimation," *7th Fault and Disturbance Analysis Conference,* April 26-27, 2004.

[50] S. Widergren, "Eastern Interconnect Phasor Project." http://phasors.pnl.gov/

[51] IEEE, "IEEE standard for synchrophasor for power systems. IEEE std. 1344-1995,"

[52] "IEEE Standard for Synchrophasors for Power Systems," *IEEE Std C37.118-2005 (Revision of IEEE Std 1344-1995),* pp. 1-57, 2006.

[53] W. Hongxia, N. Hui, and G. T. Heydt, "The impact of time delay on robust control design in power systems," *IEEE Power Engineering Winter Meeting,* vol.2, pp. 1511-1516, 2002.

[54] J. Bertsch, M. Zima, A. Suranyi, C. Carnal, and C. Rehtanz, "Experiences with and perspectives of the system for wide area monitoring of power systems," *CIGRE/IEEE PES International Symposium Quality and Security of Electric Power Delivery Systems,* pp. 5-9, 2003.

[55] D. Karlsson, M. Hemmingsson, and S. Lindahl, "Wide area system monitoring and control - terminology, phenomena, and solution implementation strategies," *IEEE Power and Energy Magazine,* vol. 2, pp. 68-76, 2004.

[56] J. F. Hauer, N. B. Bhatt, K. Shah, and S. Kolluri, "Performance of "WAMS East" in providing dynamic information for the North East blackout of August 14, 2003," *IEEE Power Engineering Society General Meeting, vol. 2*, pp. 1685-1690, 2004.

[57] X. Tong, G. Liao, X. Wang, and S. Zhong, "The analysis of communication architecture and control mode of wide area power systems control," *Proceedings Autonomous Decentralized Systems,* pp. 59-65, 2005.

[58] K. E. Holbert, G. I. Heydt, and H. Ni, "Use of satellite technologies for power system measurements, command, and control," *Proceedings of the IEEE,* vol. 93, pp. 947-955, 2005.

[59] I. Kamwa, R. Grondin, and Y. Hebert, "Wide-area measurement based stabilizing control of large power systems-a decentralized/hierarchical approach," *IEEE Transactions on Power Systems,* vol. 16, pp. 136-153, 2001.

[60] K. Tomsovic, D. E. Bakken, V. Venkatasubramanian, and A. Bose, "Designing the next generation of real-time control, communication, and computations for large power systems," *Proceedings of the IEEE,* vol. 93, pp. 965-979, 2005.

[61] B. Gou and A. Abur, "An improved measurement placement algorithm for network observability," *IEEE Transactions on Power Systems* vol. 16, pp. 819-824, 2001.

[62] X. Dongjie, H. Renmu, W. Peng, and X. Tao, "Comparison of several PMU placement algorithms for state estimation," Eighth IEE International Conference on Developments in Power System Protection, vol. 1, pp. 32 - 35, April 2004.

[63] M. Mitchell, *An Introduction to Genetic Algorithms*. Cambridge, MA: MIT Press, 1998.

[64] B. Milosevic and M. Begovic, "Nondominated sorting genetic algorithm for optimal phasor measurement placement," *IEEE Transactions on Power Systems,* vol. 18, pp. 69-75, 2003.

[65] B. Xu and A. Abur, "Observability analysis and measurement placement for systems with PMUs," *IEEE PES Power Systems Conference and Exposition, vol.2,* pp. 943-946, 2004.

[66] C. Madtharad, S. Premrudeepreechacharn, N. R. Watson, and D. Saenrak, "Measurement placement method for power system state estimation: part I," *IEEE Power Engineering Society General Meeting,* vol. 3, pp. 1632, 2003.

[67] M. Rice, G. Heydt, W. Jiang, and V. Vittal, "Design of State Estimator Measurements Based on Condition Indicators" under review for IEEE Transactions on Power Systems.

[68] M. Rice, *State Estimation and Error Analysis for Power System with Phasor Measurement Units,* Qualifying Exam, Arizona State University, Dec 2005.

[69] C. Madtharad, S. Premrudeepreechacharn, N. R. Watson, and R. Saeng-Udom, "An optimal measurement placement method for power system harmonic state estimation," *IEEE Transactions on Power Delivery,* vol. 20, pp. 1514-1521, 2005.

[70] G. M. Huang, J. Lei, and A. Abur, "A heuristic approach for power system measurement placement design," *Proceedings of the International Symposium on Circuits and Systems,* vol.3, pp. III-407-III-410, 2003.

[71] J. B. A. London, G. L. R. Brito, and N. G. Bretas, "Method for meter and RTU placement for state estimation purposes," *Conference Proceedings of IEEE Bologna Power Tech,* vol.1, pp. 6, 2003.

[72] R. L. Dykstra, "Establishing the positive definiteness of the sample covariance matrix," *The Annals of Mathematical Statistics,* vol. 41, pp. 2153 - 2154, Dec., 1970.

[73] R. C. Penney, *Linear algebra: ideas and applications*. New York: John Wiley and Sons, 1998.

[74] R. Ebrahimian and R. Baldick, "State estimator condition number analysis," *IEEE Transactions on Power Systems,* vol. 16, pp. 273-279, 2001.

[75] D. K. Faddeev and V. N. Faddeev, *Computational methods of linear algebra*. San Francisco: W. H. Freeman, 1963.

[76] J. W. Gu, G. R. Krumpholz, K. A. Clements, and P. W. Davis, "The solution of ill-conditioned power system state estimation problems via the method of Peters and Wilkinson," *IEEE Transactions on Power Apparatus and Systems*, vol. PAS-102, no. 10, pp. 3473-3480, Oct. 1983.

[77] R. Klump, R.E. Wilson, K.E. Martin, "Visualizing real-time security threats using hybrid SCADA / PMU measurement displays," Proceedings of the 38th Annual Hawaii International Conference on System Sciences, Jan., 2005.

[78] J. Depablos, V. Centeno, A.G. Phadke, M.Ingram, "Comparative testing of synchronized phasor measurement units," IEEE Power Engineering Society General Meeting, pp.948 – 954, June, 2004.

[79] S. Manfredi, M. di Bernardo, and F. Garofalo, "Small world effects in networks: an engineering interpretation," Proceedings of the 2004 International Symposium on Circuits and Systems, vol. 4, pp. 820 - 823, May 2004.
[80] D. J. Watts and S. H. Strogatz, "Collective dynamizs of 'small-world' networks," *Nature*, vol. 393, pp. 440 - 442, June 1998.
[81] A. G. Phadke, "Synchronized phasor measurements in power systems," *IEEE Computer Applications in Power,* vol. 6, pp. 10-15, 1993.
[82] R. Christie, "Power System Test Archive." www.ee.washington.edu/research/pstca/
[83] Personal communications with Xiaolin Mao, August 2006.
[84] M. B. Do Coutto Filho, J. C. Stacchini de Souza, F. M. F. de Oliveira, M. T. Schilling, "Identifying critical measurements & sets for power system state estimation," Proceedings IEEE Power Tech,, Porto, Portugal, Vol. 3, Sept. 2001.
[85] N. G. Bretas, J. B. A. London Jr., "Measurement placement design and reinforcement for state estimation purposes," IEEE Power Tech Proceedings, Porto, Vol. 3, Sept. 2001.
[86] A. Al-Atwan, H-J. Koglin, "Two aspects of local redundancy in state estimation," IEE Proceedings Generation, Transmission and Distribution, Vol. 145, No. 4, July 1998 pp. 458 – 462.
[87] E. Handschin, C. Bogers, "Theoretical and practical considerations in the design of state estimators for electric power systems," Proceedings of the International Symposium COPOC, Aug. 1975, Saõ Carlos, Brazil, pp. 104-136.
[88] H-J. Koglin, D. Oeding, K. D. Schmitt, "Local redundancy and identification of bad measuring data," Proceedings of the 9th Power System Computation Conference, Cascais, Portugal, 1987, pp. 528-534.
[89] R. Billinton, *Reliability evaluation of power systems*, 2nd ed. ed. New York: Plenum Press, 1996.
[90] B. Mcnutt, "A technique for approximating the capacity outage table based on the modeling of unit outage size," *IEEE Transactions on Power Apparatus and Systems,* vol. 103, no. 10, pp. 2891-2897, Oct. 1984.
[91] R. Ghajar and R. Billinton, "Comparison of alternative techniques for evaluating the marginal outage costs of generating systems," *IEEE Transactions on Power Systems*, vol. 8, no. 4, pp 1550 - 1556, Nov. 1993.
[92] F. Bouffard, F. D. Galian, "An electricity market with a probabilistic spinning reserve criterion," IEEE transactions on Power Systems, vol. 19, no. 1, pp 300 - 307, Feb. 2004.
[93] J. Zhu, A. Abur, M. J. Rice, G. T. Heydt, and S. Meliopoulos, "Enhanced State Estimators," PSerc Final Report, Nov. 2006.
[94] M. Rice, *Sensor Location Strategies for the Enhancement of Power System State Estimators*, Comprehensive Exam, Arizona State University, Sept. 2006.
[95] R. Billinton and A. Abdulwhab, "Short-term generating unit maintenance scheduling in a deregulated power system using a probabilistic approach," IEE Proceedings - Generation, Transmission and Distribution, vol. 150, no. 4, pp. 463 - 468, July 2003.

[96] G. A. Cucchi, D. J. Pratzon, and F. P. Witmer, "Experience with generation outage data collection procedures on a large-scale system," IEEE Transactions on Power Apparatus and Systems, vol. 95, no. 2, pp. 542 - 549, Mar. 1976.
[97] D. P. Georgiadis and N. D. Hatziargyriou, "Investigation of the effect of large wind power integration in the Greek mainland system," IEEE Power Engineering Society General Meeting, vol.4, pp. 2165 - 2170, July 2003.
[98] D. Koval, "Frequency of transmission line outages in Canada," Proceedings of the IEEE Industry Applications Society Annual Meeting, Vol. 3, pp. 2201-2208, Oct 1994.

APPENDIX A

SUMMARY OF EXAMPLES

Table A.1 Summary of Examples

Example	Intent of Example	Iterations	System	Conditions	Outcome
1	Verify (2.22) on nonlinear state estimator	4	1*	Augment H with +1 at (m+1,32) and (m+2, 89)	Equation 2.22 can predict d accurately for all iterations of the state estimation
2	Provide a base case for subsequent examples	4	1*	Signal to Noise of 10 normally distributed.	N/A
3	Observe the impact of adding an PMU on both SE accuracy and condition indicators	4	1*	PMU placed at bus 32. Signal to Noise of 10 normally distributed for power and voltage magnitude measurements.	The accuracy of the state estimation improved slightly and significant gains in the condition indicators.
4	Observe the impact of adding 5 PMUs on both SE accuracy and condition indicators	4	1*	PMUs placed at buses 25, 30, 31, 32, and 33. Signal to Noise of 10 normally distributed for power and voltage magnitude measurements.	The accuracy of the state estimation improved and significant gains in the condition indicators.
5	Observe the impact of weighting PMU on the prediction of condition indicators	4	1*	PMU placed at bus 32 and weight varied from 0 to 2.	Increasing the weight place on a PMU measurement decrease the accuracy of (2.22 – 2.24)
6	Observe the impact of the placing PMUs one-at-a-time versus all-at-once.	4	1*	PMUs placed at buses 25, 30, 31, 32, and 33.	The same buses were picked as in Example 4, however improvement was seen in the prediction of condition indicators.

Example	Intent of Example	Iterations	System	Conditions	Outcome
7	Illustrate a measurment outage table	4	1*	Condition indicators are calculated for *n*-1 contengcy of sensor outages and 0 PMUs.	This Example is a base case which Example 8 and 9 are compared to.
8	Illustrate a measurment outage table	4	1*	Condition indicators are calculated for *n*-1 contengcy of sensor outages and 1 PMU.	Decrease are seen in the maximum K_G and expected K_G compared to Example 7 and increases in minimum *d* and expected *d*.
9	Illustrate a measurment outage table	4	1*	Condition indicators are calculated for *n*-1 contengcy of sensor outages and 5 PMUs.	Decrease are seen in the maximum K_G and expected K_G compared to Example 7 and 8 and increases in minimum *d* and expected *d*.
10	Observe the impact of placing PMUs on the condition indicators	4	2**	PMUs are placed at the buses one at a time.	Equations 2.22 predicted the change in singular distance correctly. Equation 2.23 predicted the change in condition number in the gain matrix.
11	Observe the impact of placing PMUs on SE accuracy	4 – 5	2**	PMUs are placed at 0, 15, 30, … , 150. The noise is 5% for SCADA and 0.5% for PMUs.	An improvement was seen in the accuracy of the angle error and singular distance and condition number of the gain matrix.
12	Observe the impact of placing PMUs on SE accuracy	4 – 5	2**	PMUs are placed at 0, 15, 30, … , 150. The noise is 5% for SCADA and 1% for PMUs.	An improvement was seen in the accuracy of the angle error and singular distance and condition number of the gain matrix.

Example	Intent of Example	Iterations	System	Conditions	Outcome
13	Observe the impact of placing PMUs on SE accuracy	4 – 5	2**	PMUs are placed at 0, 15, 30, … , 150. The noise is 10% for SCADA and 0.5% for PMUs.	An improvement was seen in the accuracy of the angle error and singular distance and condition number of the gain matrix.
14	Observe the impact of placing PMUs on SE accuracy	4 – 5	2**	PMUs are placed at 0, 15, 30, … , 150. The noise is 10% for SCADA and 1% for PMUs.	An improvement was seen in the accuracy of the angle error and singular distance and condition number of the gain matrix.
15	Observe the impact of placing PMUs on SE accuracy	4 – 5	2**	PMUs are placed at 0, 15, 30, … , 150. The noise is 15% for SCADA and 0.5% for PMUs.	An improvement was seen in the accuracy of the angle error and singular distance and condition number of the gain matrix.
16	Observe the impact of placing PMUs on SE accuracy	4 – 5	2**	PMUs are placed at 0, 15, 30, … , 150. The noise is 15% for SCADA and 1% for PMUs.	An improvement was seen in the accuracy of the angle error and singular distance and condition number of the gain matrix.
17	Observe the impact of weighting PMU phase angle measurements on SE accuracy	4	2**	PMUs are placed at 0, 15, 30, … , 150. The noise is 15% for SCADA and 1% for PMUs. The PMU weight is 10 and SCADA weight is 1.	The impact of adding PMUs is far more signficant than in the case of unitary weighting, (Example 15).

Example	Intent of Example	Iterations	System	Conditions	Outcome
A.1	To find greatest improvement in smallest eigenvalue of the power-phase quadrant of H using (2.22)	1	1*	Augment power-phase quadrant of H with a +1 at (m+1, k).	Equation 2.22 predicted the correct location of the largest change
A.2	To see the effects of weighting the augmented measurement	1	1*	Augment power-phase quadrant of H with $0<w<2$ at (m+1, 32).	Decrease weight on the augmented measurement produced more accurate prediction d using (2.22)
A.3	Verify (2.22)	1	1*	Augment power-phase quadrant of H with +1 at (m+1, 32).	Equation 2.22 can predict the change in all eigenvalues accurately using a single row in the eigenvector matrix
A.4	To find greatest improvement in smallest eigen-value of G using (2.22)	1	1*	Augment H with +1 at (m+1, k) and (m+2, k+57).	Equation 2.22 predicted the correct location of the largest change

* System 1 is the IEEE 57 bus test bed

** System 2 is representative power system in the southwest US

APPENDIX B

EXAMPLES BASED ON SINGLE ITERATION LINEARIZED STATE ESTIMATION

B.1 Linearized Approximations of Condition Indicators Using the Power-Phase Quadrant of the H Matrix

In this Appendix, examples are presented to illustrate the use of condition indictors on first iteration gain matrix. All examples appear in detail in Appendix A. For purpose of terminology, the process matrix H is partitioned as

$$H = \begin{bmatrix} H_{P\delta} & H_{PV} \\ H_{Q\delta} & H_{QV} \end{bmatrix}$$

and $H_{P\delta}$ is termed the *power-phase quadrant* of the matrix H.

Example A.1 is performed on power-phase quadrant of the H matrix. The H matrix is constructed from measurements of System 1. Example A.1 is constructed to verify (2.22), the approximation of d, distance to the nearest singular matrix. The distance to the nearest singular matrix is also the smallest eigenvalue. In Example A.1, an extra row is augmented to the H matrix in which a single +1 is inserted in the column corresponding to the bus location at which a phasor angle measurement is added.

Figure B.1 shows that the linear approximation, noted as "Predicted," is a good indicator for which +1 change in the H will have the greatest impact on d. Both the linearized and actual change in d show the greatest improvement for a phasor measurement placed at bus 32. Figure B.1 also shows that the predicted change in d can be significantly larger than what is actually observed.

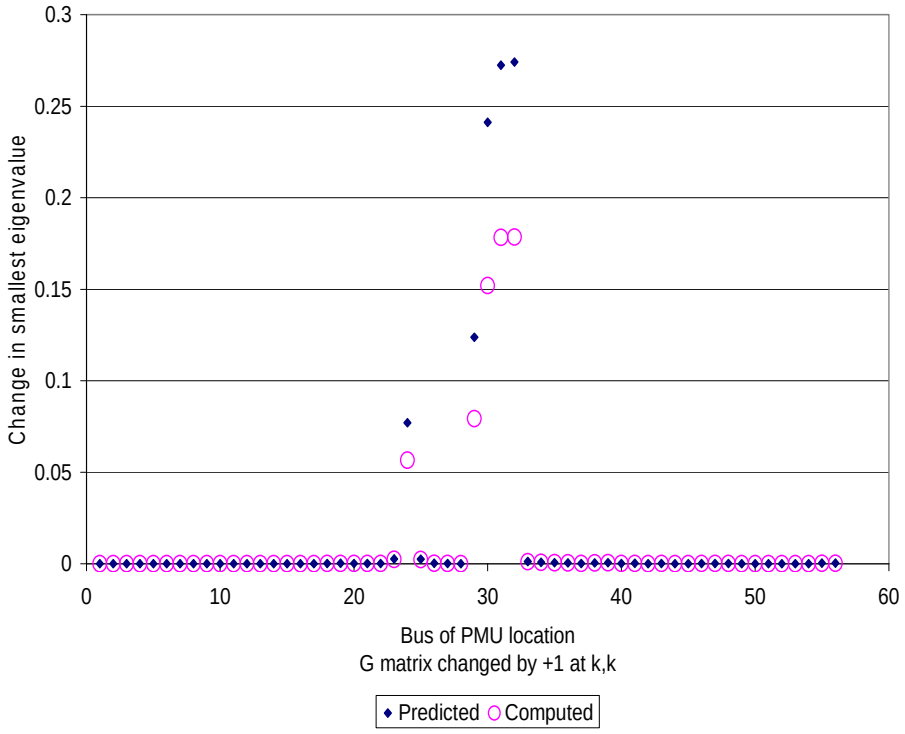

Figure B.1 Impact on singular distance of placement of a phasor measurement at a single bus (Example A.1, System 1)

Example A.2 is performed on System 1 using only the power-phase quadrant of *H*. Example A.2 will examine how the size of Δh affects the accuracy of the prediction of *d* from (2.22). The largest change in *d* in Example A.1 occurred when a phasor measurement was placed at bus 32. For Example A.2, the phasor measurement is placed at bus 32. The size of Δh will be varied from 0 to 2.

Figure B.2 depicts the predicted change in *d* using (2.22) and the actual change in *d*. It can be noted that in (2.22) there is a quadratic relationship between Δh and change in *d*. In Figure B.2, the actual change in *d* "levels off" as Δh continues to increase. This can be contributed to the smallest eigenvalue of *G* is no longer the same eigenvalue. That is, as elements of *H* change, the eigenvalues of *G* migrate. The eigenvalues of *G* "move" smoothly as $h_{i,j}$ changes and it is possible that the locus of the smallest eigenvalues will cross the locus of another eigenvalue. In this sense, the previously identified smallest eigenvalues may not longer be the smallest.

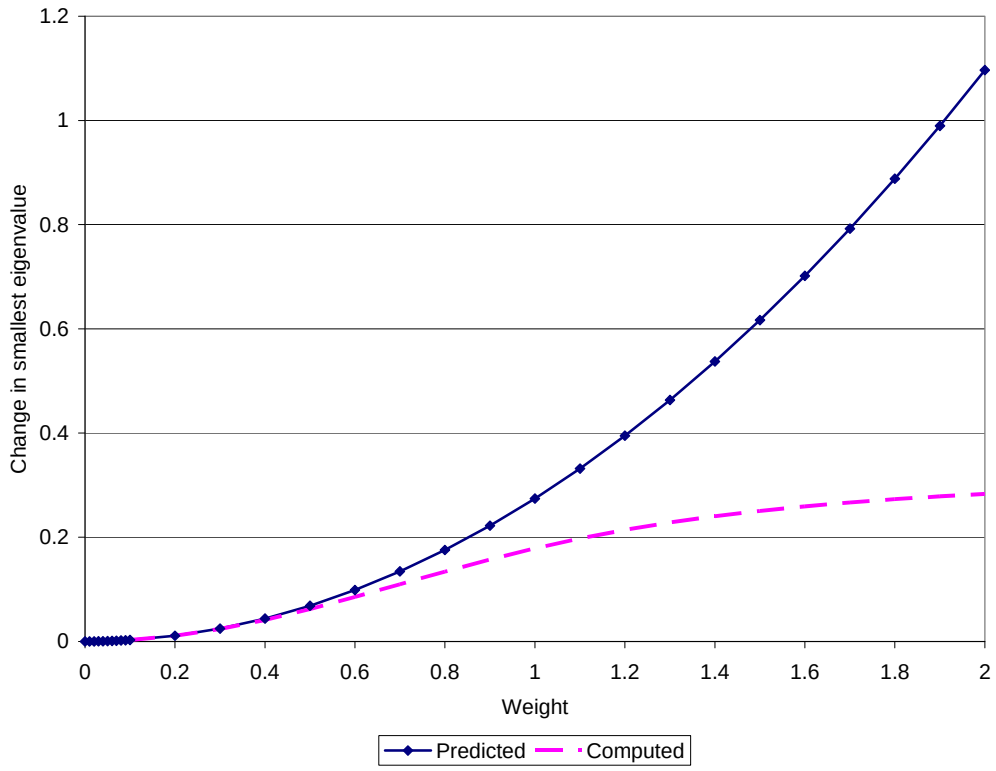

Figure B.2 Magnitude variations in Δh versus change in singular distance (Example A.2)

The leveling off in Example A.2 is attributed to smallest eigenvalue being "different" after the addition of phasor measurement; Example A.3 was constructed to confirm this hypothesis. In Example A.3 the power-phase quadrant of *H* of System 1 was used. A phasor measurement at bus 32 was augmented to the *H* matrix with a +1 in the 32nd column. Figure B.3 shows the spectrum of the eigenvalues of *G*. Note there is very little change in the eigenvalues of *G* by the addition of phasor measurement at bus 32. Also

note that the eigenvalues predicted using (2.22) agree with the actual values found after the augmentation of *H*.

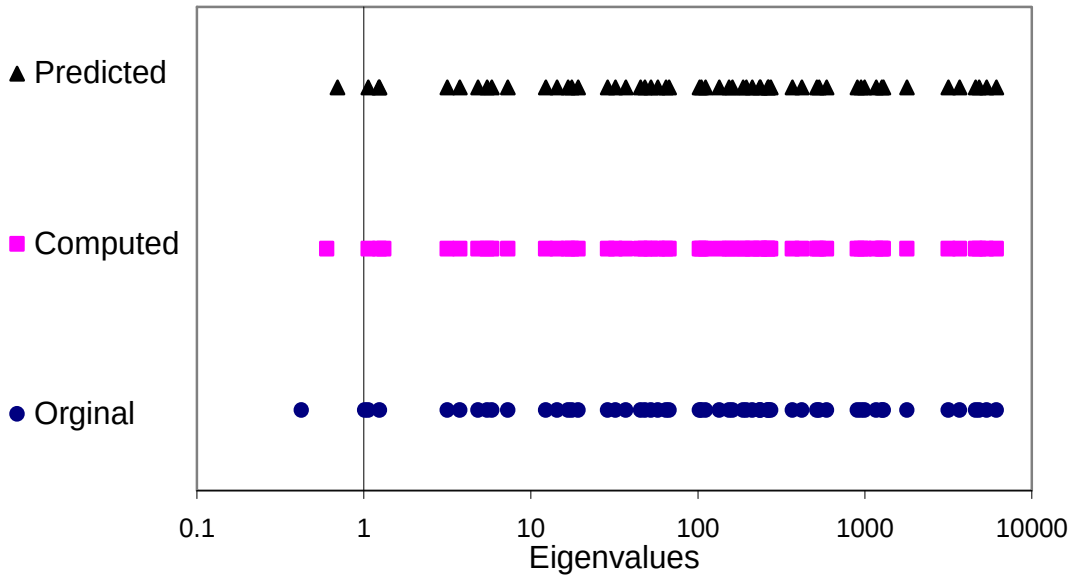

Figure B.3 Spectrum of eigenvalues of Example A.3

B.2 Linearized Approximations of Condition Indicators Using the H Matrix

The next series of examples examines the impact of the linearizations when two measurements are added, one being the phasor measurement, and two being the voltage measurement. Equation 2.22 can be used with changes in multiple columns of *H* provided the columns of *H* are linearly independent. The change in *d* will be addition of the changes in the columns of *H* mapped onto the changes in the smallest eigenvalue by (2.22).

Example A.4 is performed on System 1 using the entire *H* matrix. Example A.4 is to verify (2.22), the approximation of *d*, distance to the nearest singular matrix. In Example A.4, two rows are augmented to the *H* in which +1 is inserted in the columns corresponding to the phase angle locations at which phasor angle measurements were added.

Figure B.4 shows linear approximation, noted as "Predicted." Both the linearized and actual change in *d* show the greatest improvement for a phasor measurement placed at bus 32. Figure B.4 also shows that predicted change in *d* can be significantly larger than actual change in *d*.

Equation 2.25 is a linearized model for the change in condition number of *G* based on the change in Δh. Figure B.5 is displays the change in condition number of *G* as a voltage magnitude and phase angle measurement are added. Note that Bus 32 is the bus with greatest change in both the using (2.25) and actual change in condition number. Also note that the predicted change is much greater than the actual change.

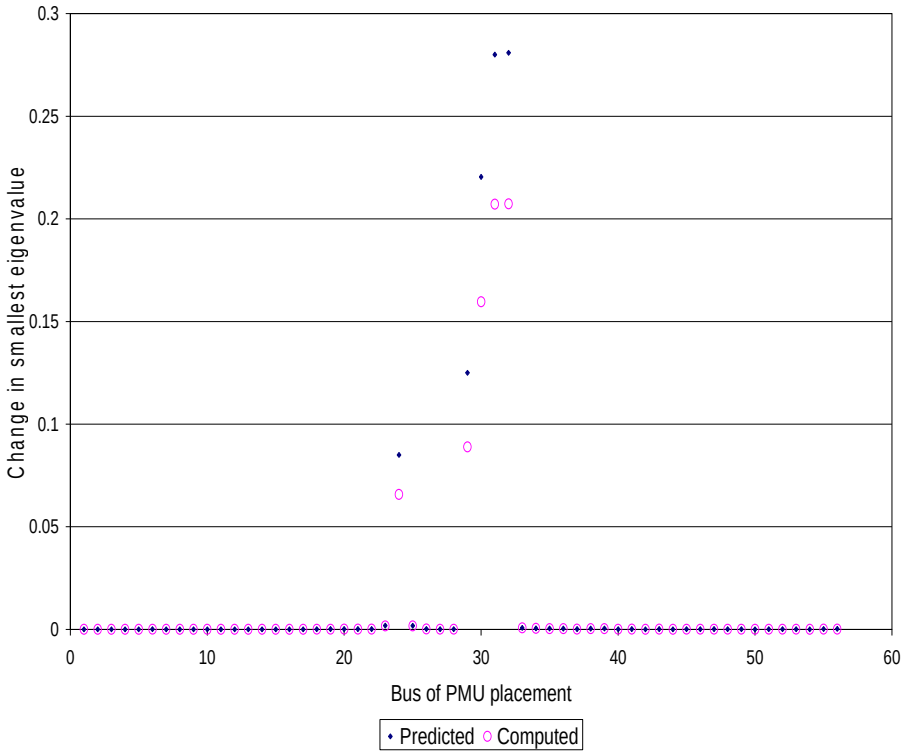

Figure B.4 Impact on singular distance by placement of a phasor measurement and voltage magnitude at one bus (Example A.4)

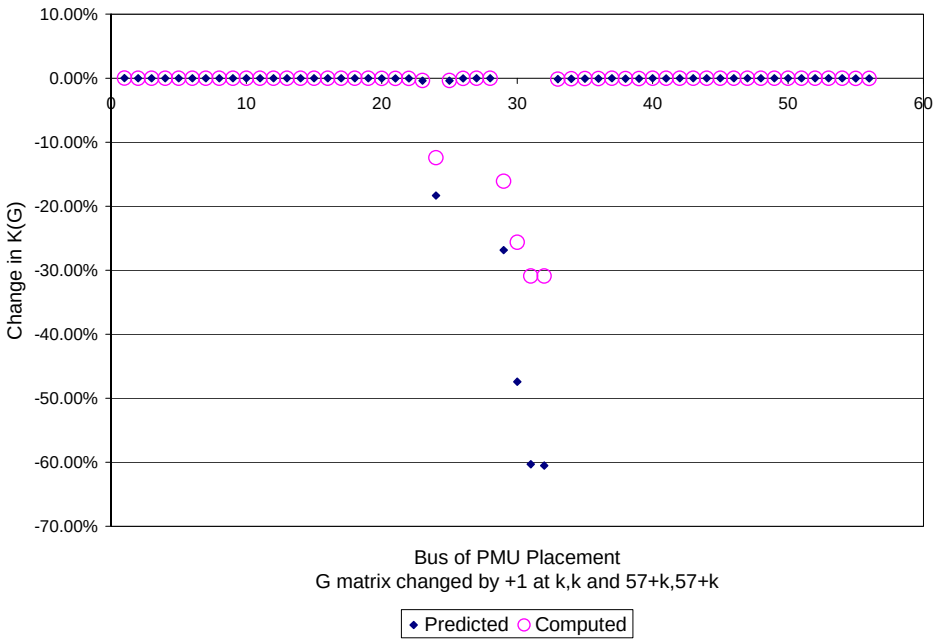

Figure B.5 Impact on condition number of *G* by placement of a phasor measurement and voltage magnitude at one bus (Example A.4)

Figure B.6 shows Example A.1 and Example A.4 on the same graph. Note that the improvement seen *d* is greater for the full *H* (Example A.4) than just the power-phase quadrant of *H* (Example A.1).

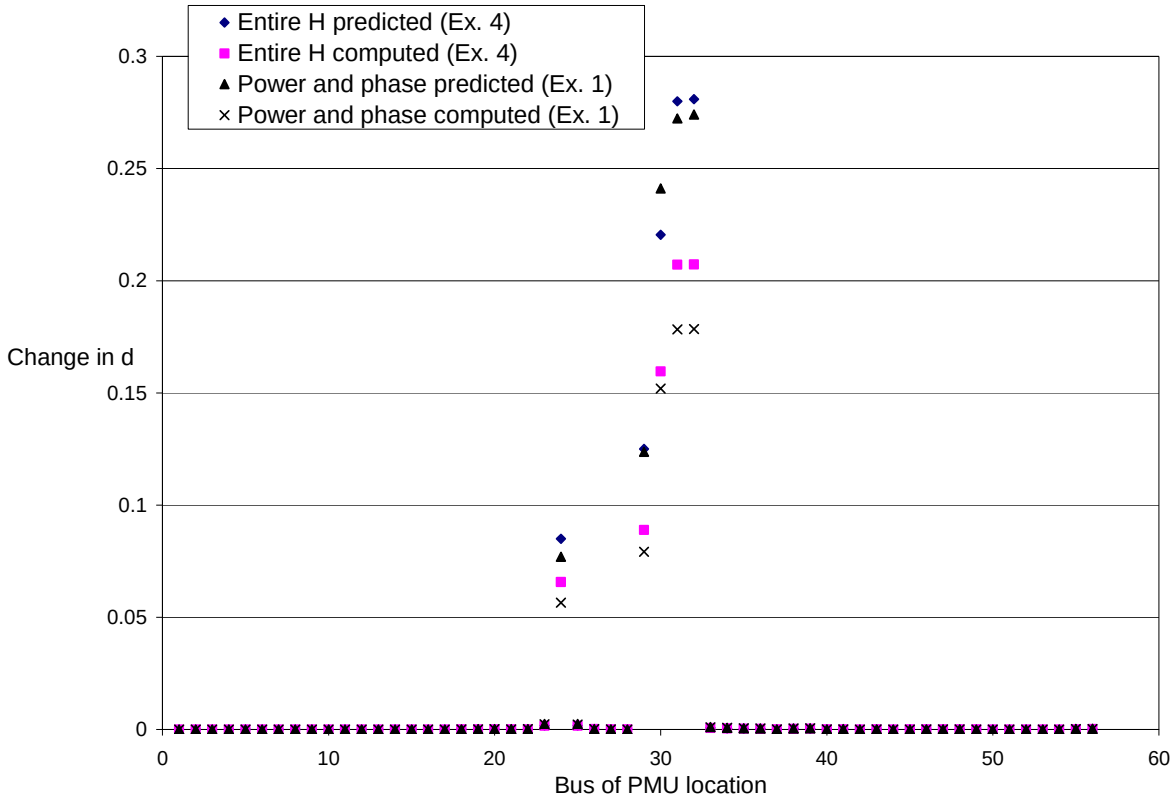

Figure B.6 Example A.1 and Example A.4 changes in singular distance

B.3 Summary of Examples

Table A.1 summarizes Examples A.1 -- A.6. The main observations are:

- Small change is seen between the prediction of the change in the smallest eigenvalue of *G* using the power-phase quadrant of *H* (Example A.1) and using the entire *H* (Example A.4) for the first iteration.
- Equation 2.22 predicted the correct location of the largest improvement of the smallest eigenvalue, *d.* However, (2.22) predicted a significantly larger estimate of improvement than the actual computed value.
- Equation 2.22 can predict all eigenvalues of *G* using limited information from the eigenvector matrix of *G*.
- Decreasing the size of Δh_{kl} will improve the accuracy of (2.22).
- The augmentation of one PMU in System 1 in Example A.4 decreased the condition number of *G* by 30.91%.

APPENDIX C

ELECTRICAL CONNECTIONS OF SYSTEM 2

Table C.1 Transmission line data for System 2

From Bus	To Bus		Series (p.u.)		Charging (p.u.)	
Number	Number	Section	Resistance	Reactance	Conductance	Susceptance
14000	14004	3	0.00000	0.00010	0.00000	0.00000
14000	14004	1	0.00000	-0.01720	0.00000	0.00000
14000	14004	2	0.00218	0.04901	0.00000	3.73739
14000	15001	0	0.00074	0.01743	0.00000	1.32274
14001	14002	1	0.00000	-0.00010	0.00000	0.00000
14001	14002	3	0.00000	-0.00010	0.00000	0.00000
14001	14002	2	0.00177	0.04189	0.00000	3.34000
14002	14003	1	0.00000	-0.01269	0.00000	0.00000
14002	14003	2	0.00077	0.01804	0.00000	1.39842
14002	14006	2	0.00098	0.02319	0.00000	1.85366
14002	14006	1	0.00000	-0.00660	0.00000	0.00000
14003	14005	3	0.00000	-0.01188	0.00000	0.00000
14003	14005	1	0.00000	-0.01188	0.00000	0.00000
14003	14005	2	0.00241	0.05865	0.00000	4.86560
14004	16000	0	0.00003	0.00030	0.00000	0.00000
14004	16001	0	0.00003	0.00030	0.00000	0.00000
14005	14006	1	0.00000	-0.00826	0.00000	0.00000
14005	14006	2	0.00081	0.01925	0.00000	1.53854
14005	15021	0	0.00040	0.00960	0.00000	0.90380
14005	15021	0	0.00040	0.00960	0.00000	0.90380
14005	15033	0	0.00000	0.00100	0.00000	0.00000
14007	15089	0	0.00020	0.00440	0.00000	0.41670
14007	15089	0	0.00020	0.00440	0.00000	0.41670
14009	15090	0	0.00000	0.00050	0.00000	0.00000
14009	15090	0	0.00000	0.00050	0.00000	0.00000
14100	14101	2	0.00855	0.08218	0.00000	0.00000
14100	14101	1	0.00000	-0.02072	0.00000	0.00000
14100	14101	1	0.00000	-0.02072	0.00000	0.00000
14100	14101	2	0.00860	0.08270	0.00000	0.00000
14100	14102	2	0.00000	0.00010	0.00000	0.00000
14100	14102	1	0.00361	0.06736	0.00000	1.02994
14100	14103	0	0.00364	0.03474	0.00000	0.53082
14101	79064	0	0.00030	0.00420	0.00000	0.07150
14102	14103	1	0.00000	0.00030	0.00000	0.00000
14102	14103	2	0.00340	0.03262	0.00000	0.49913
14201	19052	0	0.00090	0.00970	0.00000	0.01864
14202	14219	0	0.00330	0.02510	0.00000	0.05860
14202	14221	0	0.00240	0.01870	0.00000	0.04500
14203	14225	0	0.00800	0.07200	0.00000	0.15120
14203	14500	0	0.00038	0.00281	0.00000	0.00260
14204	14215	0	0.01180	0.06900	0.00000	0.14400
14205	14215	0	0.00850	0.05400	0.00000	0.09800

From Bus	To Bus		Series (p.u.)		Charging (p.u.)	
Number	Number	Section	Resistance	Reactance	Conductance	Susceptance
14205	14230	0	0.00770	0.04490	0.00000	0.09000
14206	14216	0	0.00035	0.00143	0.00000	0.31160
14206	14218	0	0.00020	0.00070	0.00000	0.17000
14206	14270	0	0.00030	0.00100	0.00000	0.06148
14207	14231	0	0.00190	0.01714	0.00000	0.05932
14207	15202	0	0.00096	0.00832	0.00000	0.03008
14207	15211	0	0.00161	0.01460	0.00000	0.05006
14209	19042	0	0.00830	0.08790	0.00000	0.16934
14209	19052	0	0.00840	0.08870	0.00000	0.17078
14210	14228	0	0.00090	0.00930	0.00000	0.03660
14210	14232	0	0.00085	0.00837	0.00000	0.00000
14210	15201	0	0.00081	0.00781	0.00000	0.02100
14212	14270	0	0.00100	0.01010	0.00000	0.22772
14212	15201	0	0.00040	0.00400	0.00000	0.00720
14216	14219	0	0.00210	0.01680	0.00000	0.03400
14216	14239	0	0.00135	0.00746	0.00000	0.01031
14217	14220	0	0.00050	0.00501	0.00000	0.01877
14217	14221	0	0.00158	0.01515	0.00000	0.03154
14217	14227	0	0.00089	0.00887	0.00000	0.02000
14218	14227	0	0.00053	0.00220	0.00000	0.53400
14219	14221	0	0.00480	0.03720	0.00000	0.07200
14219	14236	0	0.00388	0.02936	0.00000	0.06164
14220	14221	0	0.00073	0.00721	0.00000	0.02591
14221	15211	0	0.00015	0.00130	0.00000	0.00000
14221	15211	0	0.00015	0.00130	0.00000	0.00000
14221	19062	0	0.00001	0.00030	0.00000	0.00000
14222	14243	0	0.01370	0.09600	0.00000	0.16740
14222	14250	0	0.00000	0.00030	0.00000	0.00000
14222	19501	0	0.01580	0.10970	0.00000	0.19112
14225	14229	0	0.00666	0.04868	0.00000	0.09270
14226	14229	0	0.00582	0.04254	0.00000	0.08200
14226	14500	0	0.00266	0.01981	0.00000	0.04460
14226	15219	0	0.00483	0.02824	0.00000	0.06230
14226	19068	0	0.00000	0.00200	0.00000	0.00000
14228	14231	0	0.00080	0.00900	0.00000	0.03540
14230	14234	0	0.00361	0.02105	0.00000	0.04218
14231	14246	0	0.00133	0.01054	0.00000	0.01916
14231	15201	0	0.00213	0.01867	0.00000	0.06788
14231	19052	0	0.00397	0.03480	0.00000	0.12662
14231	19062	0	0.00272	0.02740	0.00000	0.13488
14232	14239	0	0.00197	0.01540	0.00000	0.05855
14232	15230	0	0.00074	0.00580	0.00000	0.01937
14233	15230	0	0.00182	0.01419	0.00000	0.03918
14234	14249	0	0.00420	0.02600	0.00000	0.04890

From Bus	To Bus		Series (p.u.)		Charging (p.u.)	
Number	Number	Section	Resistance	Reactance	Conductance	Susceptance
14235	14238	0	0.00090	0.00860	0.00000	0.01880
14236	15207	0	0.00000	0.00030	0.00000	0.00000
14236	15219	0	0.00083	0.00470	0.00000	0.01005
14238	19052	0	0.00710	0.06470	0.00000	0.14380
14241	15202	0	0.00000	0.00030	0.00000	0.00000
14243	19062	0	0.00300	0.02130	0.00000	0.03710
14246	19208	0	0.00067	0.00526	0.00000	0.00956
14249	14250	0	0.00000	0.00030	0.00000	0.00000
14350	14362	0	0.02710	0.12160	0.00000	0.01664
14350	17001	0	0.01530	0.09430	0.00000	0.01314
14350	19221	0	0.03800	0.23370	0.00000	0.03264
14352	15103	0	0.00000	0.00030	0.00000	0.00000
14356	14357	0	0.00010	0.00030	0.00000	0.00000
14356	17013	0	0.01060	0.06490	0.00000	0.00904
14356	19057	0	0.01710	0.10530	0.00000	0.01470
14356	19211	0	0.00270	0.01660	0.00000	0.00232
14357	14358	0	0.03091	0.25063	0.00000	0.02980
14357	19048	0	0.03480	0.14890	0.00000	0.01976
14357	19067	0	0.01540	0.09480	0.00000	0.01322
14358	19057	0	0.02960	0.12340	0.00000	0.01630
14359	19044	0	0.01370	0.03790	0.00000	0.00448
14359	19057	0	0.08820	0.24420	0.00000	0.02622
15001	15041	0	0.00176	0.04189	0.00000	3.32630
15011	15051	0	0.00026	0.00382	0.00000	0.41947
15011	15089	0	0.00048	0.01091	0.00000	1.06576
15021	15061	0	0.00034	0.00724	0.00000	0.68725
15021	15090	0	0.00003	0.00069	0.00000	0.64820
15021	15090	0	0.00003	0.00067	0.00000	0.62620
15021	15090	0	0.00003	0.00071	0.00000	0.53580
15031	15033	0	0.00000	0.00010	0.00000	0.00000
15032	15033	0	0.00000	0.00010	0.00000	0.00000
15034	19038	3	0.00000	-0.01800	0.00000	0.00000
15034	19038	2	0.00182	0.05144	0.00000	4.89200
15034	19038	1	0.00000	-0.01800	0.00000	0.00000
15041	15051	0	0.00046	0.00874	0.00000	0.70448
15089	15090	0	0.00020	0.00428	0.00000	0.40122
15090	15092	0	0.00000	0.00050	0.00000	0.00000
15090	15093	0	0.00020	0.00550	0.00000	0.51350
15090	15094	0	0.00000	0.00050	0.00000	0.00000
15101	15102	0	0.00135	0.00236	0.00000	0.00014
15102	15103	0	0.06184	0.18458	0.00000	0.01192
15102	15108	0	0.00056	0.00168	0.00000	0.00011
15103	19044	0	0.02706	0.08076	0.00000	0.00521
15105	15133	0	0.00030	0.00130	0.00000	0.00020

From Bus	To Bus		Series (p.u.)		Charging (p.u.)	
Number	Number	Section	Resistance	Reactance	Conductance	Susceptance
15106	15109	0	0.02469	0.11702	0.00000	0.01640
15106	15115	0	0.03040	0.14536	0.00000	0.01996
15106	15134	0	0.00901	0.01407	0.00000	0.00144
15107	15109	0	0.01739	0.09977	0.00000	0.01360
15107	15117	0	0.00988	0.04722	0.00000	0.00648
15107	15127	0	0.01327	0.03312	0.00000	0.00762
15107	15128	0	0.03472	0.06072	0.00000	0.00714
15108	15112	0	0.01742	0.05146	0.00000	0.00337
15108	17001	2	0.01319	0.11675	0.00000	0.01592
15108	17001	1	0.11333	0.39946	0.00000	0.05064
15109	15117	0	0.01282	0.06033	0.00000	0.00856
15111	15112	0	0.00004	0.00017	0.00000	0.00000
15112	15116	0	0.01617	0.47870	0.00000	0.00313
15113	15116	0	0.00178	0.00587	0.00000	0.00040
15113	15122	0	0.00321	0.01013	0.00000	0.00067
15114	15119	0	0.00549	0.01724	0.00000	0.00234
15114	15121	0	0.01218	0.04139	0.00000	0.00732
15114	15133	0	0.00160	0.00730	0.00000	0.00110
15115	15119	0	0.00711	0.03321	0.00000	0.00468
15115	15132	0	0.00117	0.00222	0.00000	0.00026
15118	15126	0	0.00290	0.01385	0.00000	0.00190
15118	15129	0	0.00430	0.02030	0.00000	0.00290
15119	15126	0	0.01638	0.07814	0.00000	0.01080
15121	15125	0	0.01000	0.03120	0.00000	0.00630
15122	15129	0	0.01422	0.06811	0.00000	0.00466
15123	15132	0	0.00119	0.00225	0.00000	0.00013
15124	15126	0	0.00046	0.00292	0.00000	0.00094
15125	15129	0	0.00888	0.02131	0.00000	0.00964
15127	15129	0	0.03392	0.10392	0.00000	0.02028
15132	15133	0	0.00040	0.00200	0.00000	0.00030
15170	19071	0	0.00000	0.00050	0.00000	0.00000
15171	19067	0	0.00000	0.00050	0.00000	0.00000
15201	15202	0	0.00120	0.00988	0.00000	0.04042
15201	15218	0	0.00141	0.01238	0.00000	0.04502
15203	15207	0	0.00136	0.00845	0.00000	0.06192
15203	15208	0	0.00110	0.00671	0.00000	0.05070
15204	15207	0	0.00101	0.00877	0.00000	0.03218
15204	15209	0	0.00067	0.00584	0.00000	0.02142
15204	15211	0	0.00610	0.03608	0.00000	0.07322
15204	15211	0	0.00611	0.03614	0.00000	0.07334
15204	15217	0	0.00031	0.00185	0.00000	0.00374
15204	15217	0	0.00031	0.00185	0.00000	0.00374
15205	15207	0	0.00082	0.00716	0.00000	0.02604
15205	15213	0	0.00080	0.00730	0.00000	0.02660

From Bus	To Bus		Series (p.u.)		Charging (p.u.)	
Number	Number	Section	Resistance	Reactance	Conductance	Susceptance
15206	15215	0	0.00948	0.05145	0.00000	0.10522
15206	15216	0	0.00237	0.01409	0.00000	0.02852
15206	15216	0	0.00237	0.01409	0.00000	0.02852
15207	15209	0	0.00123	0.01072	0.00000	0.03912
15207	15214	0	0.00314	0.01778	0.00000	0.04698
15208	15230	0	0.00109	0.00941	0.00000	0.03512
15208	19052	0	0.00249	0.02143	0.00000	0.08008
15209	15211	0	0.00385	0.02510	0.00000	0.17054
15211	19062	0	0.00003	0.00030	0.00000	0.00000
15211	19062	0	0.00002	0.00030	0.00000	0.00000
15212	15216	0	0.00187	0.01103	0.00000	0.02236
15212	19502	0	0.00000	0.00050	0.00000	0.00000
15212	19502	0	0.00000	0.00050	0.00000	0.00000
15213	15214	0	0.00229	0.01096	0.00000	0.08382
15213	15216	0	0.00148	0.01296	0.00000	0.04742
15213	15222	0	0.00315	0.01386	0.00000	0.01562
15218	15230	0	0.00050	0.00435	0.00000	0.01582
15230	19052	0	0.00157	0.01274	0.00000	0.04801
16100	16104	0	0.00101	0.01057	0.00000	0.19400
16101	16104	3	0.00511	0.05386	0.00000	0.96200
16101	16104	2	0.00000	0.00001	0.00000	0.00000
16101	16104	1	0.00000	0.00010	0.00000	0.00000
16101	16109	0	0.00407	0.04244	0.00000	0.77763
16101	17010	0	0.00002	0.00021	0.00000	0.00379
16102	16104	0	0.00498	0.05195	0.00000	0.95080
16102	16104	0	0.00491	0.05135	0.00000	0.94180
16103	16105	0	0.00063	0.00663	0.00000	0.12300
16103	16107	0	0.00817	0.08550	0.00000	1.60340
16104	16106	1	0.00508	0.04856	0.00000	1.07680
16104	16106	5	0.00000	0.00010	0.00000	0.00000
16104	16106	3	0.00592	0.06168	0.00000	1.13960
16104	16106	4	0.00000	-0.02420	0.00000	0.00000
16104	16106	2	0.00000	-0.02004	0.00000	0.00000
16105	16109	1	0.00000	0.00010	0.00000	0.00000
16105	16109	3	0.00185	0.01929	0.00000	0.35347
16105	16109	2	0.00000	-0.01737	0.00000	0.00000
16105	17005	0	0.00108	0.01185	0.00000	0.19640
16216	16217	0	0.04330	0.23308	0.00000	0.00000
16216	16220	0	0.01090	0.06078	0.00000	0.00000
16216	89992	0	0.00000	0.11142	0.00000	0.00000
16217	16220	0	0.01340	0.07974	0.00000	0.00000
16217	89991	0	0.00000	0.10983	0.00000	0.00000
16220	89990	0	0.00000	0.04913	0.00000	0.00000
17001	89989	0	0.00000	0.12131	0.00000	0.00000

From Bus	To Bus		Series (p.u.)		Charging (p.u.)	
Number	Number	Section	Resistance	Reactance	Conductance	Susceptance
17002	17004	0	0.02090	0.12609	0.00000	0.00000
17002	17009	0	0.01550	0.14199	0.00000	0.00000
17002	17105	0	0.00330	0.02919	0.00000	0.06369
17004	17013	0	0.15360	0.42814	0.00000	0.00000
17013	19064	0	0.02140	0.13140	0.00000	0.00000
19011	19012	0	0.00290	0.02317	0.00000	0.00000
19011	19012	0	0.00000	0.00760	0.00000	0.00000
19011	19022	0	0.01370	0.09500	0.00000	0.16600
19011	89984	0	0.00000	0.04921	0.00000	0.00000
19012	19022	0	0.02210	0.19372	0.00000	0.00000
19012	19042	0	0.02280	0.16653	0.00000	0.00000
19012	19082	0	0.00457	0.03292	0.00000	0.06020
19012	89983	0	0.00000	0.01000	0.00000	0.00000
19022	19042	0	0.00330	0.02916	0.00000	0.00000
19022	19314	0	0.00830	0.06278	0.00000	0.00000
19022	89982	0	0.00000	0.01144	0.00000	0.00000
19037	19315	2	0.00307	0.04261	0.00000	0.69365
19037	19315	1	0.00000	0.00001	0.00000	0.00000
19042	19204	0	0.00620	0.06590	0.00000	0.12680
19042	89981	0	0.00000	0.05233	0.00000	0.00000
19044	19065	0	0.01040	0.06380	0.00000	0.00890
19044	19066	0	0.01670	0.04690	0.00000	0.00568
19044	19600	0	0.00000	0.00050	0.00000	0.00000
19045	19215	0	0.00740	0.05120	0.00000	0.08892
19045	19410	0	0.00200	0.01510	0.00000	0.03030
19045	19410	0	0.00200	0.01510	0.00000	0.03030
19047	19064	0	0.00900	0.05550	0.00000	0.00774
19047	19221	0	0.00950	0.05820	0.00000	0.00812
19048	19222	0	0.03640	0.10210	0.00000	0.01240
19052	19055	0	0.00800	0.06350	0.00000	0.10920
19052	19061	0	0.00430	0.03230	0.00000	0.06678
19052	19500	0	0.00290	0.03020	0.00000	0.05792
19053	19315	2	0.00563	0.07809	0.00000	1.27136
19053	19315	1	0.00000	-0.04220	0.00000	0.00000
19055	19061	0	0.01820	0.11740	0.00000	0.01510
19055	19068	0	0.02200	0.11840	0.00000	0.01470
19055	19410	0	0.00740	0.05810	0.00000	0.11940
19057	19064	0	0.04590	0.14990	0.00000	0.01814
19057	19652	0	0.00000	0.00050	0.00000	0.00000
19062	19502	0	0.00420	0.03190	0.00000	0.06480
19062	19502	0	0.00420	0.03190	0.00000	0.06480
19065	19066	0	0.00840	0.05160	0.00000	0.00720
19065	19071	0	0.00840	0.05160	0.00000	0.00720
19065	19211	0	0.03100	0.19070	0.00000	0.00000

From Bus	To Bus		Series (p.u.)		Charging (p.u.)	
Number	Number	Section	Resistance	Reactance	Conductance	Susceptance
19067	19071	0	0.00830	0.05100	0.00000	0.00712
19068	19218	0	0.00868	0.09030	0.00000	0.01080
19204	19500	0	0.00770	0.00626	0.00000	0.20440
19215	19502	0	0.00170	0.01150	0.00000	0.01990
19314	19501	0	0.00475	0.03299	0.00000	0.05726
19314	89980	0	0.00000	0.05620	0.00000	0.00000
19410	89979	0	0.00000	0.28985	0.00000	0.00000
79024	79032	1	0.00000	-0.04540	0.00000	0.00000
79024	79032	2	0.00570	0.06500	0.00000	1.00700
79024	79032	1	0.00000	-0.04540	0.00000	0.00000
79024	79032	2	0.00550	0.06540	0.00000	1.00700
79024	79053	1	0.00500	0.05950	0.00000	0.91620
79024	79053	2	0.00000	-0.04170	0.00000	0.00000
79024	79053	1	0.00490	0.05980	0.00000	0.91080
79024	79053	2	0.00000	-0.04190	0.00000	0.00000
79028	79093	0	0.00327	0.01100	0.00000	0.06906
79032	89962	0	0.00000	0.02776	0.00000	0.00000
79043	79063	1	0.00000	-0.10397	0.00000	0.00000
79043	79063	2	0.01620	0.16110	0.00000	0.29490
79043	79096	1	0.00000	-0.10397	0.00000	0.00000
79043	79096	2	0.00229	0.02277	0.00000	0.04144
79093	79096	0	0.00660	0.06578	0.00000	0.11970

Table C.2 Transformer connections of System 2

From Bus	To Bus		Series (p.u.)		From Magnetizing (p.u.)	
Number	Number	Ratio	Resistance	Reactance	Conductance	Susceptance
14000	14100	0.97951	0.00021	0.01671	0.00252	-0.02094
14000	14100	0.97951	0.00019	0.01641	0.00264	-0.02487
14001	14101	1.02375	0.00018	0.01060	0.00313	-0.00686
14004	14356	1.02435	0.00057	0.04562	0.00257	-0.02958
14004	14357	1.02435	0.00055	0.04589	0.00243	-0.02487
14005	14231	0.98438	0.00011	0.00839	0.00486	-0.03666
14005	14231	0.98438	0.00011	0.00838	0.00504	-0.03948
14005	14231	0.98438	0.00007	0.00857	0.00279	-0.00315
14005	99993	1.05000	-0.00003	0.01261	0.00349	-0.03042
14006	14234	0.99590	0.00047	0.04129	0.00085	-0.00205
14006	14234	0.99590	0.00046	0.04124	0.00095	-0.00288
14007	14238	1.05000	0.00040	0.03150	0.00141	-0.00240
14100	14204	1.00000	0.00111	0.04225	0.00056	-0.00092
14101	14211	1.00000	0.00028	0.01381	0.00172	-0.00563
14101	14211	1.00000	0.00029	0.01390	0.00169	-0.00600
14102	14221	0.97500	0.00028	0.01390	0.00168	-0.00589
14102	14221	0.97500	0.00027	0.01404	0.00163	-0.00529

From Bus	To Bus		Series (p.u.)		From Magnetizing (p.u.)	
Number	Number	Ratio	Resistance	Reactance	Conductance	Susceptance
14102	14221	0.97500	0.00019	0.01328	0.00165	-0.01530
14222	14355	0.97500	0.00340	0.08392	0.00038	-0.00131
14222	14355	0.97500	0.00318	0.08594	0.00018	-0.00025
14225	14356	1.00000	0.00107	0.03440	0.00094	-0.00272
14225	14357	1.00000	0.00085	0.03516	0.00058	-0.00258
15001	16100	1.02375	0.00018	0.01456	0.00140	-0.00090
15011	99988	1.02380	0.00006	0.00298	0.00000	0.00000
15011	99989	1.02380	0.00056	0.01153	0.00000	0.00000
15021	14931	1.07763	0.00011	0.00973	0.00567	-0.02637
15021	14932	1.07763	0.00011	0.00964	0.00583	-0.02913
15021	14933	1.07763	0.00011	0.00977	0.00583	-0.03833
15034	15031	1.00000	0.00000	0.02000	0.00000	0.00000
15034	15032	1.00000	0.00000	0.02000	0.00000	0.00000
15041	99987	1.02380	0.00005	0.01308	0.00000	0.00000
15051	99985	1.05000	0.00056	0.01153	0.00000	0.00000
15051	99986	1.05000	0.00056	0.01153	0.00000	0.00000
15061	99982	1.05000	0.00015	0.01717	0.00000	0.00000
15061	99983	1.05000	0.00015	0.01717	0.00000	0.00000
15061	99984	1.05000	0.00015	0.01717	0.00000	0.00000
15094	15163	1.05000	0.00000	0.00280	0.00000	0.00000
15206	15107	1.02500	0.00000	0.04222	0.00000	0.00000
15206	15107	1.02500	0.00000	0.04065	0.00000	0.00000
15207	99988	1.00000	0.00006	0.00958	0.00000	0.00000
15207	99989	1.00000	0.00055	-0.00012	0.00000	0.00000
15215	15124	1.00000	0.00000	0.03776	0.00000	0.00000
15215	15125	1.00000	0.00000	0.03801	0.00000	0.00000
15215	99987	1.00000	0.00006	-0.00183	0.00000	0.00000
15222	99985	1.00000	0.00055	-0.00012	0.00000	0.00000
15222	99986	1.00000	0.00055	-0.00012	0.00000	0.00000
15230	99982	1.00000	0.00015	0.00553	0.00000	0.00000
15230	99983	1.00000	0.00015	0.00553	0.00000	0.00000
15230	99984	1.00000	0.00015	0.00553	0.00000	0.00000
16103	99978	1.00000	0.00013	-0.01194	0.00292	-0.01192
16105	99977	1.00000	-0.00014	-0.01249	0.00295	-0.01192
16106	16220	1.00000	0.00015	0.01614	0.00130	-0.00065
16107	99993	1.00000	0.00020	-0.00011	0.00000	0.00000
16109	17105	1.00000	0.00000	0.02827	0.00000	0.00000
16216	99978	1.00000	0.00013	0.02844	0.00000	0.00000
16217	16000	0.99526	0.00039	0.02550	0.00202	-0.00551
16217	16001	0.99526	0.00039	0.02550	0.00202	-0.00551
16220	99977	1.00000	0.00041	0.02927	0.00000	0.00000
17002	17001	1.00000	0.00000	0.09017	0.00000	0.00000
17002	17001	1.00000	0.00000	0.09183	0.00000	0.00000
17005	17004	1.02500	0.00000	0.04433	0.00000	0.00000

From Bus	To Bus		Series (p.u.)		From Magnetizing (p.u.)	
Number	Number	Ratio	Resistance	Reactance	Conductance	Susceptance
17010	17009	0.98040	0.00000	0.04444	0.00000	0.00000
19037	19011	0.97510	0.00004	0.01420	0.00000	0.00000
19038	19011	1.07520	0.00000	0.01514	0.00000	0.00000
19045	19044	0.98040	0.00000	0.03000	0.00000	0.00000
19045	19044	0.98040	0.00000	0.03000	0.00000	0.00000
19053	19054	1.00000	0.00004	0.01420	0.00000	0.00000
19054	19052	1.00000	0.00000	0.01586	0.00000	0.00000
19218	19222	1.02500	0.00000	0.03000	0.00000	0.00000
19315	19314	1.00000	0.00005	0.01795	0.00000	0.00000
79028	79031	1.00000	0.00054	0.02695	0.00000	0.00000
79032	79031	1.00000	0.00040	0.02270	0.00000	0.00000
79032	79031	1.00000	0.00040	0.02270	0.00000	0.00000
79053	19062	0.97500	0.00006	0.01614	0.00000	0.00000
79053	19062	0.97500	0.00005	0.01614	0.00000	0.00000
79053	19062	0.97500	0.00006	0.01644	0.00000	0.00000
79063	79062	1.00000	0.00100	0.04220	0.00000	0.00000
79064	79063	1.00000	0.00000	0.02333	0.00000	0.00000

Table C.3 Shunt devices connected in System 2

Bus		Shunt	
Number	Type	MW	MVAr
14101	Gen. Bus	0.00	-90.00
14216	Load Bus	0.00	35.00
14219	Load Bus	0.00	300.00
14221	Load Bus	0.00	153.00
14227	Load Bus	0.00	43.20
14356	Gen. Bus	0.00	49.20
14358	Load Bus	0.00	15.60
15101	Load Bus	0.00	28.80
15108	Load Bus	0.00	27.00
15119	Load Bus	0.00	27.00
15121	Load Bus	0.00	40.00
15207	Load Bus	0.00	150.00
16216	Load Bus	0.00	39.60
16220	Load Bus	0.00	33.10
19037	Load Bus	0.00	-48.00
19052	Load Bus	0.00	38.90
19062	Load Bus	0.00	200.00
79031	Gen. Bus	0.00	165.00

APPENDIX D

EXAMPLE OF MATLAB SCRIPTS

This appendix contains a sample of the Matlab code used in examples. The scripts below creates the *H* matrix from the downloaded text file in IEEE format with branch information of System 1 and a text file containing measurements.

```
clear
system='ieee57cdf.dat'
[Y]=IEEEtoYbus(system);
G=real(Y);
B=imag(Y);

%intial guess Flat start
[Vo,Phaseo]=IEEEintialguess(system);
V=Vo;
Phase=Phaseo;

%Mesurement Set Uses PSAT power flow solution
MeasureSet='57BaseCaseMeasure.txt';
[BusP, Pinj, BusQ, Qinj, sendQ, reciveQ, Qflow, Pflow, sendP, re-
civeP,LineIDp,LineIDq]=Measurementreader(MeasureSet);

%Branch Information for Power Flow Measurements
[send,recive,Circuit,g,b,Charging] = IEEEBranchInfo(system);
Z=[Pinj;Qinj;Pflow;Qflow];
[r,c]=find(Y~=0);
HpV=zeros(size(BusP,1),size(Y,1));
HpPhase=zeros(size(BusP,1),size(Y,1));
hPinj=zeros(size(BusP,1),1);
hQinj=zeros(size(BusQ,1),1);
for k=1:size(BusP,1)
    m=BusP(k);
    Hcolumn=0;
    Hcolumn=find(r==m);
    for l=1:size(Hcolumn)
        n=c(Hcolumn(l));
        if n~=m
            HpPhase(k,n)=V(n)*V(m)*(G(m,n)*sin(Phase(m)-Phase(n))-
B(m,n)*cos(Phase(m)-Phase(n)));
            HpPhase(k,m)=-HpPhase(k,n)+HpPhase(k,m);
            HpV(k,n)=V(m)*(G(m,n)*cos(Phase(m)-
Phase(n))+B(m,n)*sin(Phase(m)-Phase(n)));
            HpV(k,m)=V(n)*(G(m,n)*cos(Phase(m)-
Phase(n))+B(m,n)*sin(Phase(m)-Phase(n)))+HpV(k,m);
            hPinj(k,1)=V(m)*V(n)*(G(m,n)*cos(Phase(m)-
Phase(n))+B(m,n)*sin(Phase(m)-Phase(n)))+hPinj(k,1);
        else
            HpV(k,m)=V(m)*(G(m,m)*cos(Phase(m)-
Phase(m))+B(m,m)*sin(Phase(m)-Phase(m)))+HpV(k,m)+V(m)*G(m,m);
            HpPhase(k,m)=-V(n)*V(m)*(G(m,n)*sin(Phase(m)-Phase(n))-
B(m,n)*cos(Phase(m)-Phase(n)))+HpPhase(k,m)-V(m)*V(m)*B(m,m);
        end
    end
end
HqV=zeros(size(BusQ,1),size(Y,1));
```

```
HqPhase=zeros(size(BusQ,1),size(Y,1));
for k=1:size(BusQ,1)
    m=BusQ(k);
    Hcolumn=0;
    Hcolumn=find(r==m);
    for l=1:size(Hcolumn)
        n=c(Hcolumn(l));
        if n~=m
            HqPhase(k,n)=V(n)*V(m)*(-G(m,n)*cos(Phase(m)-Phase(n))-
B(m,n)*sin(Phase(m)-Phase(n)));
            HqPhase(k,m)=-HqPhase(k,n)+HqPhase(k,m);
            HqV(k,n)=V(m)*(G(m,n)*sin(Phase(m)-Phase(n))-
B(m,n)*cos(Phase(m)-Phase(n)));
            HqV(k,m)=V(n)*(G(m,n)*sin(Phase(m)-Phase(n))-
B(m,n)*cos(Phase(m)-Phase(n)))+HqV(k,m);
            hQinj(k,1)=V(m)*V(n)*(G(m,n)*cos(Phase(m)-Phase(n))-
B(m,n)*sin(Phase(m)-Phase(n)))+hQinj(k,1);
        else
            HqV(k,m)=V(n)*(G(m,n)*sin(Phase(m)-Phase(n))-
B(m,n)*cos(Phase(m)-Phase(n)))+HqV(k,m)-V(m)*B(m,m);
            HqPhase(k,m)=-V(n)*V(m)*(-G(m,n)*cos(Phase(m)-Phase(n))-
B(m,n)*sin(Phase(m)-Phase(n)))+HqPhase(k,m)-V(m)*V(m)*G(m,m);
        end
    end
end

for k=1:size(sendQ,1)
    BusS=sendQ(k);
    BusR=reciveQ(k);
    branch=0;
    S=[];
    S=find(send==BusS);
    for m=1:size(S,2)
        if recive(S(m))==BusR
            if Circuit(S(m))==LineIDq(k)
                branch=S(m);
            end
        end
    end
    if branch==0
        S=find(recive==BusS);
        for m=1:size(S,2)
          if send(S(m))==BusR
              if Circuit(S(m))==LineIDq(k)
                  branch=S(m);
              end
          end
        end
    end
    HqfPhase(k,BusS)=-V(BusS)*V(BusR)*(g(branch)*cos(Phase(BusS)-
Phase(BusR))-b(branch)*sin(Phase(BusS)-Phase(BusR)));
    HqfPhase(k,BusR)=-HqfPhase(k,BusS);
```

```
    HqfV(k,BusS)=-V(BusR)*(g(branch)*sin(Phase(BusS)-Phase(BusR))-
b(branch)*cos(Phase(BusS)-Phase(BusR)))-
2*(b(branch)+imag(Charging(branch)))*V(BusS);
    HqfV(k,BusR)=-V(BusS)*(g(branch)*sin(Phase(BusS)-Phase(BusR))-
b(branch)*cos(Phase(BusS)-Phase(BusR)));
    hQflow(k,1)=-V(BusS)*V(BusS)*(b(branch)+imag(Charging(branch)))-
V(BusR)*V(BusS)*(g(branch)*cos(Phase(BusS)-
Phase(BusR))+b(branch)*sin(Phase(BusS)-Phase(BusR)));
end

for k=1:size(sendP,1)
    BusS=sendP(k);
    BusR=reciveP(k);
    branch=0;
    S=[];
    S=find(send==BusS);
    for m=1:size(S,2)
        if recive(S(m))==BusR
            if Circuit(S(m))==LineIDp(k)
                branch=S(m);
            end
        end
    end
    if branch==0
        S=find(recive==BusS);
        for m=1:size(S,2)
          if send(S(m))==BusR
              if Circuit(S(m))==LineIDp(k)
                  branch=S(m);
              end
          end
        end
    end
    HpfPhase(k,BusS)=V(BusS)*V(BusR)*(g(branch)*sin(Phase(BusS)-
Phase(BusR))-b(branch)*cos(Phase(BusS)-Phase(BusR)));
    HpfPhase(k,BusR)=-HpfPhase(k,BusS);
    HpfV(k,BusS)=-V(BusR)*(g(branch)*cos(Phase(BusS)-Phase(BusR))-
b(branch)*sin(Phase(BusS)-
Phase(BusR)))+2*(g(branch)+real(Charging(branch)))*V(BusS);
    HpfV(k,BusR)=-V(BusS)*(g(branch)*cos(Phase(BusS)-Phase(BusR))-
b(branch)*sin(Phase(BusS)-Phase(BusR)));
    hPflow(k,1)=V(BusS)*V(BusS)*(g(branch)+real(Charging(branch)))-
V(BusR)*V(BusS)*(g(branch)*cos(Phase(BusS)-
Phase(BusR))+b(branch)*sin(Phase(BusS)-Phase(BusR)));
end

% Formation of the intial H matrix
H=[HpfPhase, HpfV; HpPhase,HpV;HqfPhase,HqfV;HqPhase,HqV];
H(:,1)=[];
Hphase=[HpfPhase;HpPhase];
Hphase(:,1)=[];
[Hprows,Hpcolomns]=size(Hphase)
Gphase=Hphase'*Hphase;
RankHphase=rank(Hphase)
```

```
[Vphase,Eigphase]=eig(Gphase);

% Testing the Equations

% Insertion of the First PMU  Effects on Just Power Phase matrix
deltG=1
for k=1:size(Vphase,1)
    PredictedEig(k,1)=Vphase(k,1)^2*deltG;
end
for k=1:Hpcolomns
    Hphasep=[Hphase;zeros(1,Hpcolomns)];
    Hphasep(Hprows+1,k)=1;
    EV=eig(Hphasep'*Hphasep);
    ExpEig(k,1)=EV(1);
    DeltaEigExp=ExpEig-Eigphase(1,1);
end
S=1:56;
plot(S,PredictedEig,'r+', S,DeltaEigExp,'go')
xlabel('G matrix changed by +1 at k,k')
ylabel('Change in smallest Eigenvalue')
legend('Predicted','Actual')
title('H of Power and Phase')
w=[0:0.01:.1,.2:.1:2];
for k=1:size(w,2)
    WPredictedEig(k,1)=Vphase(32,1)^2*w(k)^2;
    Hphasep=[Hphase;zeros(1,Hpcolomns)];
    Hphasep(Hprows+1,32)=w(k);
    EV=eig(Hphasep'*Hphasep);
    WExpEig(k,1)=EV(1);
    WDeltaEigExp(k,1)=WExpEig(k,1)-Eigphase(1,1);
end
figure
plot(w,WPredictedEig,'g--',w,WDeltaEigExp,'r:')
xlabel('Size in Change of H matrix col 32')
ylabel('Change in smallest Eigenvalue')
legend('Predicted','Actual')
title('H of Power and Phase')
for k=1:Hpcolomns
    PredictedEigDelta(k,1)=Vphase(32,k)^2*deltG;
    PreEig(k,1)=Eigphase(k,k)+PredictedEigDelta(k);

end
Hphasep=[Hphase;zeros(1,Hpcolomns)];
Hphasep(Hprows+1,32)=1;
EV=eig(Hphasep'*Hphasep);
Orginal=ones(56,1);
Predicted=2*Orginal;
Exp=3*Orginal;
K0=cond(Gphase);
KPredicted=max(PreEig)/min(PreEig);
Kactual=cond(Hphasep'*Hphasep);
figure
plot(diag(Eigphase),Orginal,'r+',PreEig,Predicted,'go',EV,Exp,'b^')
axis([0,6500,0,4])
```

```
xlabel('EigenValues')
legend('Original','Predicted','Actual')
title('H of Power and Phase')

%  PMU measures both phase and angle What would the including volt
measure
%  do
[Hrows,Hcolomns]=size(H);
G=H'*H;
RankH=rank(H);
[VG,EigG]=eig(G);

deltG=1;
kG=cond(G)
for k=1:size(Vphase,1)
    PredEigPV(k,1)=VG(k,1)^2*deltG+VG(k+57,1)^2*deltG;
    LargestEig(k,1)=VG(k,113)^2*deltG+VG(k+57,113)^2*deltG;
    deltaK(k,1)=(VG(k,113)^2-kG*VG(k,1)^2)/(EigG(1,1));
end
for k=1:56
    Hp=[H;zeros(2,Hcolomns)];
    Hp(Hrows+1,k)=1;
    Hp(Hrows+2,k+57)=1;
    EV=eig(Hp'*Hp);
    ExpEigPV(k,1)=EV(1);
    K2(k,1)=cond(Hp'*Hp);
end
DEigExpPV=ExpEigPV-EigG(1,1);
dK2=K2-kG;
figure
plot(S,PredEigPV,'r+', S,DEigExpPV,'go')
xlabel('G matrix changed by +1 at k,k and 57+k,57+k')
ylabel('Change in smallest Eigenvalue')
legend('Predicted','Actual')
title('Entire H')
figure
plot(S,deltaK,'r+', S,dK2,'go')
xlabel('G matrix changed by +1 at k,k and 57+k,57+k')
ylabel('Change in Condition Number')
legend('Predicted','Actual')
title('Entire H')
w=[0:0.01:.1,.2:.1:2];
for k=1:size(w,2)
    WPredEigG(k,1)=VG(32,1)^2*w(k)^2+VG(32+57,1)^2*w(k);
    Hp=[H;zeros(2,Hcolomns)];
    Hp(Hrows+1,32)=w(k);
    Hp(Hrows+2,32+57)=w(k);
    EV=eig(Hp'*Hp);
    WExpEigG(k,1)=EV(1);
    WDeltaEigExpG(k,1)=WExpEigG(k,1)-EigG(1,1);
end
figure
plot(w,WPredEigG,'g--',w,WDeltaEigExpG,'r:')
xlabel('Magnitude of Change of H matrix col 32')
```

```
ylabel('Change in smallest Eigenvalue')
legend('Predicted','Actual')
title('Entire H')
for k=1:Hcolomns
    PredEigDeltaG(k,1)=VG(32,k)^2*deltG+VG(32+57,k)^2*deltG;
    PreEigG(k,1)=EigG(k,k)+PredEigDeltaG(k);
end
Hp=[H;zeros(2,Hcolomns)];
Hp(Hrows+1,32)=1;
Hp(Hrows+2,32+57)=1;
EVG=eig(Hp'*Hp);
Orginal=ones(113,1);
Predicted=2*Orginal;
Exp=3*Orginal;
figure
plot(diag(EigG),Orginal,'r+',PreEigG,Predicted,'go',EVG,Exp,'b^')
%plot(diag(EigG),Orginal,'r+',PreEigG,Orginal,'go',EVG,Orginal,'b^')
axis([0,6500,0,4])
xlabel('EigenValues')
legend('Original','Predicted','Actual')
title('Entire H')
K0g=cond(G)
KPredictedg=max(PreEigG)/min(PreEigG);
Kactualg=cond(Hp'*Hp);

figure
plot(S,PredEigPV,'r+', S,DEigExpPV,'go',S,PredictedEig,'rx',
S,DeltaEigExp,'g+');
```

APPENDIX E

EXAMPLES 11, 13, 14, AND 16

E.1 Results of Examples 11, 13, 14, and 16: State Estimation Error

System 2 is tested using pseudorandom noise inserted in the power and voltage magnitude measurements at levels of 5%, 10%, and 15%. The PMU measurements are modeled with 0.5% and 1% noise. Figure 5.1 is a one line diagram of System 2. Appendix C contains information about the electrical connections in System 2. The state estimator solves 1,000 trials each with 0, 15, 30, 45, 60, 75, 90, 105, 120, 135, and 150 PMUs. The PMUs are located using the ranking done as described in Section 5.2. The PMUs are added in the order of rank. Examples presents here are:

- Example 11: 5% noise in SCADA measurements and 0.5% noise in PMU measurements
- Example 13: 10% noise in SCADA measurements and 0.5% noise in PMU measurements
- Example 14: 10% noise in SCADA measurements and 1% noise in PMU measurements
- Example 16: 15% noise in SCADA measurements and 1% noise in PMU measurements.

Examples 12 and 15 are presented in 5.3 - 5.4. Terminology used in the discussion of Example 11, 13, 14, and 16 is explained in 5.5.

The results of Examples 11, 13, 14, and 16 are depicted graphically in 16 figures. These figures are listed in Table E.1.

Table E.1 List of Figures showing results of Examples 11, 13, 14, and 16

Example	Parameter	Figure
11	Maximum voltage phase angle error	E.1
11	RMS voltage phase angle error	E.2
11	Maximum voltage magnitude error	E.3
11	RMS voltage magnitude error	E.4
13	Maximum voltage phase angle error	E.5
13	RMS voltage phase angle error	E.6
13	Maximum voltage magnitude error	E.7
13	RMS voltage magnitude error	E.8
14	Maximum voltage phase angle error	E.9
14	RMS voltage phase angle error	E.10
14	Maximum voltage magnitude error	E.11
14	RMS voltage magnitude error	E.12
16	Maximum voltage phase angle error	E.13
16	RMS voltage magnitude error	E.14
16	Maximum voltage magnitude error	E.15
16	RMS voltage magnitude error	E.16

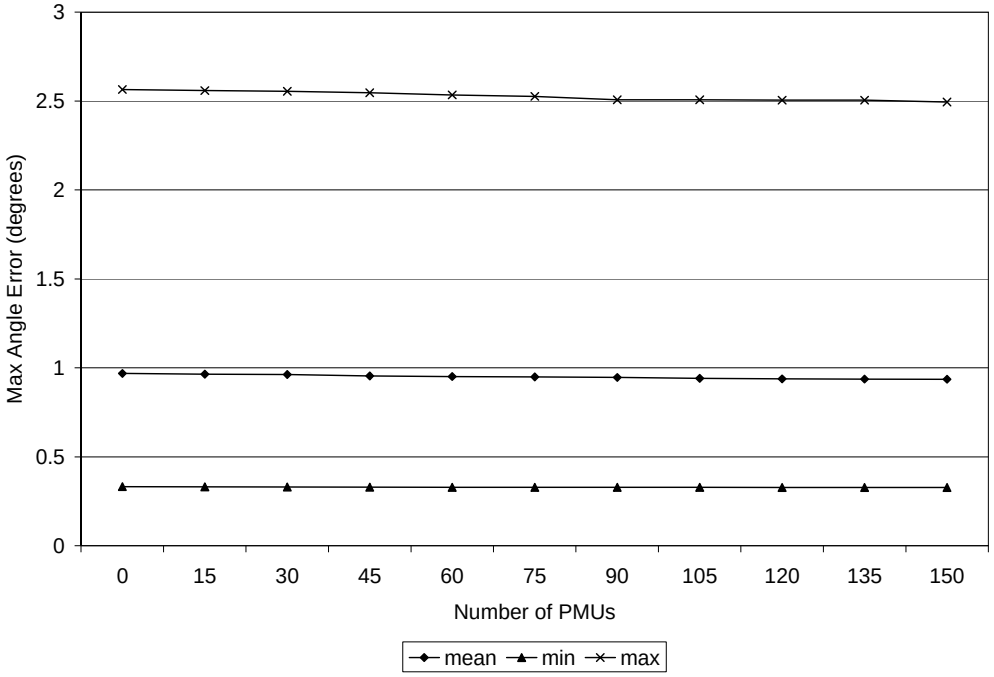

Figure E.1 Maximum voltage angle error for SCADA noise 5% and PMU noise 0.5% on System 2 (Example 11)

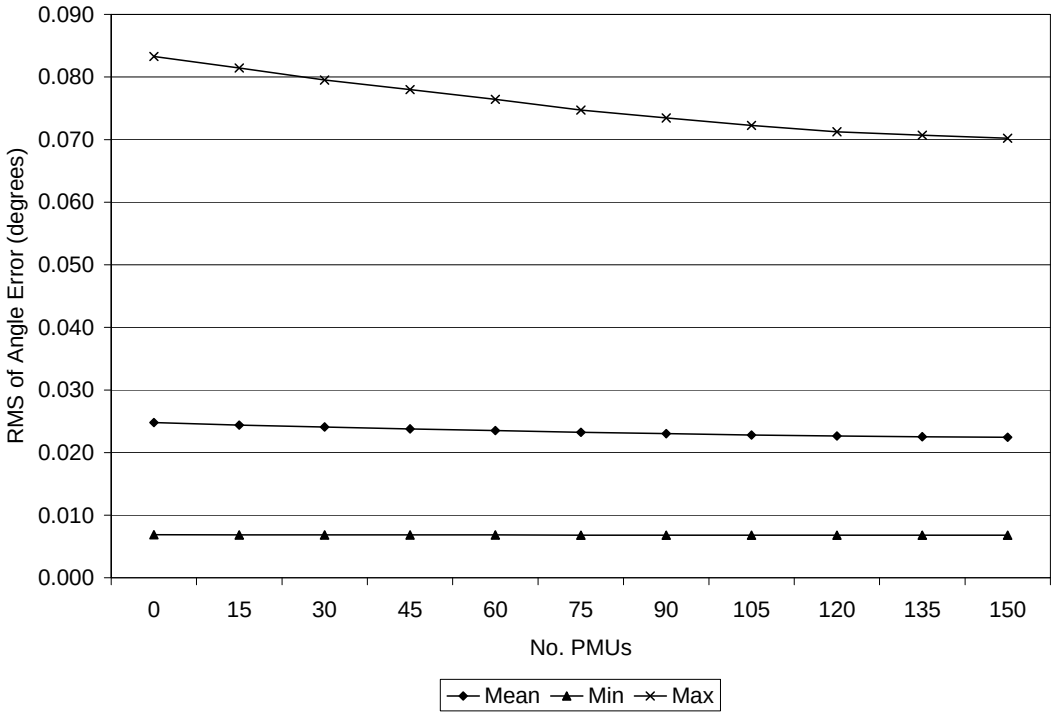

Figure E.2 RMS voltage angle error for Example 11: SCADA noise 5% and PMU noise 0.5% on System 2

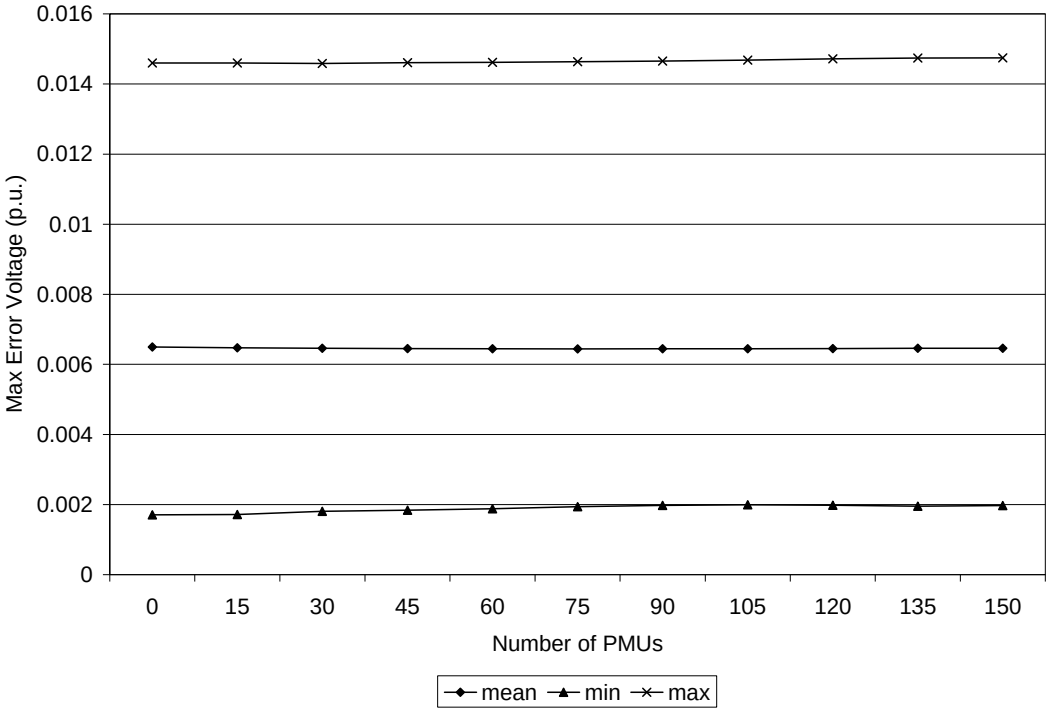

Figure E.3 Maximum voltage magnitude error for Example 11: SCADA noise 5% and PMU noise 0.5% on System 2

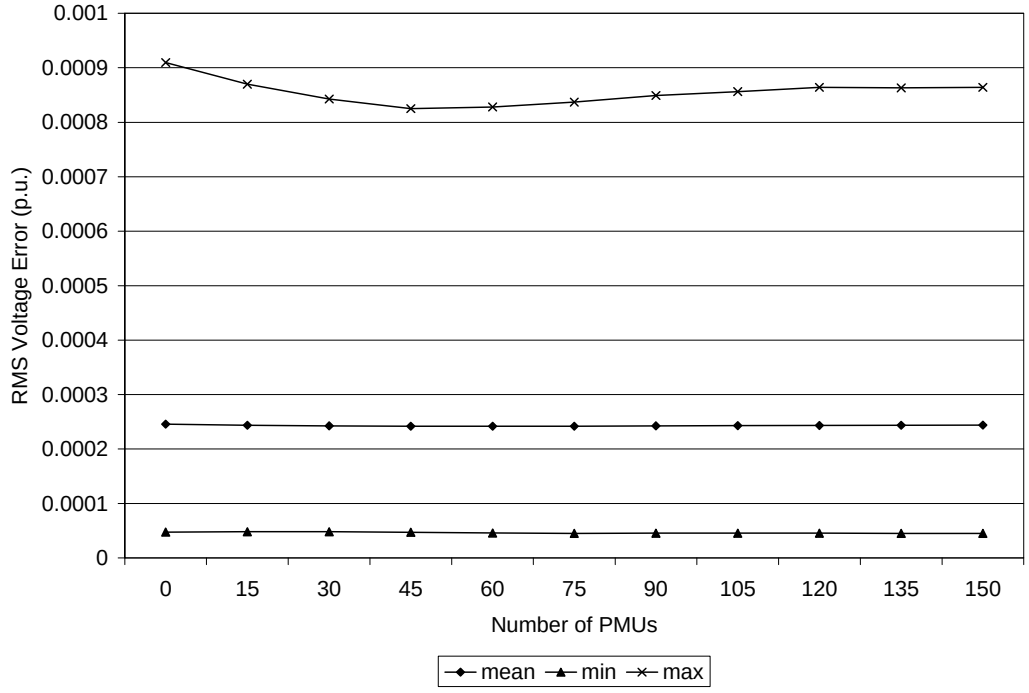

Figure E.4 RMS voltage magnitude error for Example 11: SCADA noise 5% and PMU noise 0.5% on System 2

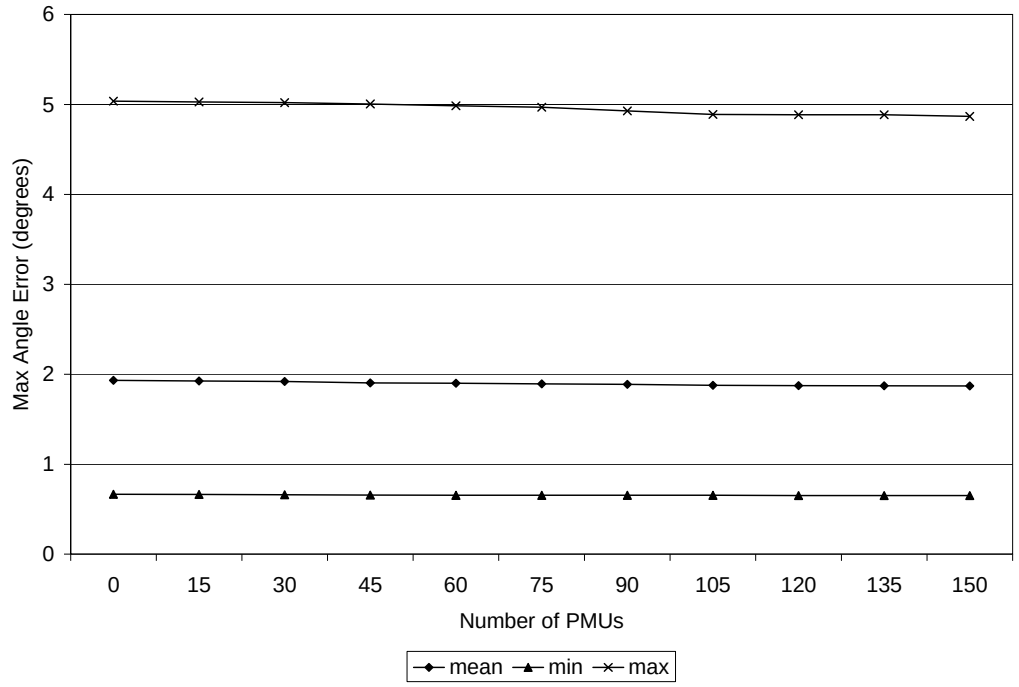

Figure E.5 Maximum voltage angle error Example 13: SCADA noise 10% and PMU noise 0.5% on System 2

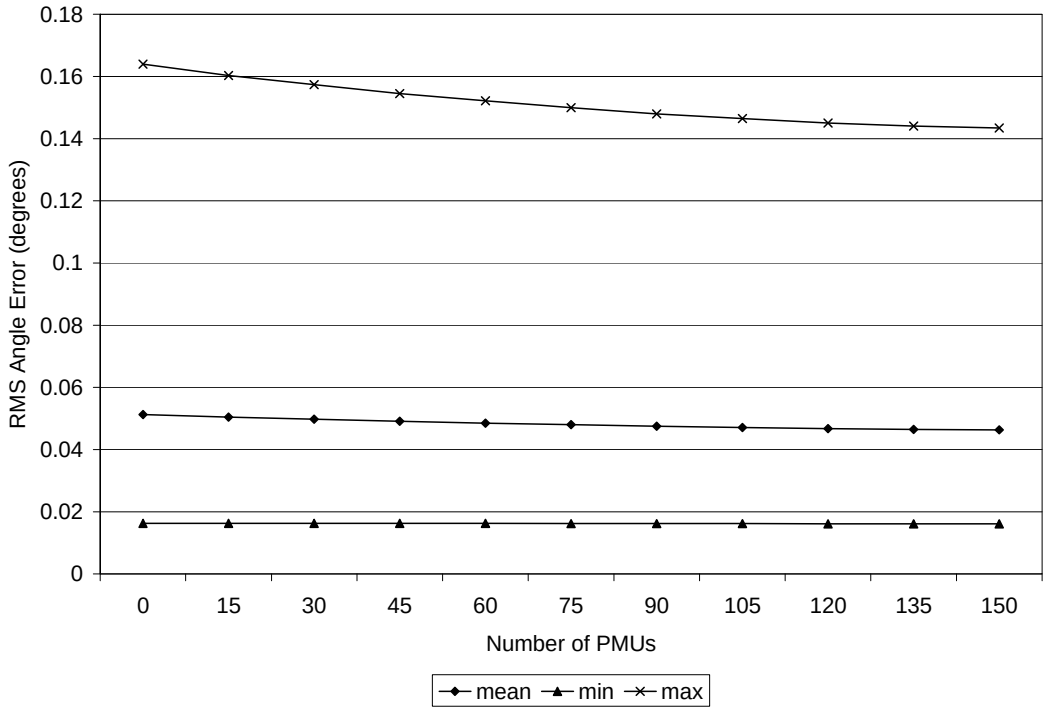

Figure E.6 RMS voltage angle error for Example 13: SCADA noise 10% and PMU noise 0.5% on System 2

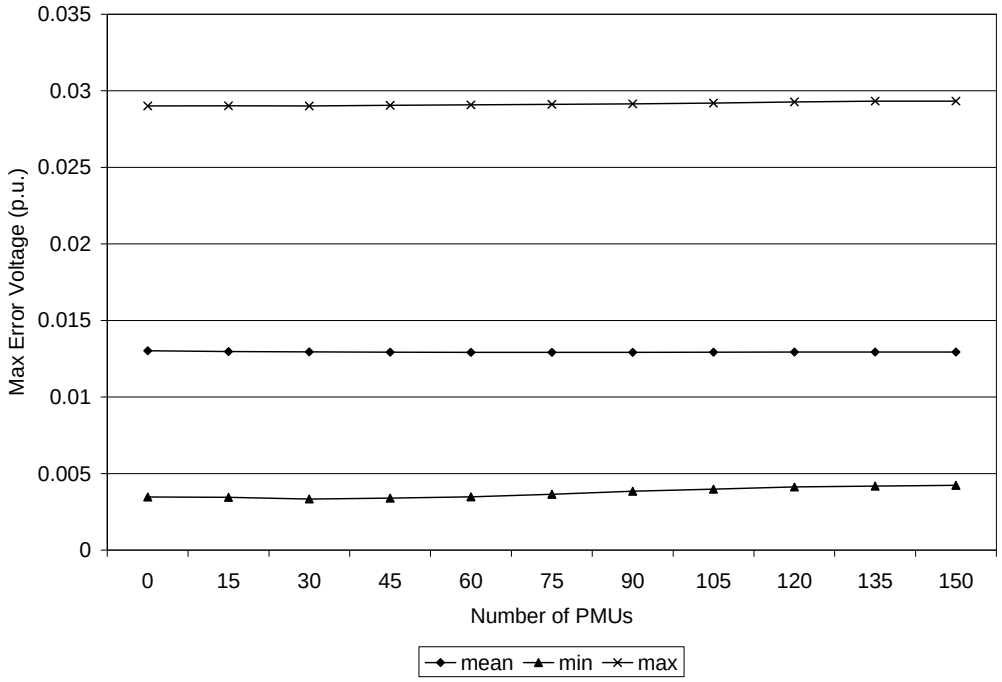

Figure E.7 Maximum voltage magnitude error for Example 13: SCADA noise 10% and PMU noise 0.5% on System 2

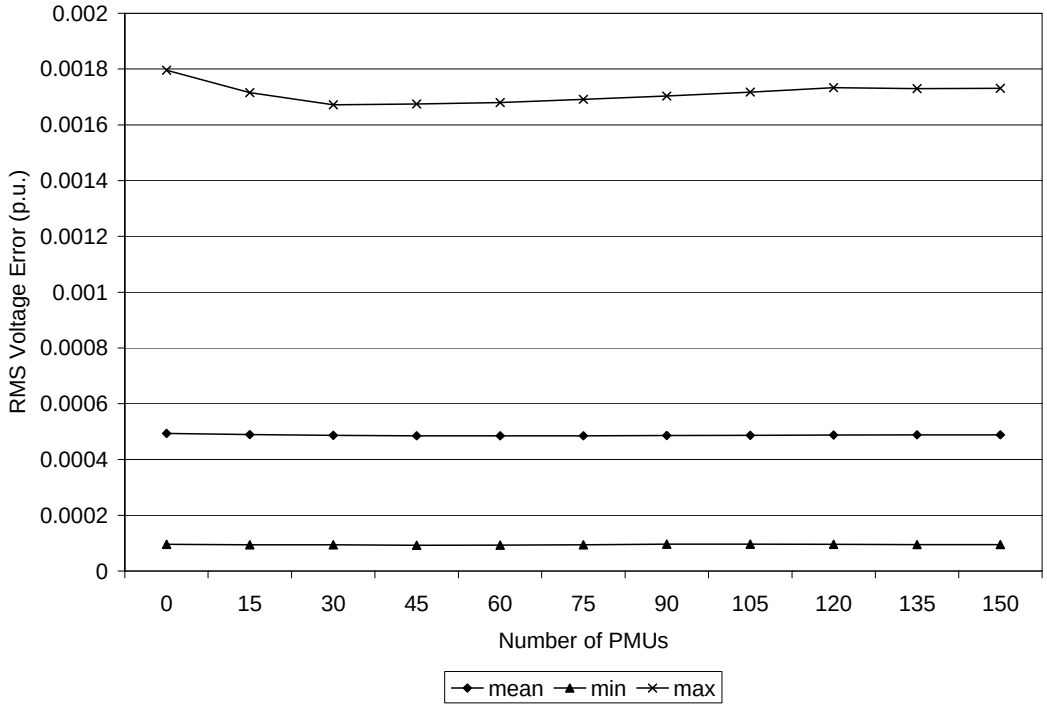

Figure E.8 RMS voltage magnitude error for Example 13: SCADA noise 10% and PMU noise 0.5% on System 2

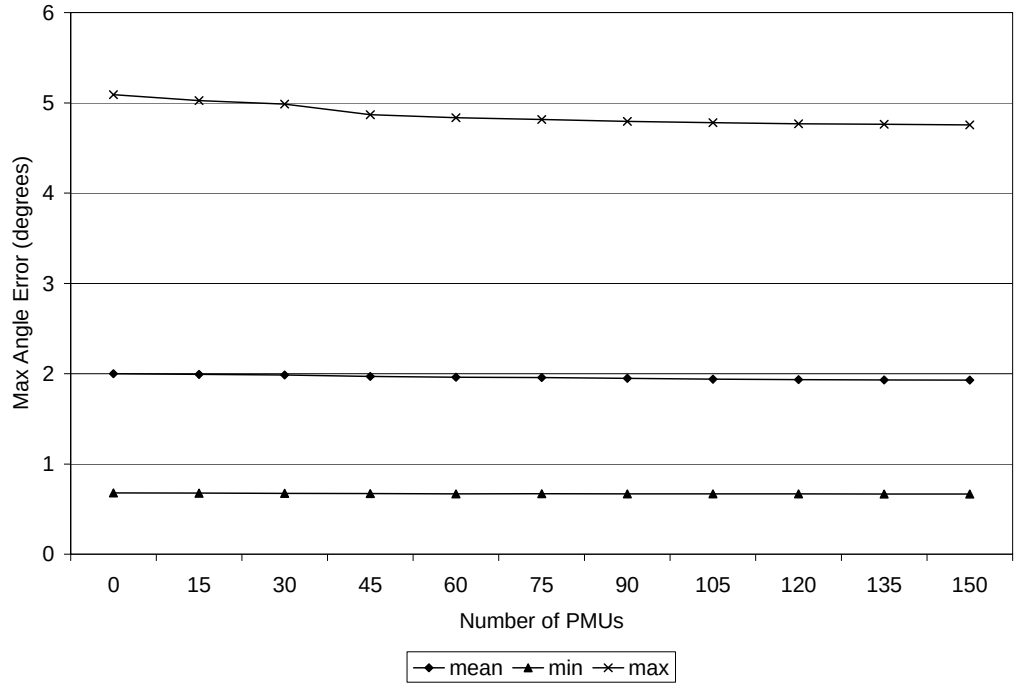

Figure E.9 Maximum voltage angle error for Example 14: SCADA noise 10% and PMU noise 1% on System 2

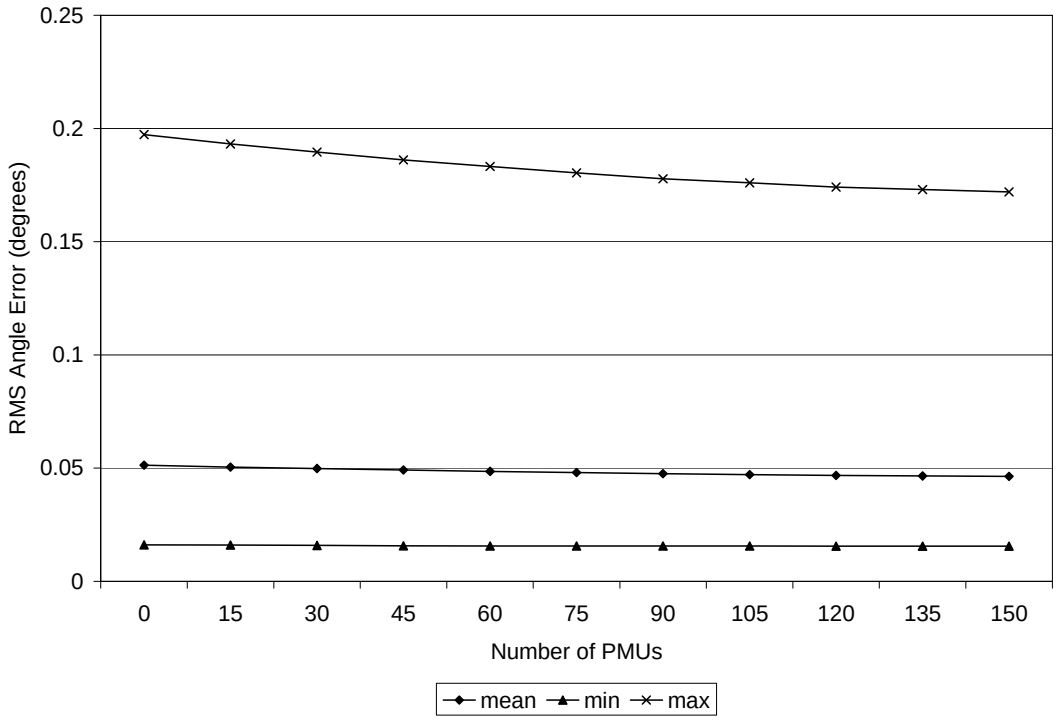

Figure E.10 RMS voltage angle error for Example 14: SCADA noise 10% and PMU noise 1% on System 2

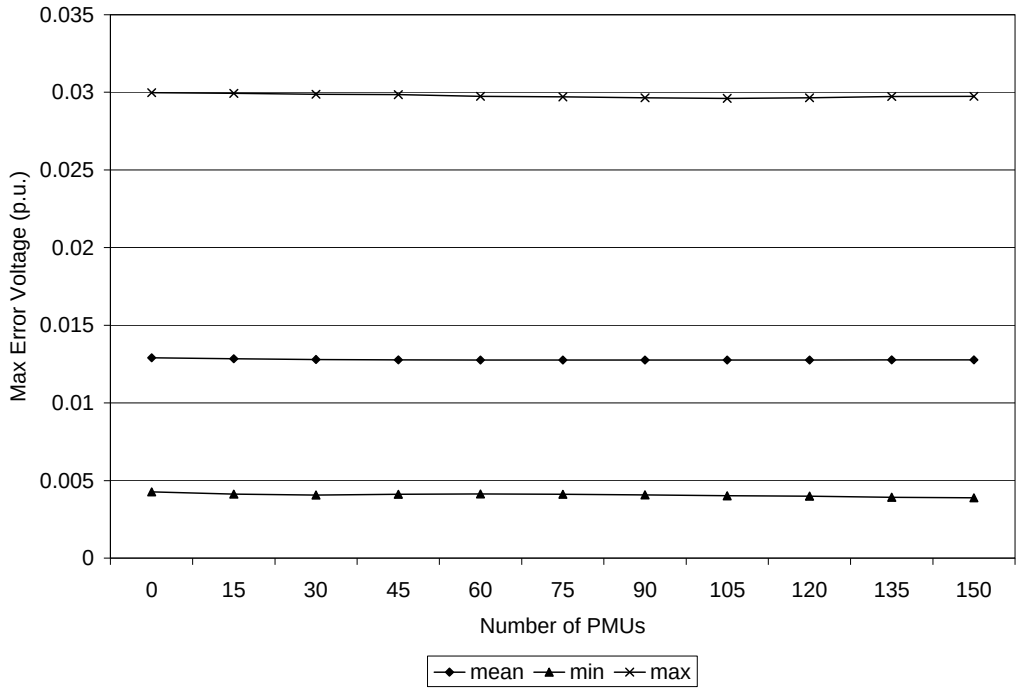

Figure E.11 Maximum voltage magnitude error for Example 14: SCADA noise 10% and PMU noise 1% on System 2

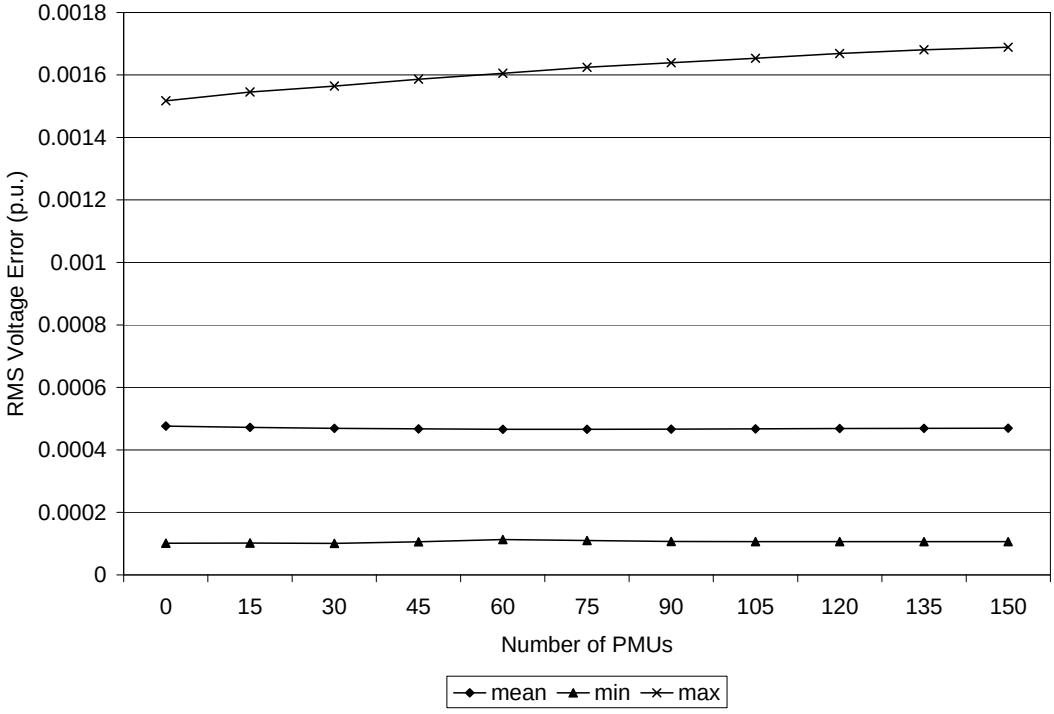

Figure E.12 RMS voltage magnitude error for Example 14: SCADA noise 10% and PMU noise 1% on System 2

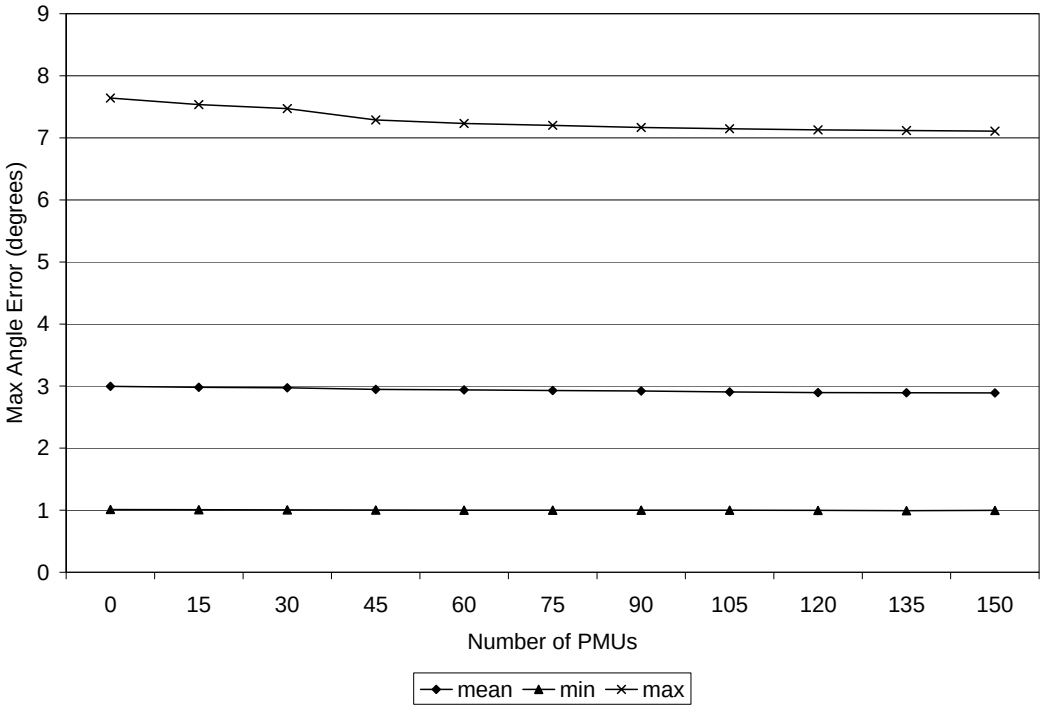

Figure E.13 Maximum voltage angle error for Example 16: SCADA noise 15% and PMU noise 1% on System 2

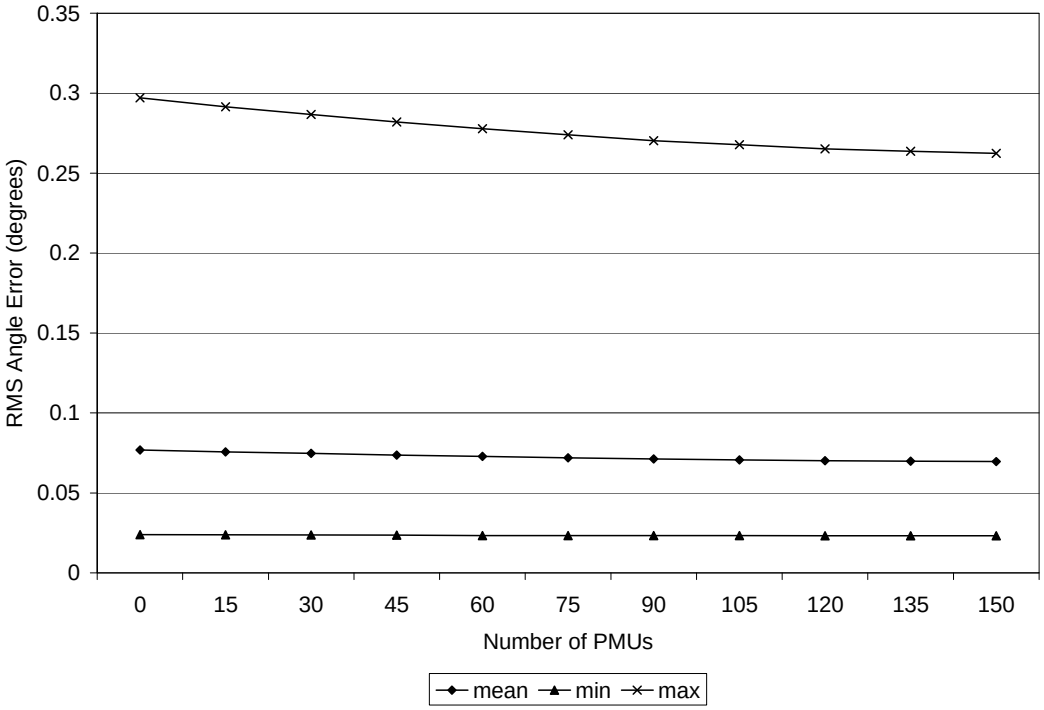

Figure E.14 RMS voltage angle error for Example 16: SCADA noise 15% and PMU noise 1% on System 2

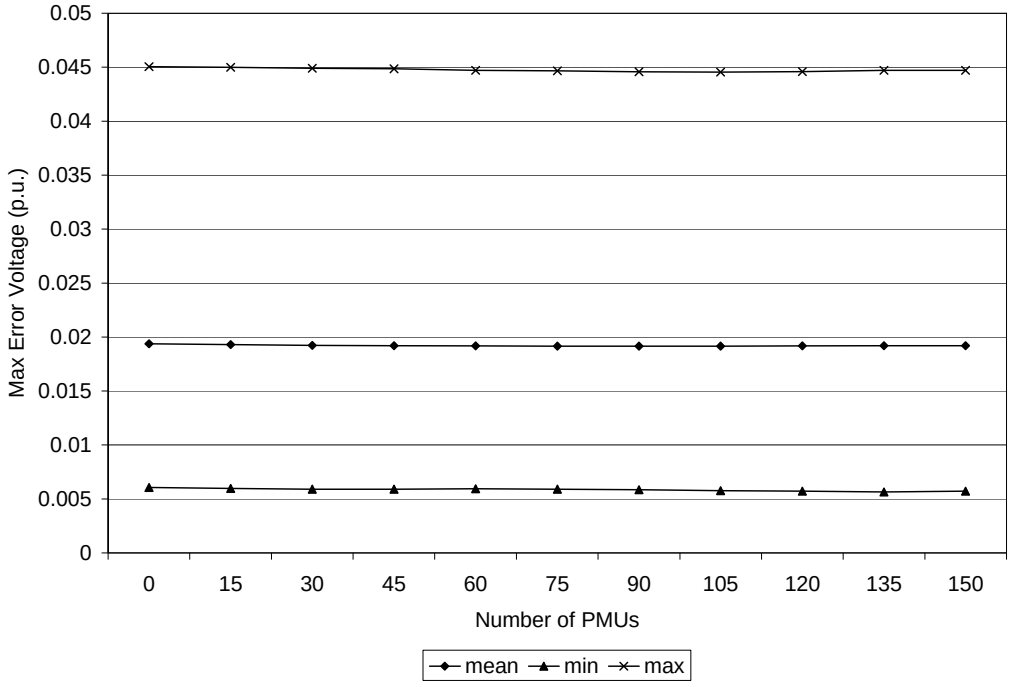

Figure E.15 Maximum voltage magnitude error for Example 16: SCADA noise 15% and PMU noise 1% on System 2

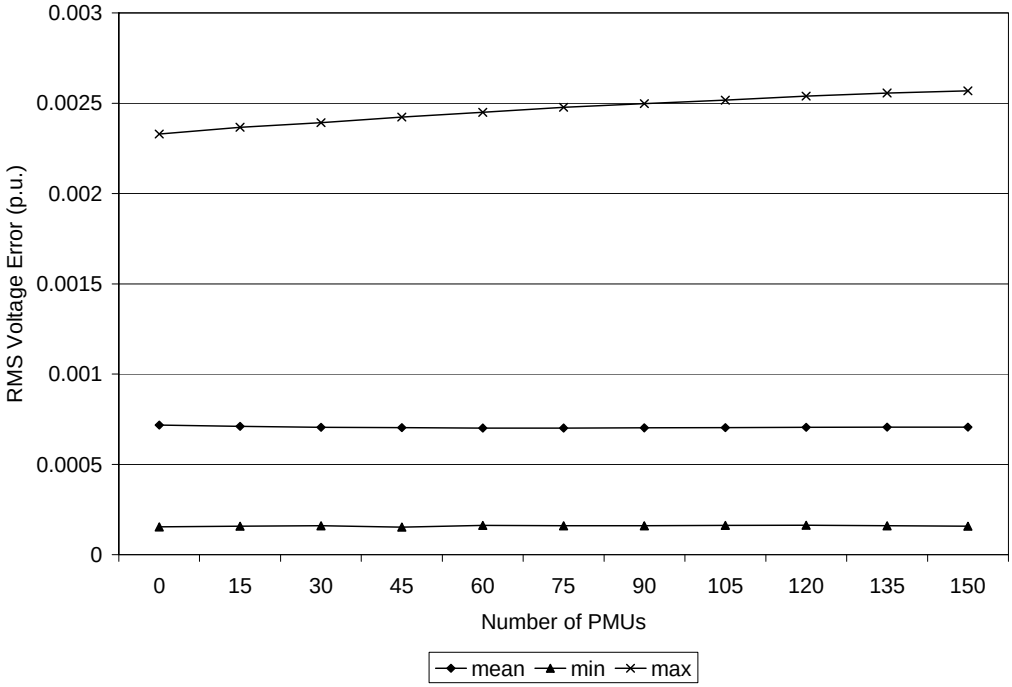

Figure E.16 RMS voltage magnitude error for Example 16: SCADA noise 15% and PMU noise 1% on System 2

E.2 Results of Examples 11, 13, 14, and 16: Condition Indicators

The condition indicators for Example 11, 13, 14, and 16 are depicted graphically. These Figures are listed in Table E.2.

Table E.2 List of Figures showing condition indicators of Examples 11, 13, 14, and 16

Example	Parameter	Figure
11	Condition number of converged G	E.17
11	Singular distance of converge G	E.18
13	Condition number of converged G	E.19
13	Singular distance of converge G	E.20
14	Condition number of converged G	E.21
14	Singular distance of converge G	E.22
16	Condition number of converged G	E.23
16	Singular distance of converge G	E.24

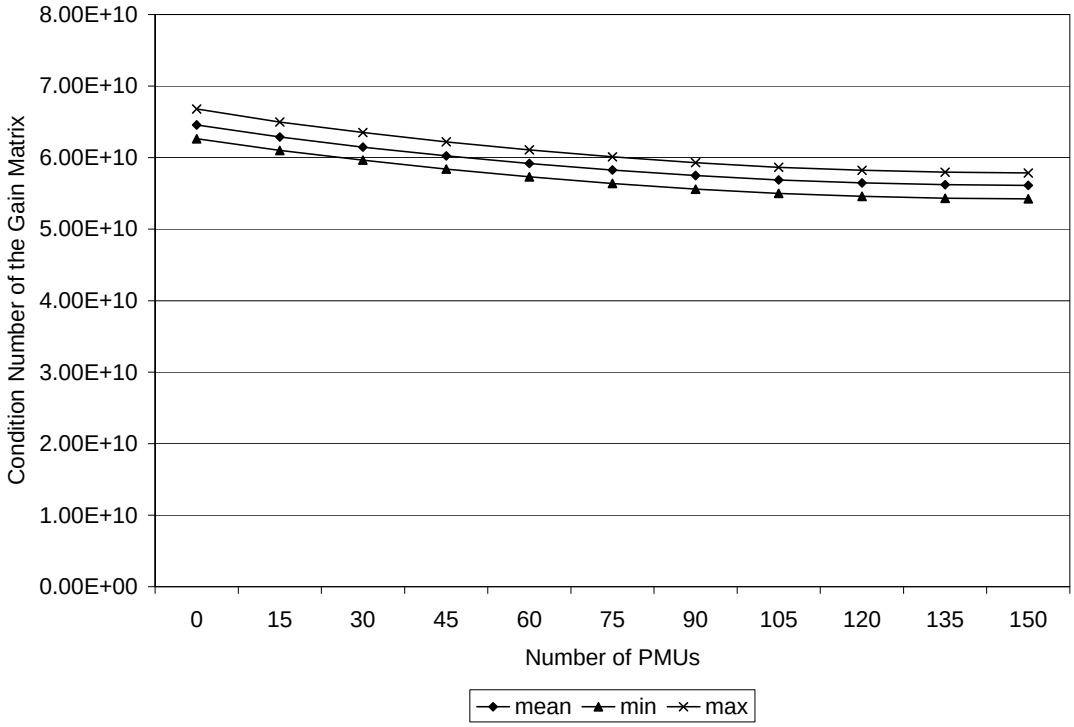

Figure E.17 System 2, K_G for solved iteration with SCADA noise 5% and PMU noise 0.5% (Example 11)

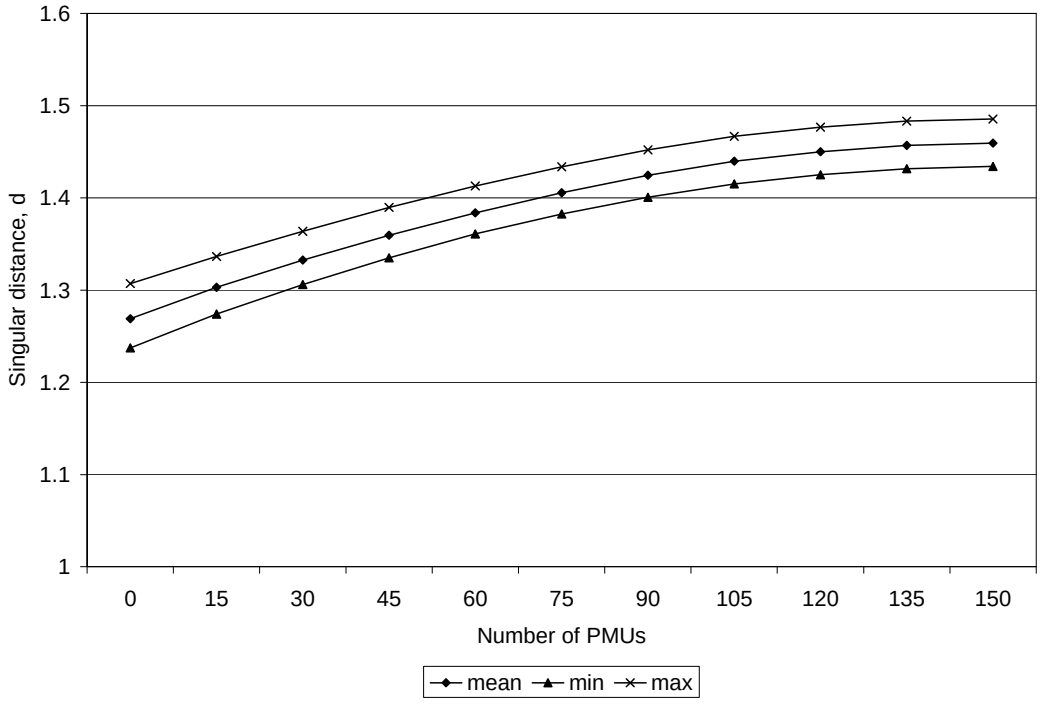

Figure E.18 System 2, *d* for solved iteration with SCADA noise 5% and PMU noise 0.5% (Example 11)

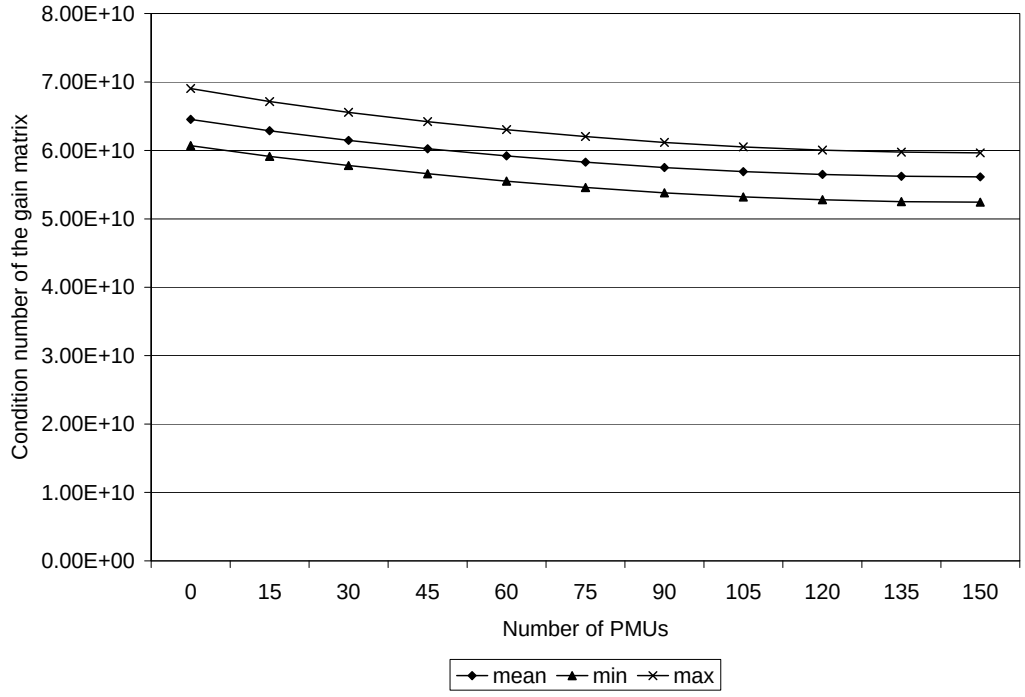

Figure E.19 System 2, K_G for solved iteration with SCADA noise 10% and PMU noise 0.5% (Example 13)

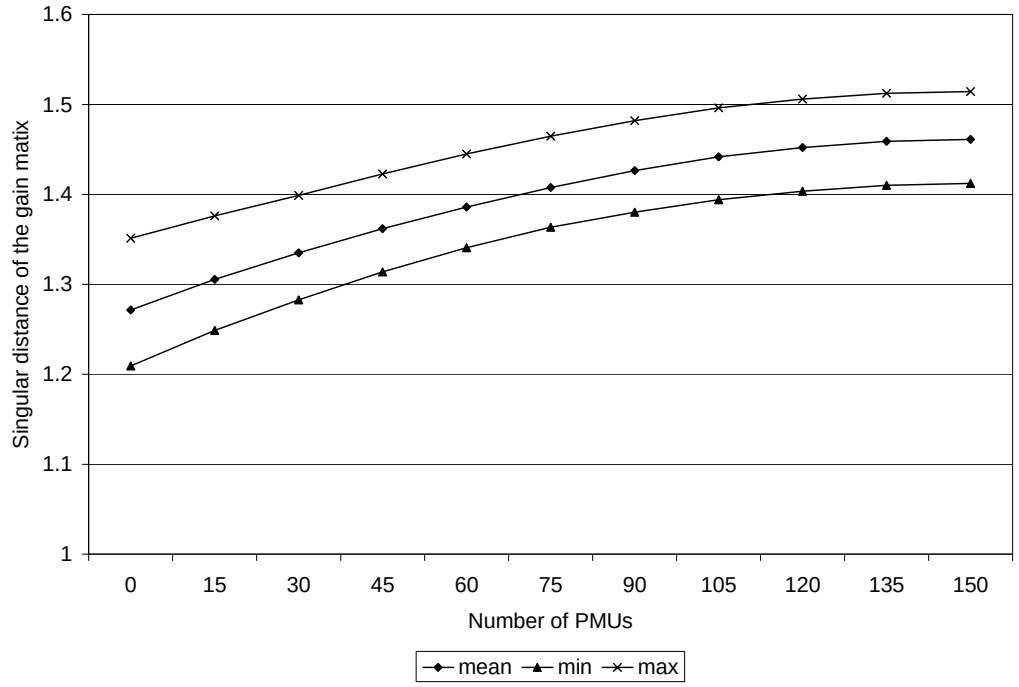

Figure E.20 System, 2 *d* for solved iteration with SCADA noise 10% and PMU noise 0.5% (Example 13)

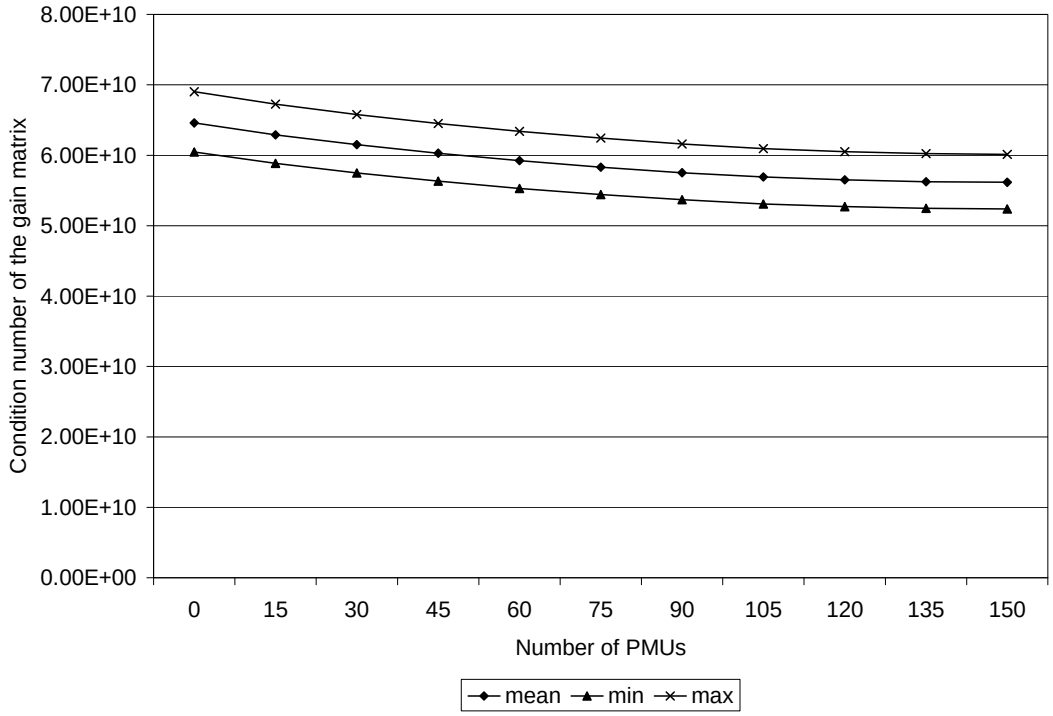

Figure E.21 System, 2 K_g for solved iteration with SCADA noise 10% and PMU noise 1% (Example 14)

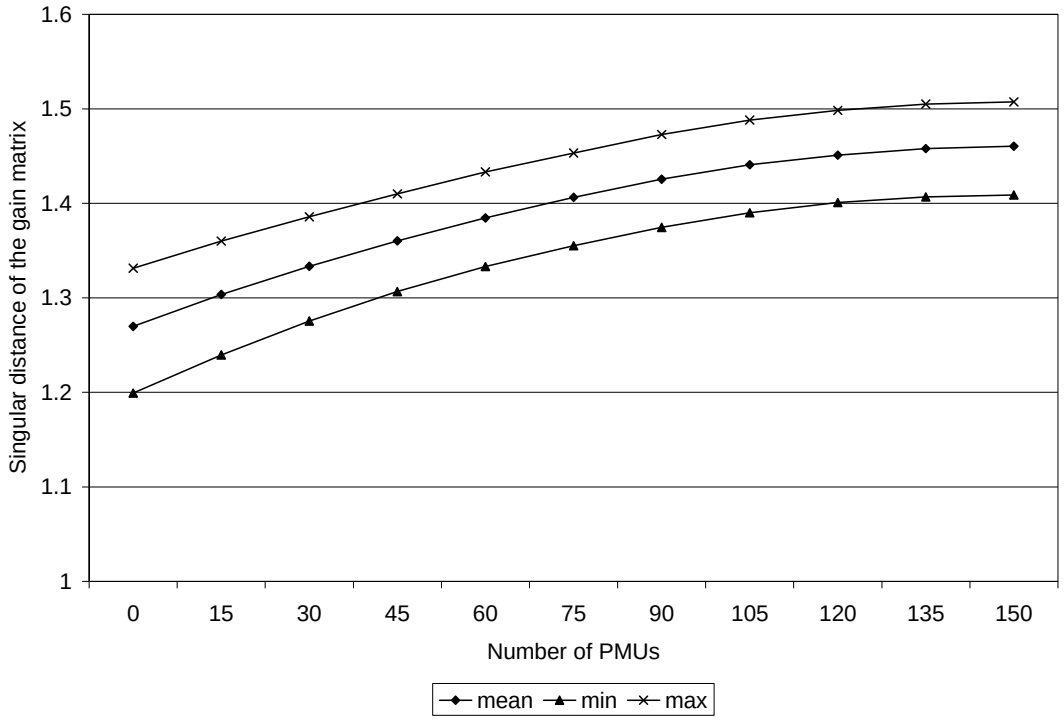

Figure E.22 System 2, d for solved iteration with SCADA noise 10% and PMU noise 1% (Example 14)

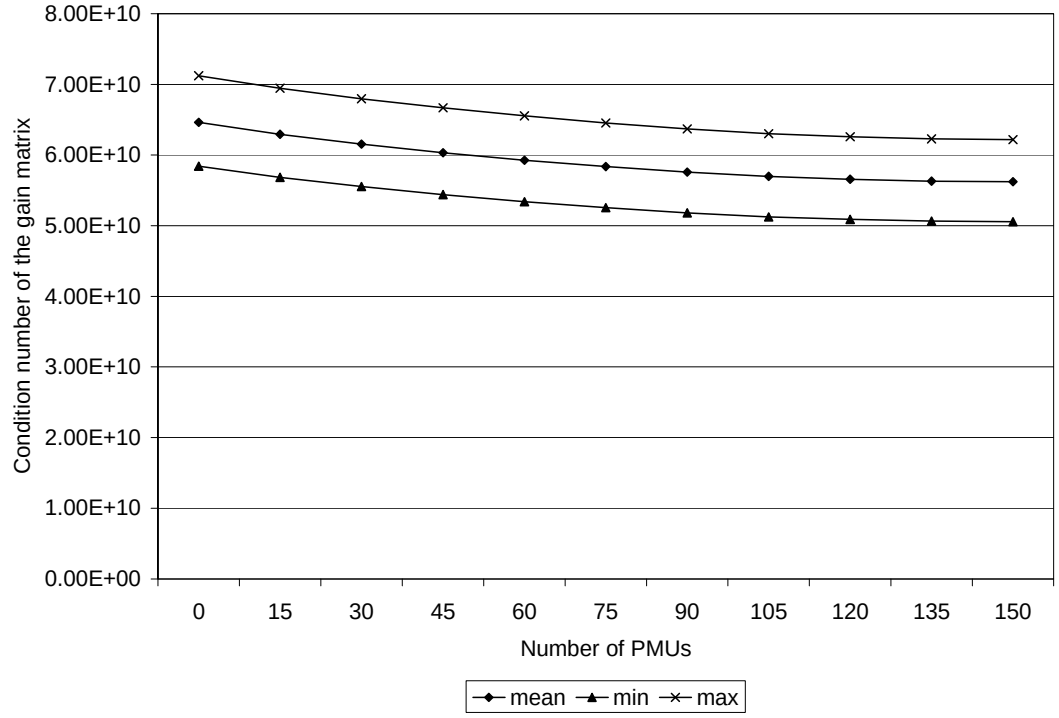

Figure E.23 System 2, K_g for solved iteration with SCADA noise 15% and PMU noise 1% (Example 16)

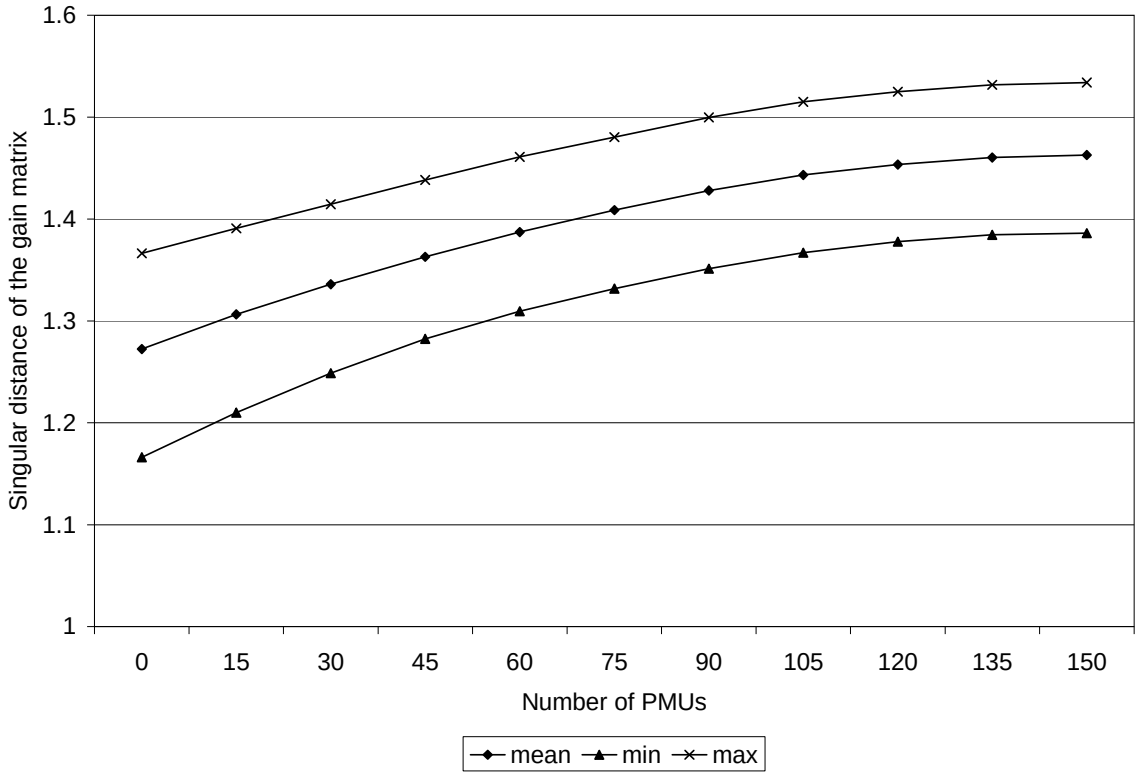

Figure E.24 System 2, *d* for solved iteration with SCADA noise 15% and PMU noise 1% (Example 16)

E.3 Summary of Examples 11, 13, 14, and 16

Table E.3 Summary of state estimation error in Examples 11, 13, 14, and 16

Example/ Figure No.	Parameter	Behavior of Parameter		
		Max from 0 to 150 PMUs	Min from 0 to 150 PMUs	Mean from 0 to 150 PMUs
11/ Figure E.1	Maximum angle error	↑ 0.07º	↓0.005º	↓0.033º
11/ Figure E.2	RMS angle error	↓ 0.011º	↓ 7.33 x10^{-5} deg	↓ 0.002º
11/ Figure E.3	Maximum voltage magnitude error	↑ 1.5 x10^{-4} p.u.	↑ 2.7 x10^{-4} p.u.	↓ 3.9 x10^{-5} p.u.
11/ Figure E.4	RMS voltage magnitude error	↓ 4.6 x10^{-5} p.u.	↓ 2.2 x10^{-6} p.u.	↓ 1.8 x10^{-6} p.u.
13/ Figure E.5	Maximum angle error	↓ 0.171º	↓ 0.015º	↓0.065º
13/ Figure E.6	RMS angle error	↓ 0.021º	↓ 1.29 x10^{-4} deg	↓ 0.005º
13/ Figure E.7	Maximum voltage magnitude error	↑ 3.2 x10^{-4} p.u.	↑ 7.7 x10^{-4} p.u.	↓ 8.7 x10^{-5} p.u.
13/ Figure E.8	RMS voltage magnitude error	↓ 6.5 x10^{-5} p.u.	↓ 7.6 x10^{-6} p.u.	↓ 4.7 x10^{-6} p.u.
14/ Figure E.9	Maximum angle error	↓ 0.335º	↓ 0.013º	↓ 0.072º
14/ Figure E.10	RMS angle error	↓ 0.025º	↓ 6.36 x10^{-4} deg	↓ 0.005º
14/ Figure E.11	Maximum voltage magnitude error	↓ 2.5 x10^{-4} p.u.	↓ 3.8 x10^{-4} p.u.	↓ 1.3 x10^{-4} p.u.
14/ Figure E.12	RMS voltage magnitude error	↑ 1.7 x10^{-4} p.u.	↑ 4.6 x10^{-6} p.u.	↓ 7.3 x10^{-6} p.u.
16/ Figure E.13	Maximum angle error	↓ 0.533º	↓ 0.016º	↓ 0.107º
16/ Figure E.14	RMS angle error	↓ 0.035º	↓ 7.6 x10^{-4} deg	↓ 0.007º
16/ Figure E.15	Maximum voltage magnitude error	↓ 3.3 x10^{-4} p.u.	↓ 3.4 x10^{-4} p.u.	↓ 2.0 x10^{-5} p.u.
16/ Figure E.16	RMS voltage magnitude error	↑ 2.4 x10^{-4} p.u.	↑ 4.6 x10^{-6} p.u.	↓ 1.1 x10^{-5} p.u.

Table E.4 Summary of condition indicators in Examples 11, 13, 14, and 16

Example/ Figure No.	Parameter	Behavior of Parameter		
		Max from 0 to 150 PMUs	Min from 0 to 150 PMUs	Mean from 0 to 150 PMUs
11/ Figure E.17	K_G	$\downarrow 8.92 \times 10^9$	$\downarrow 8.41 \times 10^9$	$\downarrow 8.43 \times 10^9$
11/ Figure E.18	d	$\uparrow 0.1785$	$\uparrow 0.1967$	$\uparrow 0.1903$
13/ Figure E.19	K_G	$\downarrow 9.42 \times 10^9$	$\downarrow 8.27 \times 10^9$	$\downarrow 8.41 \times 10^9$
13/ Figure E.20	d	$\uparrow 0.1632$	$\uparrow 0.2030$	$\uparrow 0.1896$
14/ Figure E.21	K_G	$\downarrow 8.88 \times 10^9$	$\downarrow 8.07 \times 10^9$	$\downarrow 8.43 \times 10^9$
14/ Figure E.22	d	$\uparrow 0.1760$	$\uparrow 0.2095$	$\uparrow 0.1906$
16/ Figure E.23	K_G	$\downarrow 9.05 \times 10^9$	$\downarrow 7.86 \times 10^9$	$\downarrow 8.41 \times 10^9$
16/ Figure E.24	d	$\uparrow 0.1676$	$\uparrow 0.2201$	$\uparrow 0.1903$

APPENDIX F

THE IMPACT OF WEIGHTING MEASUREMENTS ON SYSTEM 2

F.1 Infinite norm of error in Example 17

Example 17 is a 100 Monte Carlo trials simulation performed on System 2 with SCADA measurement noise level of 15% and 0.5% noise in PMU phase angle measurements. The PMU measurements have a weight of 10 and the SCADA measurements are weighted 1. In this example, the PMUs are 30 times more accurate than the SCADA measurements (i.e., SCADA noise / PMU noise = 30). Figure F.1 depicts the maximum phase angle error. Note the significant drop in maximum phase angle error as PMUs voltage phase angle measurements are added. In approximate terms, the mean of the maximum phase angle error decreases at the rate of 0.0109º per PMU phase angle measurement added. In a separated example not depicted here, if a weight of 50 is assigned to the PMU measurements, the improvement in error is about 0.0110° per PMU measurement added.

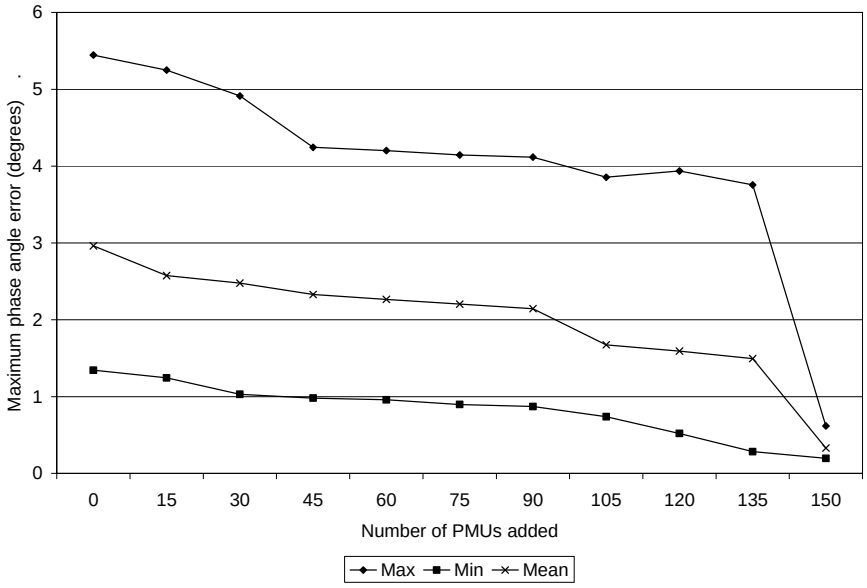

Figure F.1 Maximum phase angle error for Example 17: SCADA noise 15% and PMU noise 0.5% with PMU weight of 10

F.2 L_2 norm of error in Example 17

The RMS voltage phase angle error of Example 17 is shown in Figure F.2. Note, the significant improvement seen in RMS voltage phase angle error as PMUs are added. This improvement is significantly larger than the improvement seen in Example 15. In approximate terms, the improvement in RMS phase error is 0.0005 per added PMU, most of which occurs in the addition of the first few PMUs.

F.3 Voltage Magnitude Errors in Example 17

The maximum voltage magnitude error in Example 17 is shown in Figure F.3 and the RMS voltage magnitude error is shown in Figure F.4. Note the erratic behavior of

voltage magnitude error in Figures F.3 and F.4. This increase in voltage magnitude error in Example 17 is larger than seen in Examples 11 – 16. The increase in voltage magnitude error is due to the fact that the phase angle measurements can "push" the error away from the phase angle states and into other states estimates (i.e., voltage magnitude states). This is a drawback of weighting the PMU phase angle measurements 10 times larger than the SCADA measurements.

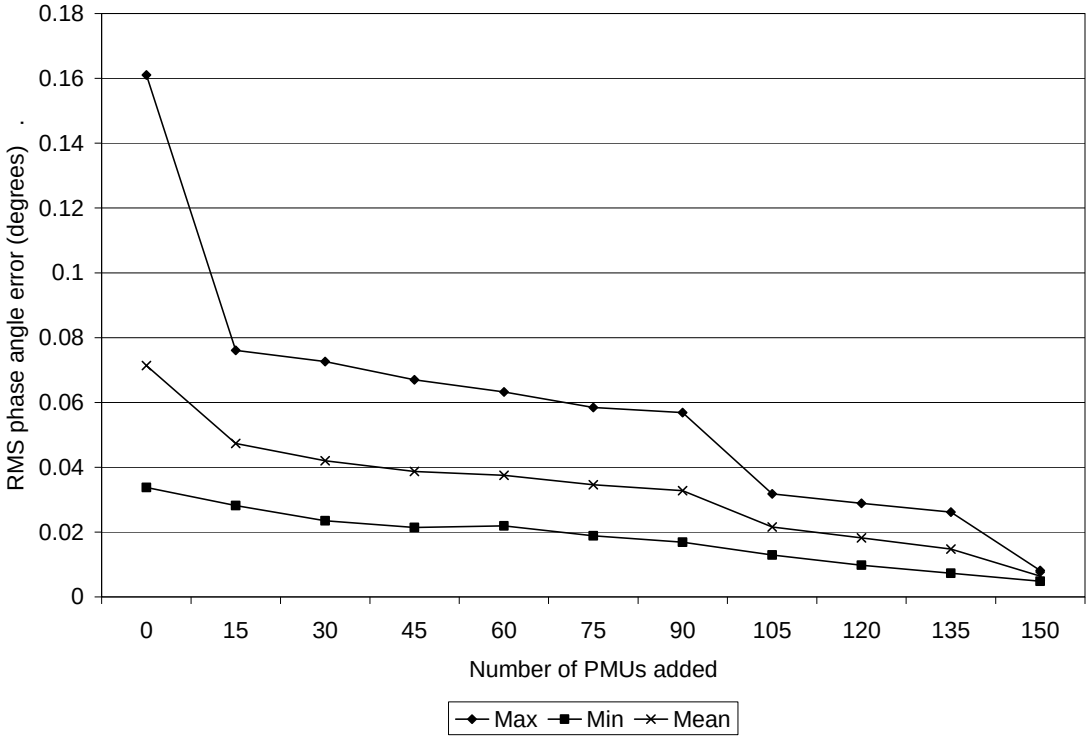

Figure F.2 RMS phase angle error for Example 17: SCADA noise 15% and PMU noise 0.5% with PMU weight of 10

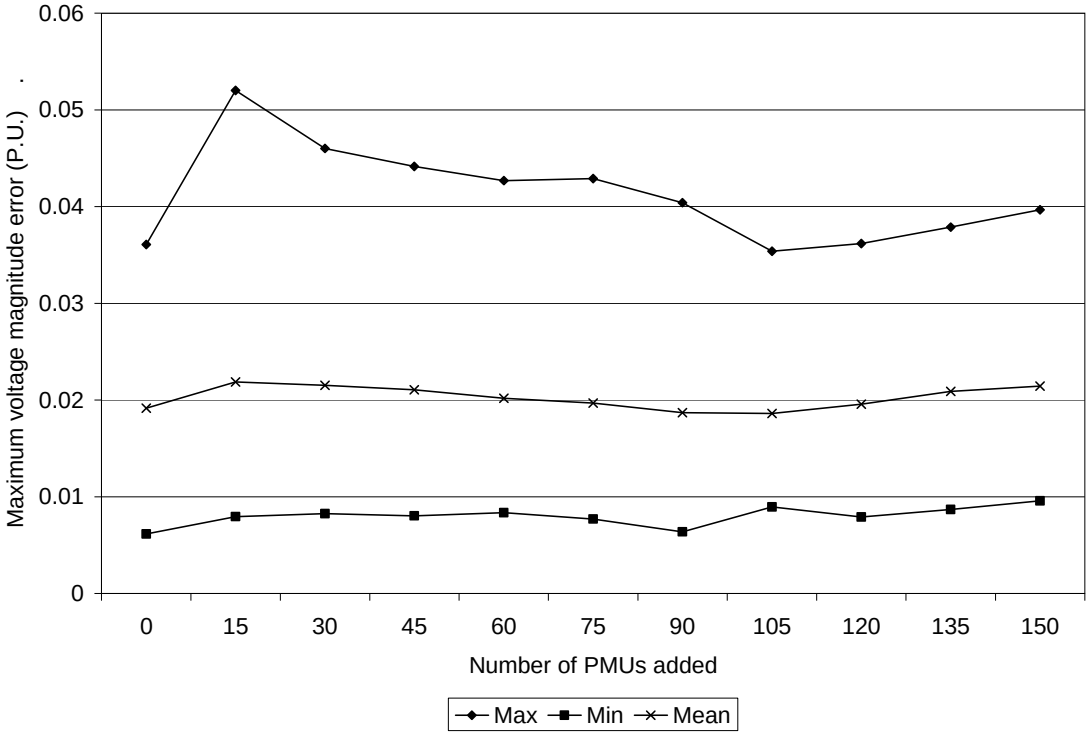

Figure F.3 Maximum voltage magnitude error for Example 17: SCADA noise 15% and PMU noise 0.5% with PMU weight of 10

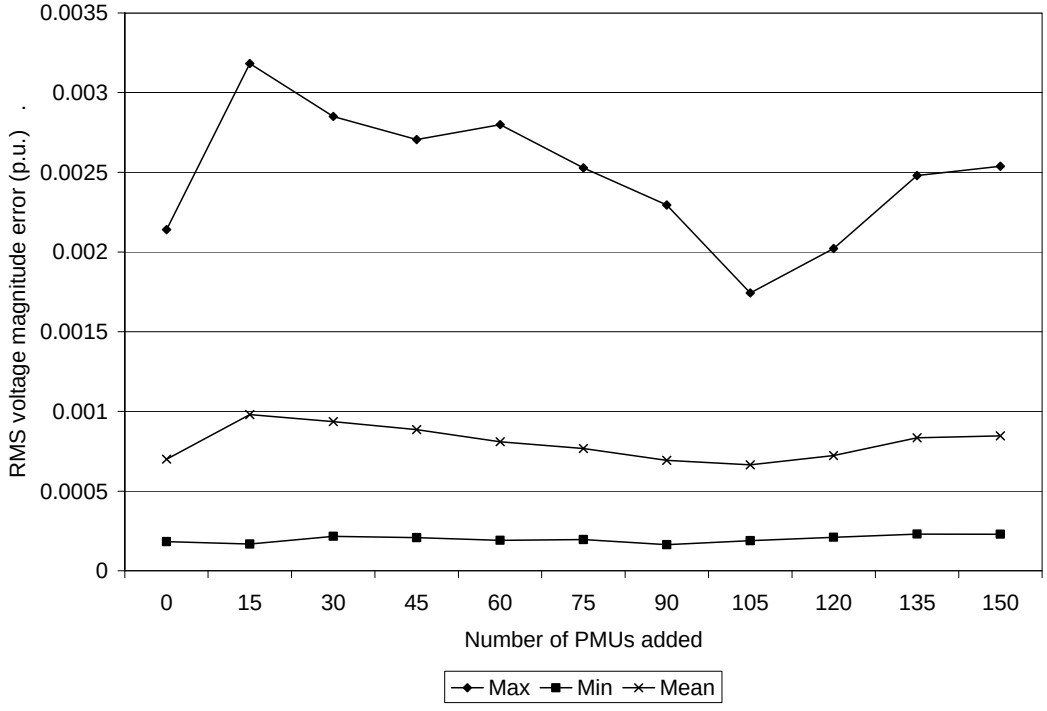

Figure F.4 RMS voltage magnitude error for Example 17: SCADA noise 15% and PMU noise 0.5% with PMU weight of 10

F.4 Condition Indicators in Example 17

Figure F.5 displays the condition number in Example 17 of the converged iteration gain matrix, K_G. Note the significant improvement in the condition number for the addition of the first 15 PMUs. The improvement in K_G from the addition of the first 15 PMUs appears inconsistent with the improvement in K_G from the addition of the subsequent PMUs. Figure F.6 depicts the singular distance of the converged iteration gain matrix, d. Note, in F.6 the improvement per PMU phase angle measurement added in d increases as more PMU phase angle measurements are added for the addition of 30th to 150th PMUs.

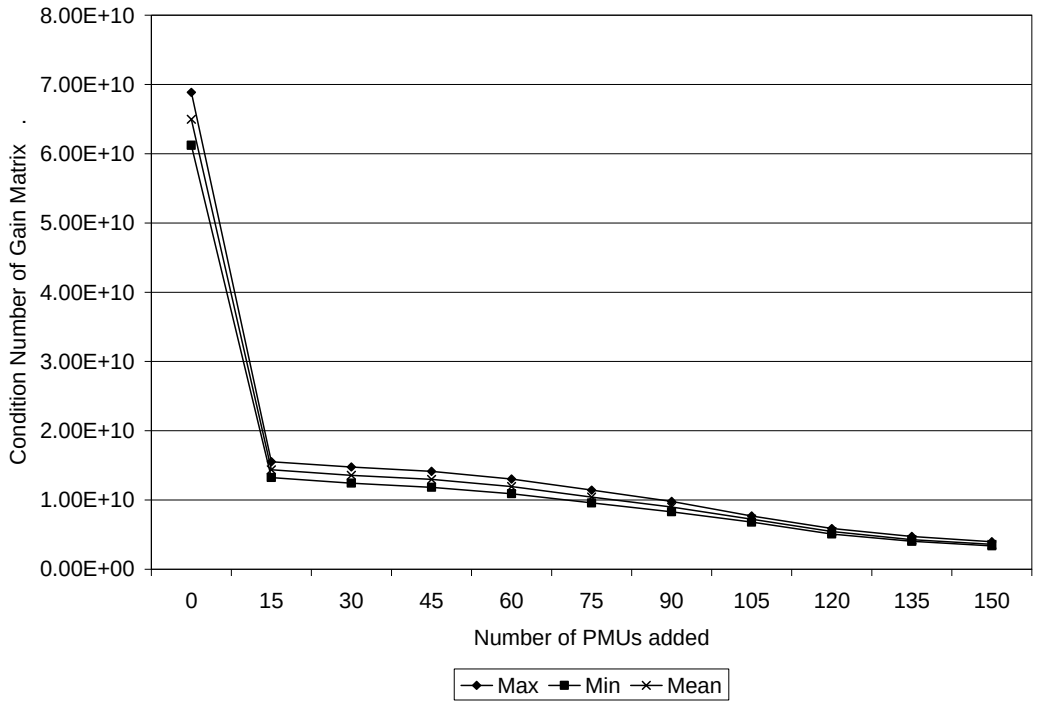

Figure F.5 K_G for solved iteration of Example 17: SCADA noise 15% and PMU noise 0.5% with PMU weight of 10

Equations (2.22) and (2.23) allow for the prediction of the change in K_G and the change in d in Example 17. These predictions are, for the addition of one PMU phase angle measurement,

$$\Delta d = 0.0254$$
$$\Delta K_G = -1.26x10^{10}.$$

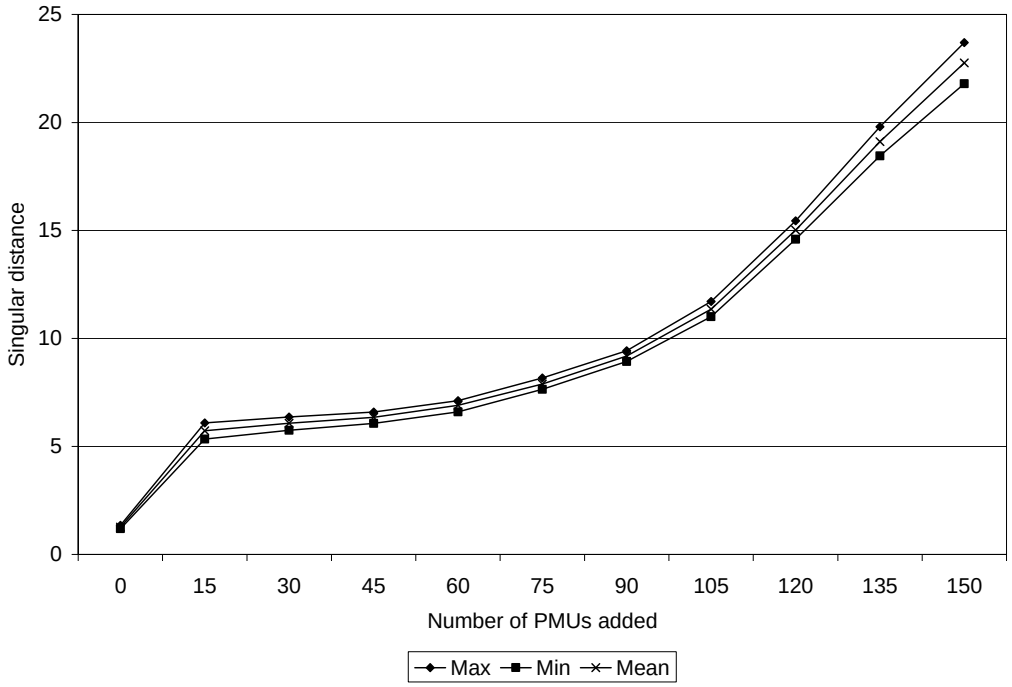

Figure F.6 Singular distance, *d*, for solved iteration of Example 17: SCADA noise 15% and PMU noise 0.5% with PMU weight of 10